Detailed chemical kinetic modeling study on gas phase partial oxidation and steam reforming of species released during biomass pyrolysis

ティムトン, ナルモン

https://doi.org/10.15017/1544007

Detailed chemical kinetic modeling study on gas phase partial oxidation and steam reforming of species released during biomass pyrolysis

by

Narumon Thimthong

(2015)

Department of Applied Science for Electronics and Materials,

Interdisciplinary Graduate School of Engineering Sciences,

Kyushu University, Japan

Contents

Chapter 1

General Introduction

1.1 Background

Demand of world's energy increases with emerging economy and growing population. A report on world energy consumption predicts an increased energy demand of 56% from 2010 to 2040 [1]. Giving impacts on increasing scarcity of fossil carbon resource and high fossil fuel prices. Although, fossil resources are not regarded as clean energy sources for an environmental point of view. One of environmental impacts is caused by the intensified using of fossil resources. Environmental concerns due to greenhouse gas emissions is motivated to increase utilizations of renewable energy sources and reduce dependence on fossil resources. As a renewable energy resource, biomass has become more important because of its several environmental and economic advantages. Biomass has a potential to be a major source of energy which is estimated to contribute of the order 10-14% of the world's energy supply [2]. For an aspect of environmental benefits, decomposition of biomass either naturally or thermal conversion processes contributes no new carbon dioxide to the atmosphere due to carbon dioxide emission roughly estimate same with carbon dioxide uptake by plant [3–5].

Biomass is a complex mixture of organic materials derived from living organisms which most often refers to as plants or plant-based materials. Which are specifically called ligno-cellulosic biomass. Biomass contains stored energy from sun via photosynthesis

process and stocks as complex molecules. The stored chemical energy in biomass is contained in the terms of cellulose, hemicellulose, and lignin components. When these components are broken by digestion, combustion, or decomposition, their stored chemical energy is released as heat. Biomass is a very versatile and various feedstock which can be converted to more valuable energy forms via a number of processes such as thermal and biological processes. Factors that influence the choice of conversion process are the type and quantity of biomass feedstock; the desired energy requirements, environmental standards, and economic conditions.

Biochemical conversion processes are suitable for biomass which have high moisture content. However, some limitations are related to biochemical methods. For example, cold climatic conditions are not suitable for anaerobic fermentation for methane digester. Fermentation to produce ethanol requires consistent biomass source, advanced equipment, and highly skilled labor [3].

1.2 Thermochemical conversion of biomass

According to some limitations of biochemical conversion process about lacks of robustness at industrial scale and produces a small number of discrete products. Thermochemical process for biomass conversion is focused of interest due to suitable for almost any types of biomass and practical for commercial scale. Thermochemical conversion process is based on the reaction of heat which allows chemical reactions to transform biomass into multiples products namely energy/power/heat generation, transportation fuels, and chemical feedstock [4,6–8]. The relative advantages of thermochemical conversion over other technologies are higher productivity which can be used in a variety of applications and

compatibility with existing infrastructure facilities. The major thermal biomass conversion techniques are combustion, gasification, and pyrolysis.

Direct combustion is the most ancient and mature technology for thermochemical conversion of biomass. It is the process of burning biomass in air to convert the chemical energy stored in biomass into heat at temperature around 800-1000^{o}C. Although, direct combustion has excellence efficiency for heat utilization, however, there are many operational and environmental challenges associated with this technology. For example, direct combustion suffered problem of ash melting at low temperature leads to bed agglomeration, fouling, scaling, and corrosion. Subsequently, the presence of sulfur, nitrogen, chlorine etc., in biomass during combustion leads to the formation of gaseous pollutants such as SOx, NOx, N_2O and HCl which cause harmful effects and undesired health impacts [9–11].

Gasification has been practiced for many years. It is a robust proven technology that can be operated either as a simple or as a more sophisticated system. Unlike direct combustion, gasification consists of two stages; firstly, pyrolysis biomass into a gaseous fuel by heating at temperature below 600^{o}C following by secondary step for partial oxidation with oxidizing agents at elevated temperature [5]. The main gasifying agent is usually air but oxygen/steam agents are also used. Difference of oxidizing agents result in different product qualities. For instant, air agent results in a low calorific power gas, despite, medium calorific power gas is obtained by using oxygen and steam oxidizing agents. The gas obtained from biomass gasification is called producer gases or prosuct gases. Product gases are a mixture of hydrogen, carbon monoxide, methane, carbon dioxide, water vapor, and small quantities of heavier hydrocarbons or nitrogen (in air gasification). Gasification is a viable options to

not only remove the problems encountered in direct combustion but also to provide cleaner fuel gases suitable for use in gas turbines and engines. In addition, the production of syngas from biomass gasification allow to synthesize other chemicals and liquid fuels which can use for chemical feedstock and transportation [10].

Pyrolysis is the first step of gasification process (Fig. 1). It is thermal decomposition of biomass at moderate temperatures in the absence of oxidizing agents so the oxidation reactions can be neglected. Pyrolysis allows transforming organic materials into a wide range of useful products (solid, liquid, gaseous). Properties and quantities of products are always varieties depending on reactor temperature, residence time, biomass type, char separation, and biomass ash content. Based on the operating conditions, pyrolysis can be classified into three regimes, conventional or slow pyrolysis, intermediate pyrolysis, fast and flash pyrolysis.

I. Conventional pyrolysis involves lower temperatures and longer residence times with the principal product is solid char.
II. Intermediate pyrolysis takes place at temperature lower than 600^{o}C with moderate reaction times to provide same proportions of gas, solid, and liquid.
III. Fast pyrolysis occurs at temperature between 500^{o}C and 650^{o}C with brief reaction times to favor production of a liquid fraction up to 70-80% of the feed biomass weight.
IV. Flash pyrolysis is similar with fast pyrolysis but it takes place at temperatures higher than 700^{o}C and have reaction times that are lower than the former. This process allows the production of a liquid fraction up to 80% of the feed biomass weight [6].

The products of pyrolysis can be used for various purpose. Products gases can be burned

to give heat for the reactor. Char can be used as fuel or fine application in the chemical industry. The major product, liquid product, in terms bio-oil can be utilized in several different ways such as energy, conventional fuels (diesel, gasoline, kerosene, methane, liquefied petroleum gas, etc.,) for transportation and power generation [6–8].

1.3 Tar problem in thermochemical conversion technology for biomass utilization

Even thermochemical comversion as pyrolysis or gasification has been sufficiently developed to yield a number of valuable products. However, the complexity of biomass and its factors such as moisture, oxygen, sulfur, nitrogen, and metal contents cause some troubles for this technology. One of the challenge problem is unavoidable products consisting of tar, particulate matter, HCl, NOx, H_2S, and SOx [12,13]. These undesired products cause harmful for downstream equipment also deteriorate gasification efficiency. Removal of impurities from gasification of biomass is usually required for most end-uses of products [9–11,14–21].

Tar is a major problematic by-product derived from biomass gasification. Tar is formed during biomass thermochemical conversion and begin to condense at reduced temperatures normally <450^{o}C. Tar is higher molecular weight hydrocarbons than benzene; consists of stable aromatic compounds, such as polycyclic aromatic hydrocarbons [22]. The appearance ranges from brown and watery to black and highly viscous. Tar trends to be refractory in the gasification process and difficult to remove. Thus tar is partly deposited on the walls of the piping and partly remaining as an aerosol in the gas. Condensing of tar on the inner surfaces of the equipment results in plugging, fouling, erosion, corrosion, and catalyst poisoning of pipes, tubes, and other components in downstream. At temperature above 400^{o}C, tar can undergo subsequent dehydration reactions to form solid char and coke that further tend to

plug up systems. Although tar is only a minor component in biomass gasification, even small amounts can significantly damage downstream facilities and deteriorate gasification efficiency. In order to prevent eventual problems, removal or control of tar is necessary before syngas can be used in any downstream equipments.

Tar in the product gas can be reduced/control with many methods including physical, thermal cracking, catalyst cracking, and non-catalytic vapor-phase reforming [22–26].

I. The physical method for removing tar such as wet scrubbers, electrostatic precipitators is principle but requires the product gas be cooled to ensure that tar is in a condensed form. And the main disadvantage of this method is water containing tar, which is classified as hazardous wastewater and its treatment adds significantly to the overall cost of the gasification plant.

II. Thermal cracking is tar cracking at higher temperature, typically above 1000^{o}C. However, thermos decomposition at high temperature lead to soot formation, which is more troublesome than the aromatics compounds. Indeed, the difficulties of achieving complete thermal cracking, in parallel with operational and economic considerations, often make thermal cracking less attractive in large-scale gasification systems.

III. Catalyst cracking is an effective method for tar elimination, but it is expensive and requires good technologies to manage/regenerate the deactivated catalyst. As well as sulfur/chlorine poisoning due to hydrogen sulfide/hydrogen chloride contained

in the product gas are likely unavoidable which caused the irreversible deactivation of the catalyst [27–32].

IV. Non-catalytic vapor-phase reforming such as steam reforming and partial oxidation aimed at a more robust technology [24]. This process reduced tar by converting into permanent gases. The process deal with volatile matter which release during the initial stage of biomass gasification (pyrolysis). The volatiles frequently contain tarry components in addition to steam as well as non-condensable gases such as hydrogen, carbon monoxide, carbon dioxide, and methane. So an exhaustive reforming of tar in the volatiles into dry gas is thus highly desirable in order to reduce the cost of further expensive gas treatment facilities.

1.4. Non catalytic partial oxidation and steam reforming

Non-catalytic partial oxidation or steam reforming is a practical and effective method for tar removal from the thermochemical conversion of biomass. In the presence of oxygen during gasification accelerates destruction of primary tar products. Many studies have successfully applied a partial oxidation approach to control the tar concentration [15,33–36]. Su et al. [36], who found that oxygen significantly impacts the conversion of tar and developed a flow reactor to predict tar destruction under partial oxidation conditions. Hosokai et al. investigated the gas-phase partial oxidation of nascent volatiles from the rapid pyrolysis of cedar sawdust in two-stage reactor and claimed that the amount of oxygen and the temperature were critical parameters for controlling tar concentrations [15]. J. Ahrenfeldt et al., 2013 emphasized that high temperature between 800-1050°C and excess air ratios

between 0-0.7 contribute positively to the direct tar destruction in the producer gas of wood pellets pyrolysis [34].

In addition to partial oxidation, steam reforming provides additional advantages not only for tar removal, but also in terms of ensuring a hydrogen-rich content in the end-products. Hydrogen production from steam reforming process have been paying interest in recent studies to apply for transportation and will promote to be a fundamental raw material/feedstock in many fields such as petroleum, chemical engineering, chemical fertilizer and metallurgical industries [37–40]. Wang et al., 2009 reported that when steam was supplied into the two-stage reformer, the tar residual rate in reformed gases decreased, in contrat, increased the hydrogen yields when increasing steam ratio (H_2O/C, 0-1.0) [41].

1.5. Numerical simulation as detailed chemical kinetic model

Regarding to the process for non-catalytic vapor-phase of tar reforming is extremely complex with ten to thousands reactions (Fig. 2). Thus a kinetic model would be useful for understanding those reactions. Kinetic model is a key approach for developing the technology to reduce tars and is critically important for the design and efficient operation of biomass-based thermochemical conversion systems. Traditional lumping models have been widely used in studies of biomass thermal chemical conversion (Table 1). However, in the lumping approach, tars are grouped as one or more different lumps in addition with kinetic parameters are determined by numerical fitting [42–46]. Therefore, this practical but simplified model is limited with respect to predicting the product gas composition at the molecular level.

To overcome the disadvantages of the lumping approach, Ranzi et al. used lumping

approach for woody biomass and developed the detailed chemical kinetic model (DCKM) to study secondary vapor-phase reactions which the DCKM consists of 2808 reactions and 138 species. The DCKM comprises thousands of elementary reactions of stable species as well as intermediates (including radical species) for vapor phase reaction [47–50]. DCKM has an advantage to understand both the conversion of feedstock and formation of products [48–52]. With a DCKM, the concentration of each individual molecules in the gas phase can be directly used as input information without lumping chemical species. Also, the kinetic parameters (frequency factor and activation energy) of individual elementary reactions are provided based on experimental studies and theory. Norinaga et al. extended and developed a DCKM that incorporates more than 8000 elementary reaction steps and more than 500 chemical species to predict the vapor-phase cracking of nascent volatiles generated from the fast pyrolysis of cellulose [49,50] and coffee extraction residue [48]. Table 1 summarized previous studies on the biomass vapor-phase reforming with both lumping approach and DCKM.

1.6. Scope of the thesis

Thermochemical conversion of biomass requires tar removal technology in order to achieve the successful thermochemical applications. Non-catalytic vapor-phase reforming of nascent volatiles derived from biomass primary pyrolysis is promising method to reduce/control tar during biomass pyrolysis/gasification. However, non-catalytic vapor-phase reforming is a complex process that likely consisting of uncountable chemical reactions (Fig. 1.2). To provide deeper understanding of those complex reactions, it is crucial to achieve extensive tar formation and consumption as the molecular level.

Although the kinetic modeling of tar has already reported from many researchers [35,47,53,54], to date, there are no study examining tar reforming behaviors in the vapor-phase in the molecular level. Hence a numerical simulation based on detailed chemical kinetic model (DCKM) for tar reforming is chosen in this work to simulate the vapor-phase reforming of nascent volatiles derived from biomass fast pyrolysis, which have great advantages in the deeper understanding of tar formation/reduction during biomass thermochemical conversion technology.

The purpose of thesis is to simulate the non-catalytic vapor-phase reforming (partial oxidation and steam reforming) of nascent volatiles derived from biomass fast pyrolysis by using DCKM to provide a deeper understanding of tar formations as molecular level.

The thesis consists of five chapters, each chapters are briefly summarized as follows:

Chapter 1: General introduction

First chapter gives general introduction of this study. To sum up the background of biomass as an alternative energy resource, thermochemical conversion technology for biomass utilization, tar problem in biomass thermochemical conversion process, tar removal/control technologies, and numerical simulation to provide deeper understanding of tar decomposition in non-catalytic vapor-phase reforming technology. Indeed, this chapter systematically explain the challenge and purpose of this work.

Chapter 2: Kinetic Modeling of Non-Catalytic Partial Oxidation of Nascent Volatiles Derived from Fast Pyrolysis of Woody Biomass with Detailed Chemistry

This chapter, a DCKM consisting of more than 8000 elementary reaction steps and

more than 500 chemical species was applied with plug flow reactor model and a developed global reaction to simulate the partial oxidation of nascent volatiles (NV) in a two-stage reactor. The first stage was designed for fast biomass pyrolysis and the second effected the partial oxidation of the NV derived from cedar sawdust fast pyrolysis. The computations were performed for temperatures of 700 and 800°C, and at O/C = 0 as well as O/C from 0.1 to 1.1 with constant intervals of 0.2. Then the DCKM was critically evaluated by comparing the predictions of major and minor products (typically found in the refractory post-gasification tar) with the experimental results obtained from gas phase partial oxidation of nascent volatiles in a tubular and vertical two-stage reactor (TSR) [15].

Chapter 3: Numerical study on steam reforming of biomass tar with detailed chemical kinetic model

In chapter 3, the detailed chemical kinetic model (DCLM) was used to simulate steam reforming of biomass tar generated from fast pyrolysis of cedar wood chips. The computation was performed in the plug flow reactor model couple with DCKM and global reaction to simulate pyrolysis at 750°C and reforming of nascent volatiles (NV) at 900°C. Global reactions accounting for soot steam reforming was tested to improve the model capabilities. Thus major and minor products from the predictions of steam reforming of the NV at 900^{o}C with H_2O/C = 0, 0.5, and 1.0 and partial oxidation of the NV at 900^{o}C with O/C = 0, 0.15, and 0.3 were investigated. Comparisons of the computational predictions and experimentally observed trends in two-stage gasifier [41] were also carried for critical evaluation of the DCKM.

Chapter 4: Predictive capability of an existing detailed chemical kinetic model for non-catalytic vapor-phase reforming of nascent volatiles derived from various woody biomass fast pyrolysis

Chapter 4 demonstrats the predictive capability of an existing detailed chemical kinetic model (DCKM) by applying the DCKM to simulate vapor-phase reforming of nascent volatiles (NV) derived from different biomasses. This study had concentrated on the partial oxidation conditions of the NV derived from empty fruit bunches (EFB) and bagasse (BG), to emphasis the comprehensive predictive capability of the DCKM. The partial oxidation of the NV derived from EFB fast pyrolysis was numerically simulated for temperatures of 700°C with O_2/C = 1.23 mol/mol. In addition, the partial oxidation of the NV derived from BG fast pyrolysis was numerically simulated for various reforming temperatures varying at 700, 800, and 900°C with O_2/C = 0.08 mol/mol. The numerical simulation performed in the batch reactor model with the DCKM and global reaction for the missing products in the NV. Consequently the computational results were compared with experimental results obtained in the second stage of the two-stage reactor for partial oxidation of NV derived from EFB and BG, separately. Further study are encoruaged to establish more sophisticated approach to approximate the missing products for both experimentally (to identify the species) and numerically (to provide the appropriate kinetic parameters).

Chapter 5: General conclusions

The final chapter, the results of each chapters including in this thesis are summarized.

References

[1] A. Pandey, T. Bhaskar, M. Stöcker, R.K. Sukumaran, Recent Advances in Thermo-Chemical Conversion of Biomass, 2015.

[2] P. McKendry, Energy production from biomass (part 1): overview of biomass, Bioresour. Technol. 83 (2002) 37–46.

[3] M. Verma, S. Godbout, S.K. Brar, O. Solomatnikova, S.P. Lemay, J.P. Larouche, Biofuels production from biomass by thermochemical conversion technologies, Int. J. Chem. Eng. 2012 (2012).

[4] A. Yerramili, Francis Tuluri, Energy Resources Utilization and Technologies, 2012.

[5] J. Dewulf, Herman Van Langenhove, Renewables-Based Technology Sustainability Assessment, WILEY Seri, 2006.

[6] A. V Bridgwater, Review of fast pyrolysis of biomass and product upgrading, Biomass and Bioenergy. 38 (2012) 68–94.

[7] G. Lorenzini, C. Biserni, G. Flacco, Solar Thermal and Biomass Energy, WIT Press, 2010.

[8] E. Dahlquist, Technologies for Converting Biomass to Useful Energy Series: Sustainable Energy Developments 4 Erik Dahlquist, 2013.

[9] M.D. Brown, E.G. Baker, L.K. Mudge, Environmental design considerations for thermochemical biomass energy, Biomass. 11 (1986) 255–270.

[10] D.C. Dayton, B.M. Jenkins, S.Q. Turn, R.R. Bakker, R.B. Williams, D. Belle-Oudry, et al., Release of Inorganic Constituents from Leached Biomass during Thermal Conversion, Energy & Fuels. 13 (1999) 860–870.

[11] A.A. Khan, W. de Jong, P.J. Jansens, H. Spliethoff, Biomass combustion in fluidized bed boilers: Potential problems and remedies, Fuel Process. Technol. 90 (2009) 21–50.

[12] P. McKendry, Energy production from biomass (part 2): conversion technologies, Bioresour. Technol. 83 (2002) 47–54.

[13] M. Asadullah, Biomass gasification gas cleaning for downstream applications: A comparative critical review, Renew. Sustain. Energy Rev. 40 (2014) 118–132.

[14] I. De Bari, D. Barisano, M. Cardinale, D. Matera, F. Nanna, D. Viggiano, Air Gasification of Biomass in a Downdraft Fixed Bed: A Comparative Study of the Inorganic and Organic Products Distribution, Energy & Fuels. 14 (2000) 889–898.

[15] S. Hosokai, K. Kishimoto, K. Norinaga, C.-Z. Li, J. Hayashi, Characteristics of Gas-Phase Partial Oxidation of Nascent Tar from the Rapid Pyrolysis of Cedar Sawdust at 700−800 °C, Energy & Fuels. 24 (2010) 2900–2909.

[16] X.T. Li, J.R. Grace, C.J. Lim, a. P. Watkinson, H.P. Chen, J.R. Kim, Biomass gasification in a circulating fluidized bed, Biomass and Bioenergy. 26 (2004) 171–193.

[17] T. Okuno, N. Sonoyama, J. Hayashi, C.-Z. Li, C. Sathe, T. Chiba, Primary Release of Alkali and Alkaline Earth Metallic Species during the Pyrolysis of Pulverized Biomass, Energy & Fuels. 19 (2005) 2164–2171.

[18] K. Salo, W. Mojtahedi, Fate of alkali and trace metals in biomass gasification, Biomass and Bioenergy. 15 (1998) 263–267.

[19] X. Wei, U. Schnell, K.R.G. Hein, Behaviour of gaseous chlorine and alkali metals during biomass thermal utilisation, Fuel. 84 (2005) 841–848.

[20] H. Knoef, ed., Handbook Biomass Gasification.pdf, 2005.

[21] P. McKendry, Energy production from biomass (part 3): gasification technologies, Bioresour. Technol. 83 (2002) 55–63.

[22] K. Maniatis, A.A.C.M. Beenackers, Introduction: tar protocols., IEA gasification tasks, Biomass and Bioenergy. 18 (2000) 1–4.

[23] C. Li, K. Suzuki, Tar property, analysis, reforming mechanism and model for biomass gasification—An overview, Renew. Sustain. Energy Rev. 13 (2009) 594–604.

[24] J. Han, H. Kim, The reduction and control technology of tar during biomass gasification/pyrolysis: An overview, Renew. Sustain. Energy Rev. 12 (2008) 397–416.

[25] T.A. Milne, R.J. Evans, Biomass Gasifier "Tars": Their Nature, Formation, and Conversion, Fuel Energy Abstr. 39 (1998) 283.

[26] L. Devi, K.J. Ptasinski, F.J.J.. Janssen, A review of the primary measures for tar elimination in biomass gasification processes, Biomass and Bioenergy. 24 (2003) 125–140.

[27] R. Trane, S. Dahl, M.S. Skjøth-Rasmussen, A.D. Jensen, Catalytic steam reforming of bio-oil, Int. J. Hydrogen Energy. 37 (2012) 6447–6472.

[28] S. Schmidt, S. Giesa, A. Drochner, H. Vogel, Catalytic tar removal from bio syngas—Catalyst development and kinetic studies, Catal. Today. 175 (2011) 442–449.

[29] R.N. Singh, S.P. Singh, J.B. Balwanshi, Tar removal from Producer Gas : A Review, 3 (2014) 16–22.

[30] J. HEPOLA, P. SIMELL, Sulphur poisoning of nickel-based hot gas cleaning catalysts in synthetic gasification gasII. Chemisorption of hydrogen sulphide, Appl. Catal. B Environ. 14 (1997) 305–321.

[31] K. Tomishige, T. Miyazawa, T. Kimura, K. Kunimori, N. Koizumi, M. Yamada, Resistance to sulfur poisoning of hot gas cleaning catalysts for the removal of tar from the pyrolysis of cedar wood, Appl. Catal. B Environ. 60 (2005) 299–307.

[32] Z. Abu El-Rub, E.A. Bramer, G. Brem, Review of Catalysts for Tar Elimination in Biomass Gasification Processes, Ind. Eng. Chem. Res. 43 (2004) 6911–6919.

[33] P.A. Jenssen, E. Larsen, K.H. Jørgensen, Tar reduction by partial oxidation, in: Proceedings of the 9th European bioenergy conference (1996), pp. 1371–1375, 1996: p. 1996.

[34] J. Ahrenfeldt, H. Egsgaard, W. Stelte, T. Thomsen, U.B. Henriksen, The influence of partial oxidation mechanisms on tar destruction in TwoStage biomass gasification, Fuel. 112 (2013) 662–680.

[35] M.P. Houben, H.C.D. Lange, A.A. V. Steenhoven, Tar reduction through partial combustion of fuel gas, Fuel. 84 (2005) 817–824.

[36] Y. Su, Y. Luo, Y. Chen, W. Wu, Y. Zhang, Experimental and numerical investigation of tar destruction under partial oxidation environment, Fuel Process. Technol. 92 (2011) 1513–1524.

[37] T. Chen, C. Wu, R. Liu, Steam reforming of bio-oil from rice husks fast pyrolysis for hydrogen production., Bioresour. Technol. 102 (2011) 9236–40.

[38] J. Remón, F. Broust, J. Valette, Y. Chhiti, I. Alava, A.R. Fernandez-Akarregi, et al., Production of a hydrogen-rich gas from fast pyrolysis bio-oils: Comparison between homogeneous and catalytic steam reforming routes, Int. J. Hydrogen Energy. 39 (2014) 171–182.

[39] D. Li, C. Ishikawa, M. Koike, L. Wang, Y. Nakagawa, K. Tomishige, Production of renewable hydrogen by steam reforming of tar from biomass pyrolysis over supported Co catalysts, Int. J. Hydrogen Energy. 38 (2013) 3572–3581.

[40] D. Rennard, R. French, S. Czernik, T. Josephson, L. Schmidt, Production of synthesis gas by partial oxidation and steam reforming of biomass pyrolysis oils, Int. J. Hydrogen Energy. 35 (2010) 4048–4059.

[41] Y. Wang, T. Namioka, K. Yoshikawa, Effects of the reforming reagents and fuel species on tar reforming reaction., Bioresour. Technol. 100 (2009) 6610–4.

[42] J. Corella, M.A. Caballero, M.-P. Aznar, C. Brage, Two Advanced Models for the Kinetics of the Variation of the Tar Composition in Its Catalytic Elimination in Biomass Gasification, Ind. Eng. Chem. Res. 42 (2003) 3001–3011.

[43] E. Ranzi, A. Cuoci, T. Faravelli, A. Frassoldati, G. Migliavacca, S. Pierucci, et al., Chemical Kinetics of Biomass Pyrolysis, Energy & Fuels. 22 (2008) 4292–4300.

[44] C. Dupont, L. Chen, J. Cances, J.-M. Commandre, A. Cuoci, S. Pierucci, et al., Biomass pyrolysis: Kinetic modelling and experimental validation under high temperature and flash heating rate conditions, J. Anal. Appl. Pyrolysis. 85 (2009) 260–267.

[45] E.-J. Shin, M.R. Nimlos, R.J. Evans, Kinetic analysis of the gas-phase pyrolysis of carbohydrates, Fuel. 80 (2001) 1697–1709.

[46] P. Morf, P. Hasler, T. Nussbaumer, Mechanisms and kinetics of homogeneous secondary reactions of tar from continuous pyrolysis of wood chips, Fuel. 81 (2002) 843–853.

[47] M. Nowakowska, O. Herbinet, A. Dufour, P.-A. Glaude, Detailed kinetic study of anisole pyrolysis and oxidation to understand tar formation during biomass combustion and gasification, Combust. Flame. 161 (2014) 1474–1488.

[48] T. Shoji, K. Norinaga, O. Masek, J. Hayashi, Numerical Simulation of Secondary Gas Phase Reactions of Coffee Grounds with a Detailed Chemical Kinetic Model, J. Japan Inst. Energy. Vol. 89 (2010) 955–961.

[49] K. Norinaga, T. Shoji, S. Kudo, J. Hayashi, Detailed chemical kinetic modelling of vapour-phase cracking of multi-component molecular mixtures derived from the fast pyrolysis of cellulose, Fuel. 103 (2013) 141–150.

[50] K. Norinaga, H. Yang, R. Tanaka, S. Appari, K. Iwanaga, Y. Takashima, et al., A mechanistic study on the reaction pathways leading to benzene and naphthalene in cellulose vapor phase cracking, Biomass and Bioenergy. 69 (2014) 144–154.

[51] K. Norinaga, H. Yatabe, M. Matsuoka, J. Hayashi, Application of an Existing Detailed Chemical Kinetic Model to a Practical System of Hot Coke Oven Gas Reforming by Noncatalytic Partial Oxidation, Ind. Eng. Chem. Res. 49 (2010) 10565–10571.

[52] N. Thimthong, S. Appari, R. Tanaka, K. Iwanaga, S. Kudo, J. Hayashi, et al., Kinetic modeling of non-catalytic partial oxidation of nascent volatiles derived from fast pyrolysis of woody biomass with detailed chemistry, Fuel Process. Technol. (2015).

[53] J. Corella, J.M. Toledo, M.-P. Aznar, Improving the Modeling of the Kinetics of the Catalytic Tar Elimination in Biomass Gasification, Ind. Eng. Chem. Res. 41 (2002) 3351–3356.

[54] L. Devi, K.J. Ptasinski, F.J.J.G. Janssen, Decomposition of Naphthalene as a Biomass Tar over Pretreated Olivine: Effect of Gas Composition, Kinetic Approach, and Reaction Scheme, Ind. Eng. Chem. Res. 44 (2005) 9096–9104.

[55] A.L. Brown, D.C. Dayton, J.W. Daily, A study of cellulose pyrolysis chemistry and global kinetics at high heating rates, Energy and Fuels. 15 (2001) 1286–1294.

Table 1 Summary of studies on the biomass pyrolysis and its vapor-phase reforming with lumping approach and DCKM

Researcher, year	Title	Kinetic model	Number of species (lumps)/ Number of reactions	Notes	Ref. no.
A. Brown, 2001	A Study of Cellulose Pyrolysis Chemistry and Global Kinetics at High Heating Rates	Lumping model for cellulose pyrolysis	7/ 7	Temperature effect on decomposition characteristics of cellulose was reproduced	[55]
P. Morf, 2002	Mechanisms and kinetics of homogeneous secondary reactions of tar from continuous pyrolysis of wood chips	Lumping model for conversion of tar from wood chip pyrolysis	5/ 4	Decomposition characteristics of gravimetric tar and formation of naphthalene were reproduced by lumping kinetic model	[46]
J. Corella, 2003	Two Advanced Models for the Kinetics of the Variation of the Tar Composition in Its Catalytic Elimination in Biomass Gasification	Lumping model for catalytic decomposition of tar from biomass pyrolysis	6/ 11	Decomposition characteristics of tar from biomass characteristics were reproduced by lumping kinetic model	[42]
E. Ranzi, 2008	Chemical Kinetics of Biomass Pyrolysis	Lumping model of woody biomass and detailed chemical kinetic model of secondary vapor phase reactions	138/ 2808	Formations characteristics of char and light hydrocarbons were reproduced	[43]
K. Norinaga, 2013	Detailed chemical kinetic modelling of vapor-phase cracking of multi-component molecular mixtures derived from the fast pyrolysis of cellulose	DCKM for vapor-phase cracking of cellulose	more than 500/ 8000	Formation characteristics of products from hydrogen to toluene during vapor-phase cracking of cellulose pyrolysis gas were reproduced	[49]
M. Nowakowska, 2014	Detailed kinetic study of anisole pyrolysis and oxidation to understand tar formation during biomass combustion and gasification	DCKM for vapor-phase cracking and combustion of anisole	303/ 1922	Temperature effect on formation characteristics of products from hydrogen to acenaphthylene during anisole pyrolysis and oxidation were reproduced	[47]

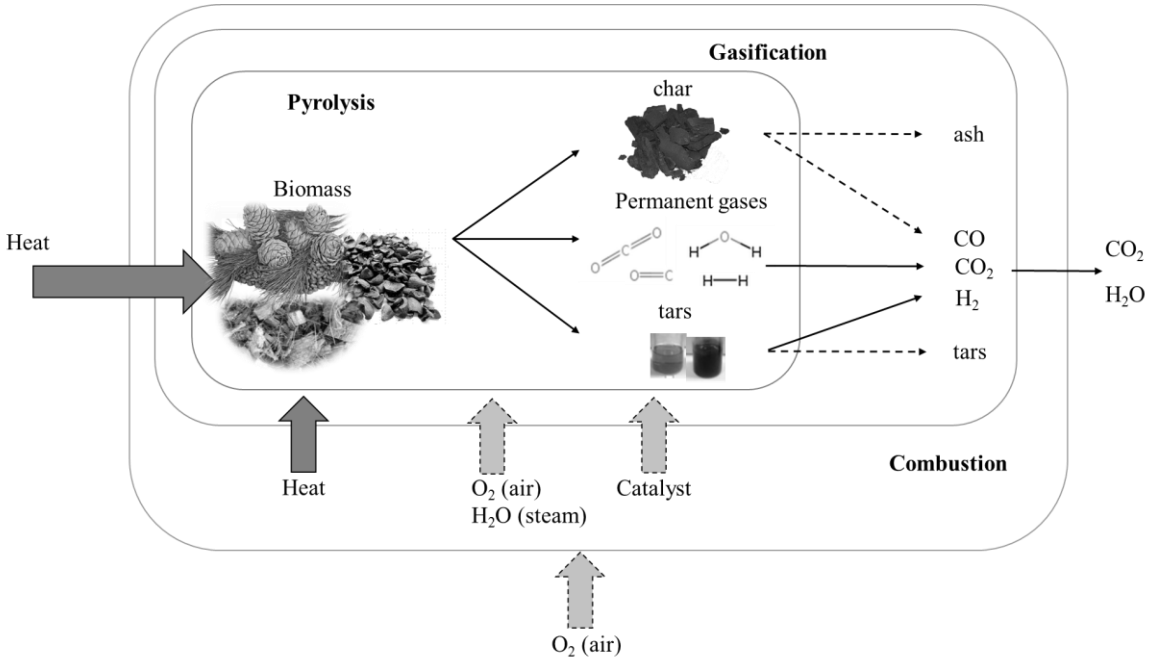

Fig. 1 Schematic presentation of gasification as one of the thermochemical conversion processes [20]

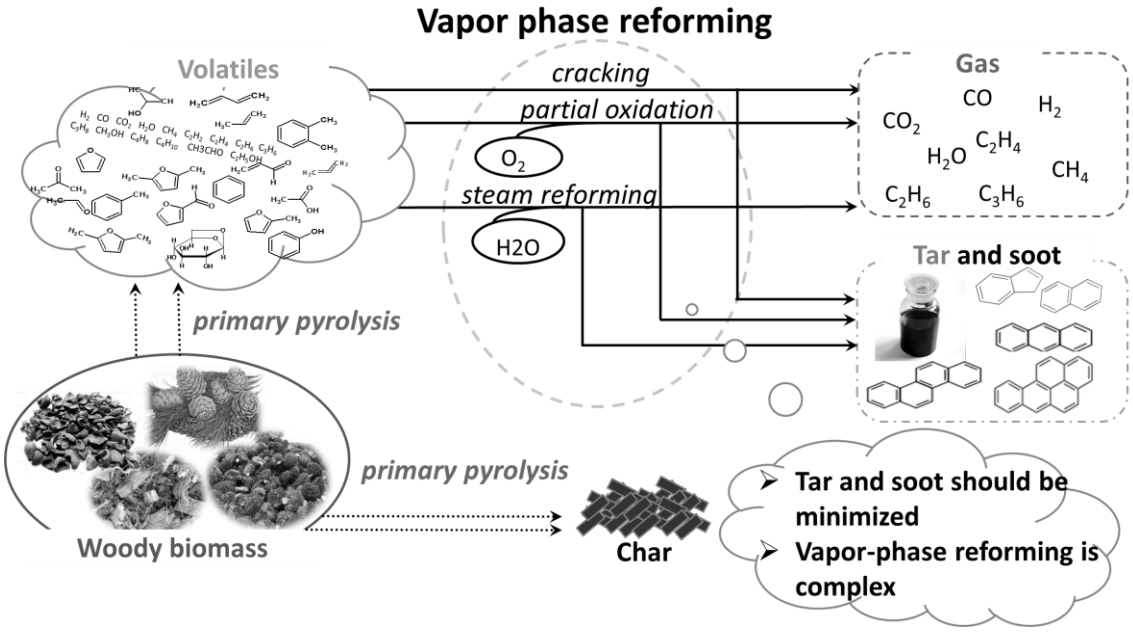

Fig. 2 Schematic diagram of vapor-phase reforming of nascent volatiles derived from biomass fast pyrolysis

Chapter 2

Kinetic Modeling of Non-Catalytic Partial Oxidation of Nascent Volatiles Derived from Fast Pyrolysis of Woody Biomass with Detailed Chemistry

2.1. Introduction

Biomass is a promising source of renewable energy, and effective and efficient technologies are needed to implement its practical application. As a feedstock comprising both organic and inorganic elements, biomass exhibits a variety of morphologies and physical characteristics. The thermal conversion of biomass through direct combustion suffers from problems of corrosion/erosion and the accumulation of inorganic solids caused by the alkali-containing species in the biomass. Biomass gasification by thermal decomposition followed by the partial combustion of the producer gas is a viable option to not only remove the problems encountered in direct combustion but also to provide cleaner fuel gases suitable for use in gas turbines and engines [1–10]. Biomass gasification products mainly consist of syngas, light hydrocarbons, and trace amounts of H_2S, HCl, NH_3, tar, and solid particles [10,11].

Among the products obtained from biomass gasification, tar is considered to be problematic, as even small amounts can significantly damage downstream equipment and deteriorate gasification efficiency. Therefore, tar control or removal measures are essential for the successful implementation of gasification technology, in terms of producing clean fuel gas as well as easy control and continuous operation [12,13]. Several methods have been reported [14] to remove tar both physically [15,16] and chemically

[4,16–21]. Non-catalytic partial oxidation for vapor-phase reforming is a promising technique that can reduce the amount of tar [4,21–24]. Su et al. [21], who found that oxygen significantly impacts the conversion of tar and non-condensable gases, developed a flow reactor to predict tar destruction under partial oxidation conditions. Indeed, Hosokai et al. investigated the gas-phase partial oxidation of nascent volatiles from the rapid pyrolysis of cedar sawdust in two-stage reactor and claimed that the amount of O_2 and the temperature were critical parameters for controlling tar concentrations [4].

A deeper understanding of tar formation and consumption behaviors during the vapor phase reactions of biomass nascent volatiles—which consists of hundreds to tens of thousands of chemical reactions—is a key approach for developing the technology to reduce tars. A kinetic model would be useful for understanding those reactions, but limited studies have been reported. Traditional lumping models have been widely used in studies of biomass thermal chemical conversion. However, in the lumping approach, tars are grouped as one or more different lumps and kinetic parameters are determined by numerical fitting [25–29]. Therefore, this practical but simplified model is limited with respect to predicting the product gas composition at the molecular level.

Detailed chemical kinetic models (DCKM) which comprise thousands of elementary reactions of stable species as well as intermediates (including radical species) for vapor phase reaction of biomass related material have been developed to overcome the disadvantages of the lumping approach [30–33]. With a DCKM, the concentration of each individual molecules in the gas phase can be directly used as input information without lumping chemical species. Also, the kinetic parameters (frequency factor and activation energy) of individual elementary reactions are provided based on experimental studies and theory. Norinaga et al. developed a DCKM that incorporates more than 8000

elementary reaction steps and more than 500 chemical species which has the potential to predict the vapor-phase cracking of nascent volatiles generated from the fast pyrolysis of cellulose [32,33].

With regard to the kinetic modelling of partial oxidation, no studies have been reported that analyze the partial oxidation of volatiles derived from the primary pyrolysis of biomass by using the DCKM. This is the first attempt to use the DCKM to predict the partial oxidation of nascent volatiles derived from woody biomass (cedar sawdust) fast pyrolysis. The DCKM [32] is used to describe the volatiles' partial oxidation. The initial molecular compositions for DCKM were derived experimentally from the primary pyrolysis of cedar sawdust. There are several missing products which are difficult to identify experimentally that are considered in the simulation by introducing global reactions. The model was critically evaluated by comparing the predicted and experimental results from the secondary vapor-phase partial oxidation of volatile components from cedar sawdust fast pyrolysis [4].

2.2. Methods

2.2.1. Experimental

2.2.1.1. Biomass sample

Japanese cedar sawdust with particle sizes ranging from 350 to 590 μm was dried and then used as the biomass feedstock. Carbon and hydrogen mass fractions were 50.2 and 6.3% on a dry sample basis, respectively.

2.2.1.2. Gas phase partial oxidation of nascent volatiles

The reported experimental data for the partial oxidation (POx) of nascent volatiles

(NV) [4] were used for the critical evaluation of the kinetic model. A tubular and vertical two-stage reactor (TSR) was employed; the first and second stages were designed for fast pyrolysis of the biomass sample and the thermal cracking/POx of the NV, respectively. The sample was fed continuously into the first stage of the TSR at a rate of 0.09–0.21 g/min for 15 min. The temperature of the first stage was held at 700 or 800°C, at which the sawdust was rapidly pyrolyzed to char and volatiles. The char was retained on the quartz frit at the reactor bottom, while the volatiles were swept through the frit under a forced flow of primary nitrogen. The volatiles were then introduced into the second stage of the tubular reactor after dilution with secondary nitrogen or an oxygen/nitrogen mixture with a flow rate of either 1.6 L STP/min and 700°C or 1.4 L STP/min and 800°C. Both the flow rates were fixed so that the residence time of the volatiles in the isothermal zone of the second stage was 3.0 s. The O/C ratio was used as the parameter to describe the composition of the mixture entering the second stage of the TSR; it is defined as the ratio of the number of oxygen atoms in the supplied O_2 gas to the total number of carbon atoms in the NV, and varies between 0 and 1.1. The temperature of the second stage of the tubular reactor was the same as that of the first. All the products passing through the reactor outlet were recovered by a mist filter, two cold traps, and a gas bag, and analyzed off-line. Detailed descriptions of the POx experimental set-up as well as the product analysis are given elsewhere [4].

2.2.1.3. Pyrolysis gas chromatography

Analytical pyrolysis experiments were conducted with an originally designed setup [32] to approximate the molecular composition of the NV, and to monitor the secondary gas-phase cracking of the NV. A U-shaped two-stage tubular reactor (UTSR), divided into two zones by a quartz wool filter (one side for the fast pyrolysis of cedar sawdust and the

other for the cracking of the nascent volatiles), was used as a pyrolyzer. Approximately 1.0 mg of the sample was wrapped with a sheet of stainless wire mesh (SUS316, 15 mm × 15 mm) with a mesh opening of 45 μm and dried under vacuum at room temperature overnight. The wrapped sample was weighed immediately after drying to determine the exact dry mass of the sample, which was subsequently fixed at the upper part of the UTSR. The UTSR was connected to the streamline of a gas chromatograph (GC). After stabilizing the heated section of the UTSR at the desired temperature (700 or 800°C), the sample was dropped into the bottom of the first zone where it underwent fast pyrolysis. The nascent volatiles formed by pyrolysis were swept into the second zone. The residence times of the volatiles in the second zone were varied from 0.2 to 4.1 s by adjusting the volume of the second reactor. The detailed experimental procedure and product analysis are given elsewhere [32].

2.2.2. Modeling approach

2.2.2.1. Plug-flow reactor model for TSR

The POx of the NV in the second stage of the TSR (length = 0.7 m) shown in Fig. 1 was numerically simulated with the PLUG code in the DETCHEM program package (DETCHEM^{PLUG}) [34]. DETCHEM^{PLUG} is designed for the modelling of a non-dispersive one-dimensional flow of a chemically reacting ideal gas mixture under steady-state conditions. The reaction mechanism and boundary conditions (such as the composition and velocity of the feed gas at the inlet of the second stage, the pressure, and the temperature profile along the flow direction) are required for the computations and are summarized in Table 1. The computations were performed for temperatures of 700 and 800°C, and at O/C = 0 as well as O/C from 0.1 to 1.1 with constant intervals of 0.2. A

detailed description of the plug-flow computations can also be found elsewhere [35].

2.2.2.2. Batch reactor model for UTSR

The vapor-phase cracking of the NV in the UTSR was numerically simulated with the BATCH code in the DETCHEM program package (DETCHEM^{BATCH}) [34]. DETCHEM^{BATCH} was designed for the computational analysis of time-dependent homogeneous reaction systems. Calculations were performed under isobaric and isothermal conditions. The composition of the NV, temperature, and pressure are the boundary conditions required for the computations and are also summarized in Table 1. A detailed description of the batch reactor computations can be found elsewhere [34].

2.2.2.3. Reaction mechanism

A detailed chemical kinetic model (DCKM) for predicting biomass secondary gas-phase reactions was developed. The reaction mechanisms and thermodynamic data are provided as Supplemental Information. The DCKM consists of 548 species and 8159 elementary reaction steps, and the model has been critically evaluated for the secondary vapor-phase reactions of cellulose [32,33] and coffee extraction residues [31]. A global reaction was added to the DCKM to account for the decomposition of the gas-chromatographically inseparable components included in the NV. The rate constants of the global reactions at both 700 and 800°C were estimated empirically.

2.3. Results and discussion

2.3.1. Approximation of the molecular composition of NV derived from cedar sawdust fast pyrolysis

The molecular composition of the NV is one of the required inputs for conducting

numerical simulations with the DCKM. Thus, analytical pyrolysis experiments using a UTSR that was directly connected to GC instruments were performed to provide experimental data on the product distributions in the fast pyrolysis of the biomass sample.

Table 2 lists the yields of the products at pyrolysis temperatures of 700 and 800°C and a vapor phase residence time of 0.2 s. Exhaustive analysis with three different GC instrumental configurations enabled the identification and quantification of 52 pyrolysates. The total mass fractional amounts of the identified products including char accounted for 77 and 89% of the sample fed at 700 and 800°C, respectively; the lost 23 and 11% mass fractions are unexplained at this time. The missing materials likely correspond to products which condense at the inner wall of the line between the UTSR and the GC and/or are not separated chromatographically due to their high molecular mass. Based on the elemental balances among the feed and products, the C:H:O atomic ratios were estimated to be 2:3:1 and 6:5:1 for the missing products at 700 and 800°C, respectively.

2.3.2. Global reactions for reactions of missing components included in NV

The DCKM employed here showed an acceptably fine capability for predicting the concentration profiles of major products such as hydrogen, carbon monoxide, carbon dioxide, and methane in the vapor-phase cracking of cellulose at 700 and 800^{o}C [32]. The molecular composition of the volatiles derived from the fast pyrolysis of cellulose fine particles could be almost perfectly defined experimentally, since most of the products were gas-chromatographically separable. This suggests that, as long as the molecular composition of the pyrolysis products are properly defined, the DCKM can provide fair predictions of the major product formation profiles in the subsequent vapor-phase

reactions. Unfortunately, however, some of the products included in the NV could not be identified and were missing.

To understand the significance of the missing products on the product distribution in the subsequent vapor-phase reactions, further analytical pyrolysis experiments were performed that varied the vapor-phase residence time of the NV. The pyrolysis experiments were numerically simulated by the DCKM with the batch-reactor model. The solid lines in Fig. 2 shows the computation results with neglecting the reactions of the missing products (K = 0). When the missing products were neglected by substitution with an inert gas such as nitrogen in the composition of the NV, the computational results for hydrogen, carbon monoxide, and methane were under-predicted compared with the UTSR experiment, whereas carbon dioxide was accurately predicted. The composition of the carbon dioxide is more or less constant at entire range of the residence time as observed from the pyrolysis experiments with the USTR. Due to this reason, carbon dioxide is not considered in the global reaction, in fact, this composition is well predicted alone with the DCKM.

The under-predictions found for the yields of hydrogen, carbon monoxide, and methane likely originate from the lack of information about the reactions of the missing products included in the NV. The under-predictions of the computational yields versus the experimental ones could potentially be minimized by assuming in the simulation that the missing products undergo chemical reactions.

To account for the formation of hydrogen, carbon monoxide, and methane, the global reaction for the missing products at 700°C was formulated as;

$C_8H_{12}O_4 \rightarrow 2\ H_2 + 1.5\ CH_4 + 4\ CO + 0.5\ C_2H_4 + \text{Soot}\ (C_2)$.

The solid lines in Fig. 2 (K = 0.3) are computation results obtained by the DCKM combined with the global reaction. The kinetic constant k_{G700} of the global reaction was optimized to be 0.3 s^{-1}, which minimized the gap between the computational and experimental results.

Without a global reaction at 800°C, the yields of hydrogen, carbon monoxide, and methane were under-predicted. Similarly, the global reaction for the missing products at 800°C was formulated as

$C_6H_5O \rightarrow CO + CH_4 + Soot\ (C_4H_1)$,

where the kinetic constant was optimized as k_{G800} = 0.8 s^{-1} (Fig. 3). The global reaction along with the DCKM at 800°C affected the predictions of major products composition slightly. This may be due to the small amount of missing products (11%) in the NV at this temperature.

2.3.3. Numerical simulation of the POx of the NV in the second stage of the TSR

A plug-flow reactor model coupled with both the DCKM and the global reaction was used to simulate the POx of the NV derived from cedar sawdust at 700 and 800°C. The distribution of the species concentrations along the axial length of the second stage of the TSR from the plug-flow simulation is shown in Fig. 4 (O/C ratio 0.5 and 700°C). Oxygen is completely consumed in the initial part of the reactor (~0.015 m), and major changes are observed between the reactor inlet and the next 0.1 m length of the reactor. The product distributions along the reactor reveal increasing yields of carbon monoxide, carbon dioxide, and water. Decreases in hydrogen, methane, and C_2–C_4 hydrocarbon yields along the TSR length are observed. Also, the yields of mono-aromatic compounds

decrease in the presence of oxygen, whereas the yields for di-aromatic compounds increase slowly along the length of the reactor.

2.3.4. Critical evaluation of the kinetic model

The numerical results of the species concentrations at the reactor exit as a function of O/C ratio were compared with the experimentally obtained results from the gas-phase POx of NV in the TSR. Figure 5 shows these comparisons for partial oxidation at 700^{o}C. The DCKM well predicts the vapor-phase POx of the NV at 700°C under varying O/C conditions. When the O/C ratio increases, hydrogen (Fig. 5 a) and methane (Fig. 5 d) decrease; these predictions are well correlated with the experimental data at different O/C ratios. The decreasing trend in hydrogen yield may be explained primarily by the abundant oxygen that is available for hydrogen oxidation. An increasing O/C ratio also affects the methane partial oxidation. The methane steam reforming reaction is enhanced by the formation of steam from hydrogen oxidation, which results in a decreased methane yield with increasing O/C ratio. The model also well predicts the experimental results for carbon monoxide (Fig. 5 b) and carbon dioxide (Fig. 5 c), which increase with increasing O/C ratio. The increasing trend in carbon dioxide yield is due to carbon monoxide oxidation and perhaps also from the water gas shift reaction. The carbon monoxide yield increases due to partial oxidation and the steam reforming reactions of methane and light hydrocarbons.

In addition to the major products, the DCKM results also capture the experimentally observed trends for the minor gas-phase hydrocarbons and aromatics. Although the partial oxidation products contain very low yields of C_2–C_4 hydrocarbons and aromatic compounds (< 3 mol-C/100-mol-C-fuel), these can nevertheless be used to validate the

DCKM in this work. The amounts of minor products such as ethylene, ethane, acetaldehyde, propylene, propane, C_4 hydrocarbons, benzene, and naphthalene could be predicted and validated by the experimental data. Discrepancies were observed between the simulations and experiments for ethylene (Fig 6 a), which is somewhat overestimated at low O/C ratios, and ethane (Fig 6 b), which is slightly underestimated at high O/C ratios. The decreasing trends of ethylene and ethane yields with increasing O/C ratio are mainly due to partial oxidation. The acetaldehyde yields are given in Fig. 6 c. Acetaldehyde is consumed with increasing O/C ratio, and good agreement is observed with the experimental measurements. Fair agreement is observed for propylene (Fig. 6 d) and propane (Fig. 7 a); although there are small gaps between the predictions and experimental measurements, the results show that propane and propylene are mainly consumed by oxygen atom addition reactions. The amounts of C_4 are also validated by the experimental measurements (Fig 7 b), and the predictions show fair reproduction of the experimental trends.

The yields of aromatic products, which are constituents of tar, are presented in Fig. 7. Calculated benzene (Fig. 7 c) yields at different O/C ratios reproduce the experimental results, although they were slightly over-predicted at lower O/C ratios and under-predicted at higher O/C ratios. These contradictory results might be related to the complexity of benzene formation, which involves many reactions [32]. The model predictions for naphthalene perfectly capture the experimental profiles (Fig. 7 d), suggesting that the major reactions leading to naphthalene are incorporated into the current kinetic model and that their rate parameters are reasonable. Overall, the numerical simulations with DCKM indicate decreasing yields of aromatic compounds with increasing O/C ratios, and reveal that these tar compounds can be effectively reduced in

the partial oxidation process.

The predictions of major and minor product yields suggested that the DCKM is fairly capable to predict the experimental trends. The major and minor product yields were under-predicted when only the DCKM was used. The model predictions are satisfactory when adding the global reaction along with the DCKM. This may be due to the missing products (high molecular mass compounds) were decomposed into the major products during the NV reforming.

Comparisons between the model predictions and experimental results from the gas-phase POx of NV in the TSR at 800^{o}C are presented in Fig. 8. The model can also reproduce the experimentally observed trends well showing that the DCKM can capture the experimentally observed trends for the effect of not only oxygen to fuel ratio but also the temperature on the product distributions in the POx of the NV from cedar sawdust. In this study, the DCKM predictive capabilities are exhaustively studied in regard with the both major and minor products. Fair agreements were obtained between the predictions and the experimental concentration profiles of the major products, as well as minor products such as benzene and naphthalene, which are important precursors/constituents of tar. This level of capabilities cannot be expected from the traditional lumping approach and strongly enhances the significance of this approach in modeling complex biomass thermo-chemistries.

2.4. Conclusions

The non-catalytic partial oxidation of gas mixtures from the fast pyrolysis of cedar sawdust was simulated with a DCKM. A global reaction was combined with the DCKM to represent the cracking of experimentally ill-defined constituents in the NV. The NV

were approximated by 52 chemical species. The resultant kinetic model, with 8159 reactions and 548 species, was further coupled with a plug-flow reactor model to reproduce the two-stage pyrolysis experiments. The predictions agreed well with the experimental concentration profiles of the major products, as well as minor products such as benzene and naphthalene, which are important constituents of tar. With almost no adjustable parameters in the kinetic model, such agreement are derived at molecular level.

References

[1] M.D. Brown, E.G. Baker, L.K. Mudge, Environmental design considerations for thermochemical biomass energy, Biomass. 11 (1986) 255–270.

[2] D.C. Dayton, B.M. Jenkins, S.Q. Turn, R.R. Bakker, R.B. Williams, D. Belle-Oudry, et al., Release of Inorganic Constituents from Leached Biomass during Thermal Conversion, Energy & Fuels. 13 (1999) 860–870.

[3] I. De Bari, D. Barisano, M. Cardinale, D. Matera, F. Nanna, D. Viggiano, Air Gasification of Biomass in a Downdraft Fixed Bed: A Comparative Study of the Inorganic and Organic Products Distribution, Energy & Fuels. 14 (2000) 889–898.

[4] S. Hosokai, K. Kishimoto, K. Norinaga, C.-Z. Li, J. Hayashi, Characteristics of Gas-Phase Partial Oxidation of Nascent Tar from the Rapid Pyrolysis of Cedar Sawdust at 700−800°C, Energy & Fuels. 24 (2010) 2900–2909.

[5] A.A. Khan, W. de Jong, P.J. Jansens, H. Spliethoff, Biomass combustion in fluidized bed boilers: Potential problems and remedies, Fuel Process. Technol. 90 (2009) 21–50.

[6] X.T. Li, J.R. Grace, C.J. Lim, a. P. Watkinson, H.P. Chen, J.R. Kim, Biomass gasification in a circulating fluidized bed, Biomass and Bioenergy. 26 (2004) 171–193.

[7] T. Okuno, N. Sonoyama, J. Hayashi, C.-Z. Li, C. Sathe, T. Chiba, Primary Release of Alkali and Alkaline Earth Metallic Species during the Pyrolysis of Pulverized Biomass, Energy & Fuels. 19 (2005) 2164–2171.

[8] K. Salo, W. Mojtahedi, Fate of alkali and trace metals in biomass gasification, Biomass and Bioenergy. 15 (1998) 263–267.

[9] X. Wei, U. Schnell, K.R.G. Hein, Behaviour of gaseous chlorine and alkali metals during biomass thermal utilisation, Fuel. 84 (2005) 841–848.

[10] H. Knoef, ed., Handbook Biomass Gasification. 2005.

[11] M. Asadullah, Biomass gasification gas cleaning for downstream applications: A comparative critical review, Renew. Sustain. Energy Rev. 40 (2014) 118–132.

[12] C. Li, K. Suzuki, Tar property, analysis, reforming mechanism and model for biomass gasification-An overview, Renew. Sustain. Energy Rev. 13 (2009) 594–604.

[13] P. McKendry, Energy production from biomass (part 3): gasification technologies, Bioresour. Technol. 83 (2002) 55–63.

[14] J. Han, H. Kim, The reduction and control technology of tar during biomass gasification/pyrolysis: An overview, Renew. Sustain. Energy Rev. 12 (2008) 397–416.

[15] A. Paethanom, S. Nakahara, M. Kobayashi, P. Prawisudha, K. Yoshikawa, Performance of tar removal by absorption and adsorption for biomass gasification, Fuel Process. Technol. 104 (2012) 144–154.

[16] Y. Wang, T. Namioka, K. Yoshikawa, Effects of the reforming reagents and fuel species on tar reforming reaction., Bioresour. Technol. 100 (2009) 6610–4.

[17] S. Schmidt, S. Giesa, A. Drochner, H. Vogel, Catalytic tar removal from bio syngas—Catalyst development and kinetic studies, Catal. Today. 175 (2011) 442–449.

[18] M.P. Aznar, M.A. Caballero, J. Gil, J.A. Martín, J. Corella, Commercial steam reforming catalysts to improve biomass gasification with steam-oxygen mixtures. 2. Catalytic tar removal, Ind. Eng. Chem. Res. 37 (1998) 2668–2680. http://www.scopus.com/inward/record.url?eid=2-s2.0-0032105553&partnerID=tZOtx3y1.

[19] J. Corella, A. Orío, J.-M. Toledo, Biomass Gasification with Air in a Fluidized Bed: Exhaustive Tar Elimination with Commercial Steam Reforming Catalysts, Energy & Fuels. 13 (1999) 702–709.

[20] L. Ma, J.F.M. Denayer, G. V. Baron, Improving catalytic hot gas cleaning in biomass gasification by oxygen addition, in: AIChE 100 - 2008 AIChE Annu. Meet. Conf. Proc., 2008. http://www.scopus.com/inward/record.url?eid=2-s2.0-79953828165&partnerID=tZOtx3y1.

[21] Y. Su, Y. Luo, Y. Chen, W. Wu, Y. Zhang, Experimental and numerical investigation of tar destruction under partial oxidation environment, Fuel Process. Technol. 92 (2011) 1513–1524.

[22] P.A. Jenssen, E. Larsen, K.H. Jørgensen, Tar reduction by partial oxidation, in: Proceedings of the 9th European bioenergy conference (1996), pp. 1371–1375, 1996: p. 1996.

[23] J. Ahrenfeldt, H. Egsgaard, W. Stelte, T. Thomsen, U.B. Henriksen, The influence of partial oxidation mechanisms on tar destruction in TwoStage biomass gasification, Fuel. 112 (2013) 662–680.

[24] M. Houben, H. Delange, A. Vansteenhoven, Tar reduction through partial combustion of fuel gas, Fuel. 84 (2005) 817–824.

[25] J. Corella, M.A. Caballero, M.-P. Aznar, C. Brage, Two Advanced Models for the Kinetics of the Variation of the Tar Composition in Its Catalytic Elimination in Biomass Gasification, Ind. Eng. Chem. Res. 42 (2003) 3001–3011.

[26] E. Ranzi, A. Cuoci, T. Faravelli, A. Frassoldati, G. Migliavacca, S. Pierucci, et al., Chemical Kinetics of Biomass Pyrolysis, Energy & Fuels. 22 (2008) 4292–4300.

[27] C. Dupont, L. Chen, J. Cances, J.-M. Commandre, A. Cuoci, S. Pierucci, et al., Biomass pyrolysis: Kinetic modelling and experimental validation under high temperature and flash heating rate conditions, J. Anal. Appl. Pyrolysis. 85 (2009) 260–267.

[28] E.-J. Shin, M.R. Nimlos, R.J. Evans, Kinetic analysis of the gas-phase pyrolysis of carbohydrates, Fuel. 80 (2001) 1697–1709.

[29] P. Morf, P. Hasler, T. Nussbaumer, Mechanisms and kinetics of homogeneous secondary reactions of tar from continuous pyrolysis of wood chips, Fuel. 81 (2002) 843–853.

[30] M. Nowakowska, O. Herbinet, A. Dufour, P.-A. Glaude, Detailed kinetic study of anisole pyrolysis and oxidation to understand tar formation during biomass combustion and gasification, Combust. Flame. 161 (2014) 1474–1488.

[31] T. Shoji, K. Norinaga, O. Masek, J. Hayashi, Numerical Simulation of Secondary Gas Phase Reactions of Coffee Grounds with a Detailed Chemical Kinetic Model, J. Japan Inst. Energy. Vol. 89 (2010) 955–961.

[32] K. Norinaga, T. Shoji, S. Kudo, J. Hayashi, Detailed chemical kinetic modelling of vapour-phase cracking of multi-component molecular mixtures derived from the fast pyrolysis of cellulose, Fuel. 103 (2013) 141–150.

[33] K. Norinaga, H. Yang, R. Tanaka, S. Appari, K. Iwanaga, Y. Takashima, et al., A mechanistic study on the reaction pathways leading to benzene and naphthalene in cellulose vapor phase cracking, Biomass and Bioenergy. 69 (2014) 144–154.

[34] Deutschmann O., S. Tischer, S. Kleditzsch, C.C. V.M. Janardhanan, M.H. D. Chatterjee, N. Mladenov, H. D. Minh and H. Karadeniz, DETCHEM Software package, 2.5 ed., (2014).

[35] K. Norinaga, V.M. Janardhanan, O. Deutschmann, Detailed chemical kinetic modeling of pyrolysis of ethylene, acetylene, and propylene at 1073–1373 K with a plug-flow reactor model, Int. J. Chem. Kinet. 40 (2008) 199–208.

Table 1. Boundary conditions for numerical simulations

Experiment	Reactor model	Mechanism	Conditions	
			Temperature	Linear velocity
POx at 2nd stage in TSR	PLUG	**DCKM** - 548 species - 8159 elementary step like reactions **Global reaction** - $C_8H_{12}O_4$ → 2 H_2 + 1.5 CH_4 + 4 CO + 0.5 C_2H_4 + Soot (C_2), k_{G700} = 0.3 s^{-1}.	700°C	0.237 m/s
		- C_6H_5O → CO + CH_4 + Soot (C_4H_1), k_{G800} = 0.8 s^{-1}.	800°C	0.237 m/s
Thermal cracking of NV in UTSR	BATCH	**DCKM** - 548 species - 8159 elementary step like reactions	700°C, 800°C	-

Table 2: Primary pyrolysis product distribution

	Mass fraction	**700° C**			**Mass fraction**	**800° C**		
Feed biomass	100	**C** 50.20	**H** 6.30	**O** 43.50	100	**C** 50.20	**H** 6.30	**O** 43.50
Products (Volatiles)								
Hydrogen	0.39	0.00	0.39	0.00	1.25	0.00	1.25	0.00
Carbon monoxide	24.96	10.70	0.00	14.26	36.000	15.44	0.00	20.56
Carbon dioxide	8.23	2.25	0.00	5.98	8.040	2.19	0.00	5.85
Water	10.00	0.00	1.12	8.88	15.900	0.00	1.78	14.12
Methane	2.78	2.08	0.70	0.00	4.810	3.60	1.21	0.00
Acetylene	0.16	0.15	0.01	0.00	0.263	0.24	0.02	0.00
Ethylene	2.21	1.89	0.32	0.00	4.351	3.73	0.63	0.00
Ethane	1.29	1.03	0.26	0.00	0.432	0.35	0.09	0.00
Propadiene	0.02	0.02	0.00	0.00	0.035	0.03	0.00	0.00
Methyl-acethylene	0.11	0.10	0.01	0.00	0.105	0.09	0.01	0.00
Propylene	2.00	1.71	0.29	0.00	0.499	0.43	0.07	0.00
Propane	0.44	0.36	0.08	0.00	0.022	0.02	0.00	0.00
Methanol	1.30	0.49	0.16	0.65	0.461	0.17	0.06	0.23
Acetaldehyde	1.95	1.06	0.18	0.71	0.081	0.04	0.01	0.03
1-Butene	2.38	2.04	0.34	0.00	0.332	0.28	0.05	0.00
n-Butane	0.12	0.10	0.02	0.00	0.006	0.01	0.00	0.00
Ethanol	0.08	0.04	0.01	0.03	0.009	0.00	0.00	0.00
2-Butyne	0.36	0.20	0.03	0.13	0.006	0.00	0.00	0.00
Cyclopropene	0.36	0.23	0.03	0.10	0.020	0.01	0.00	0.01
Furan	0.44	0.31	0.03	0.10	0.051	0.04	0.00	0.01
Acetone	0.27	0.17	0.02	0.08	0.088	0.06	0.01	0.03
2-Propanol	0.00	0.00	0.00	0.00	0.000	0.00	0.00	0.00
2-methyl-1,3-Butadiene	0.02	0.02	0.00	0.00	0.005	0.00	0.00	0.00
1,4-Pentadiene	0.12	0.11	0.01	0.00	0.074	0.06	0.01	0.00
1-Pentene	0.03	0.02	0.00	0.00	0.002	0.00	0.00	0.00
Acetic-acid	0.59	0.24	0.04	0.32	0.198	0.08	0.01	0.11
Cyclopentadiene	0.19	0.17	0.02	0.00	0.338	0.31	0.03	0.00
Methyl-furan	0.16	0.12	0.01	0.03	0.016	0.01	0.00	0.00
2,5-Dimethylfuran	0.12	0.09	0.01	0.03	0.005	0.00	0.00	0.00
Hydroxy-acetone	0.29	0.14	0.02	0.12	0.039	0.02	0.00	0.02
Benzene	0.11	0.10	0.01	0.00	1.421	1.31	0.11	0.00
Dimethyl-furan	0.00	0.00	0.00	0.00	0.000	0.00	0.00	0.00
Toluene	0.28	0.26	0.02	0.00	0.670	0.61	0.06	0.00
Fural	0.23	0.14	0.01	0.08	0.081	0.05	0.00	0.03
Ethylbenzene	0.08	0.07	0.01	0.00	0.072	0.07	0.01	0.00
Phenylacetylene	0.00	0.00	0.00	0.00	0.020	0.02	0.00	0.00
Styrene	0.10	0.10	0.01	0.00	0.216	0.20	0.02	0.00
Phenol	0.85	0.65	0.05	0.14	0.285	0.22	0.02	0.05
Benzofuran	0.09	0.08	0.00	0.01	0.124	0.10	0.01	0.02
Indene	0.18	0.17	0.01	0.00	0.188	0.17	0.01	0.00
Cresol	0.29	0.23	0.02	0.04	0.069	0.05	0.01	0.01
3-Methyl-1, 2-Benzenediol	0.12	0.08	0.01	0.03	0.063	0.04	0.00	0.02
Naphthalene	0.18	0.17	0.01	0.00	0.192	0.18	0.01	0.00
Naphthalene,1-methyl-	0.00	0.00	0.00	0.00	0.047	0.04	0.00	0.00

Naphthalene,2-methyl-	0.00	0.00	0.00	0.00	0.059	0.05	0.00	0.00
1-Butene-3-yne	0.02	0.02	0.00	0.00	0.027	0.02	0.00	0.00
1,2-Butadiene	0.01	0.01	0.00	0.00	0.003	0.00	0.00	0.00
1,3-Butadiene	0.54	0.48	0.06	0.00	0.537	0.48	0.06	0.00
1-Butyne	0.01	0.01	0.00	0.00	0.001	0.00	0.00	0.00
1-Hexen-3-yne	0.00	0.00	0.00	0.00	0.025	0.02	0.00	0.00
Cyclohexane	0.02	0.02	0.00	0.00	0.000	0.00	0.00	0.00
2,3-Butanedione	0.06	0.03	0.00	0.02	0.015	0.01	0.00	0.01
Total (volatiles)	63.45	28.42	4.35	31.75	77.55	30.89	5.58	41.09
Char (N_2)	13.26	11.46	0.17	0.91	11.55	10.01	0.08	0.44
Unknown (difference)	23.29	10.32	1.78	10.84	10.9	9.3	0.64	1.97
Total	100	50.20	6.3	43.5	100	50.2	6.3	43.5

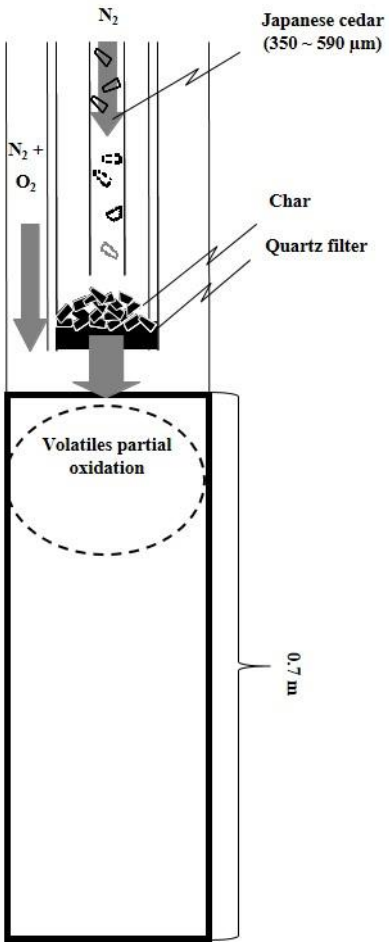

Fig. 1 Schematic representation of the idealized plug-flow reactor for numerical simulations. A two-stage tubular reactor (TSR), consisting of two sections divided by a quartz filter, is externally heated by an electric furnace. Fast pyrolysis of cedar sawdust particles in the upstream section of the TSR generates nascent volatiles, which are partially oxidized downstream in the second stage of the reactor.

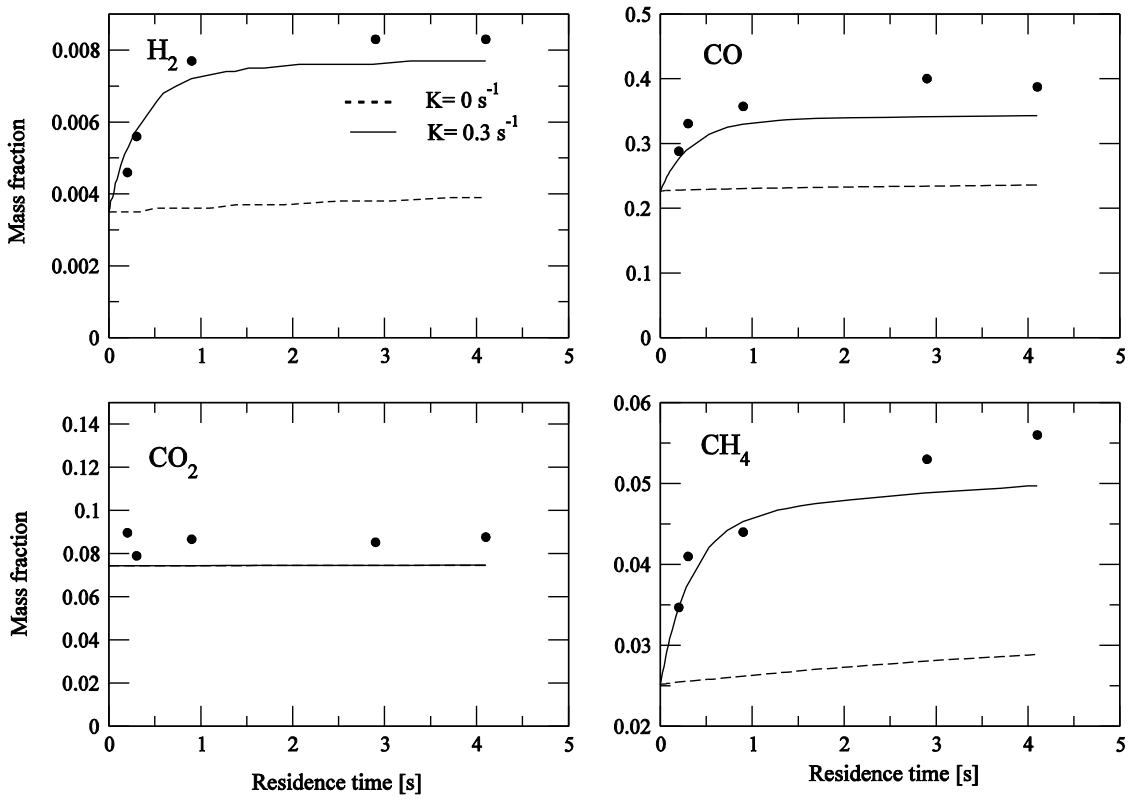

Fig. 2 A comparison between the model predictions at K= 0 and K= 0.3 s^{-1}, and fast pyrolysis experiment of cedar sawdust at 700°C for major gas phase species. The solid and dashed lines show the model predictions with and without global reaction, respectively.

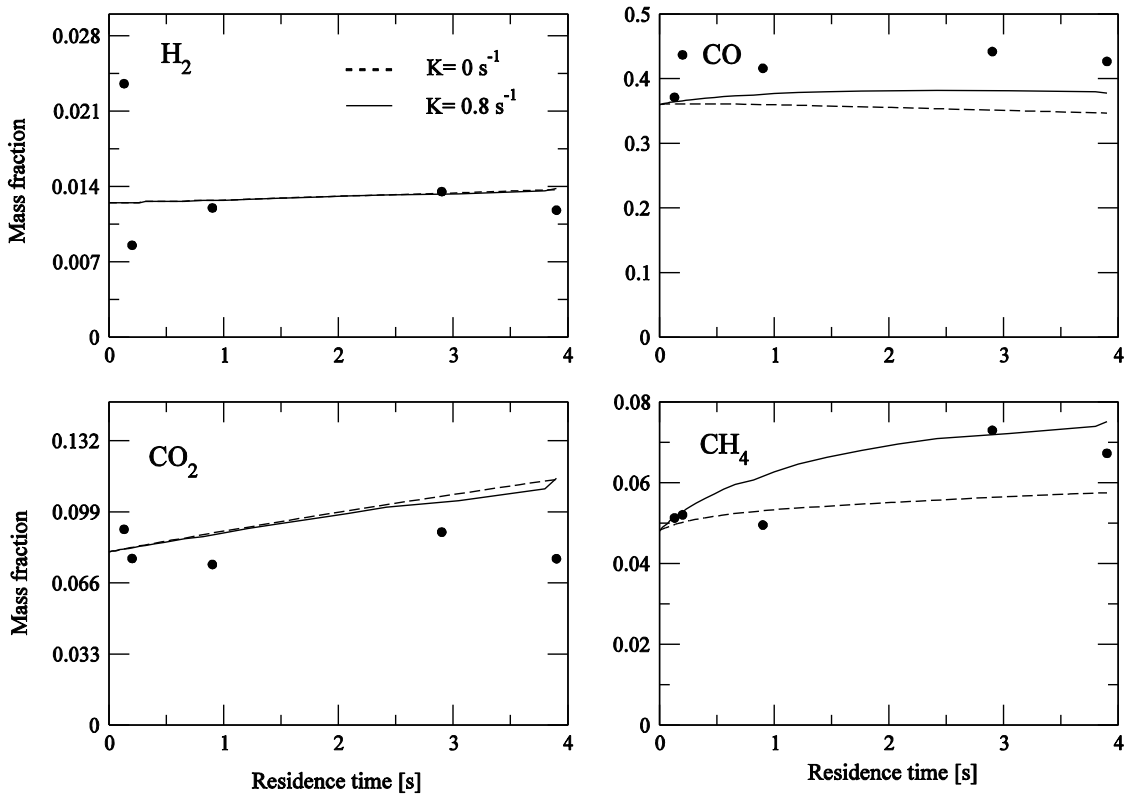

Fig. 3 A comparison between the model predictions at K= 0 and K= 0.8 s^{-1}, and fast pyrolysis experiment of cedar sawdust at 800°C for major gas phase species. The solid and dashed lines show the model predictions with and without global reaction, respectively.

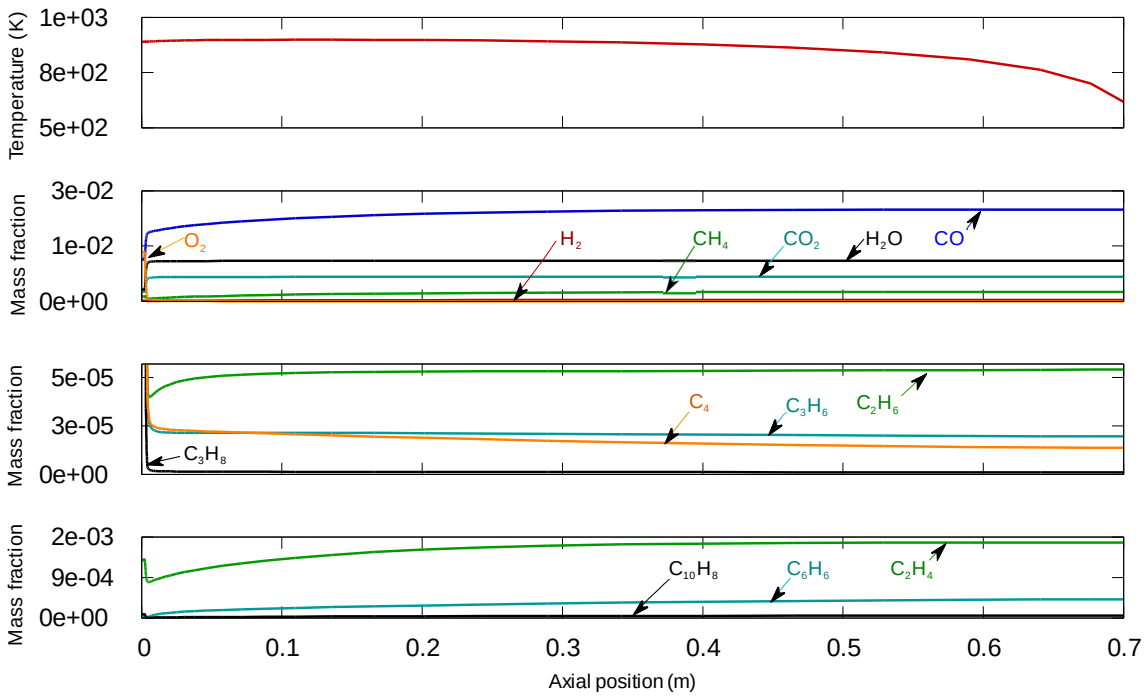

Fig. 4 Distributions of temperature and species concentrations along the axial length of the plug-flow reactor.

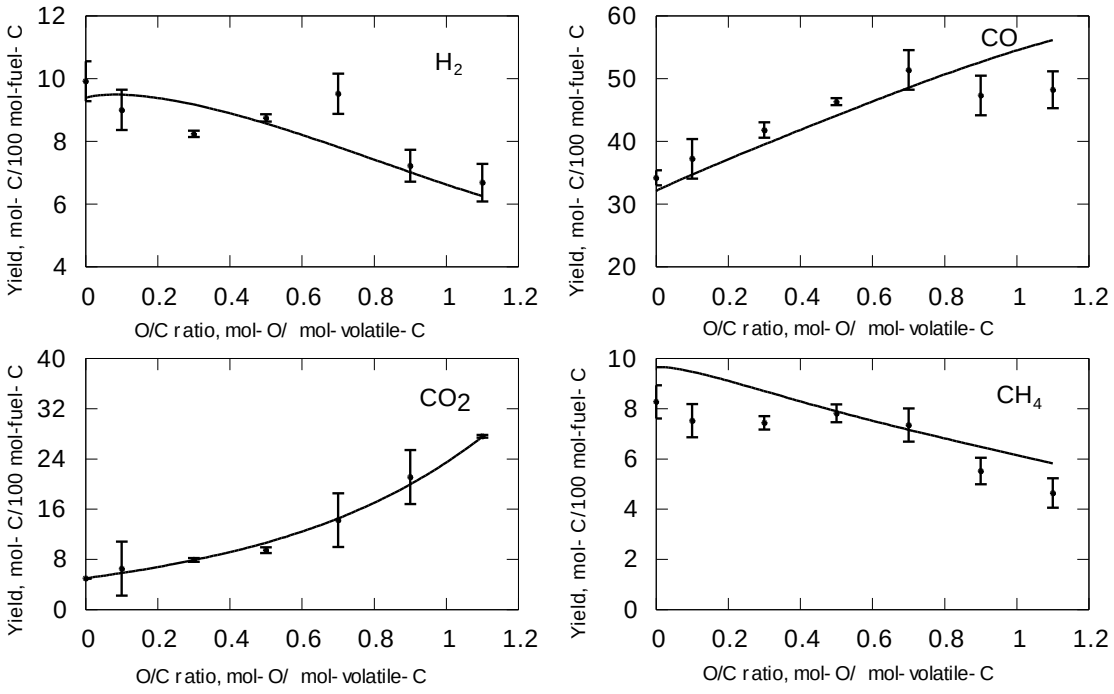

Fig. 5 Comparisons between model predictions and experimental observations under isothermal conditions (700^{o}C) for the major gas-phase species H_2, CO, CO_2, and CH_4. Error bars show the standard error in the experimental measurements and solid lines show the model predictions.

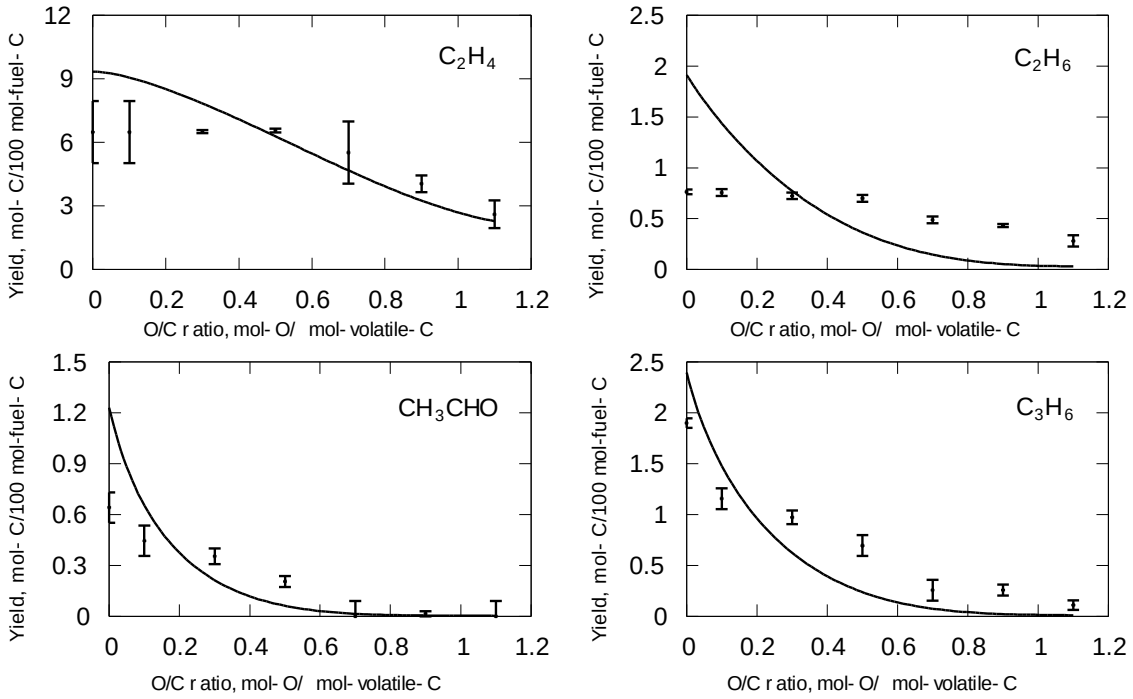

Fig. 6 Comparisons between model predictions and experimental observations under isothermal conditions (700°C) for the minor gas-phase species C_2H_4, C_2H_6, CH_3CHO, and C_3H_6. Error bars show the standard error in the experimental measurements and solid lines show the model predictions.

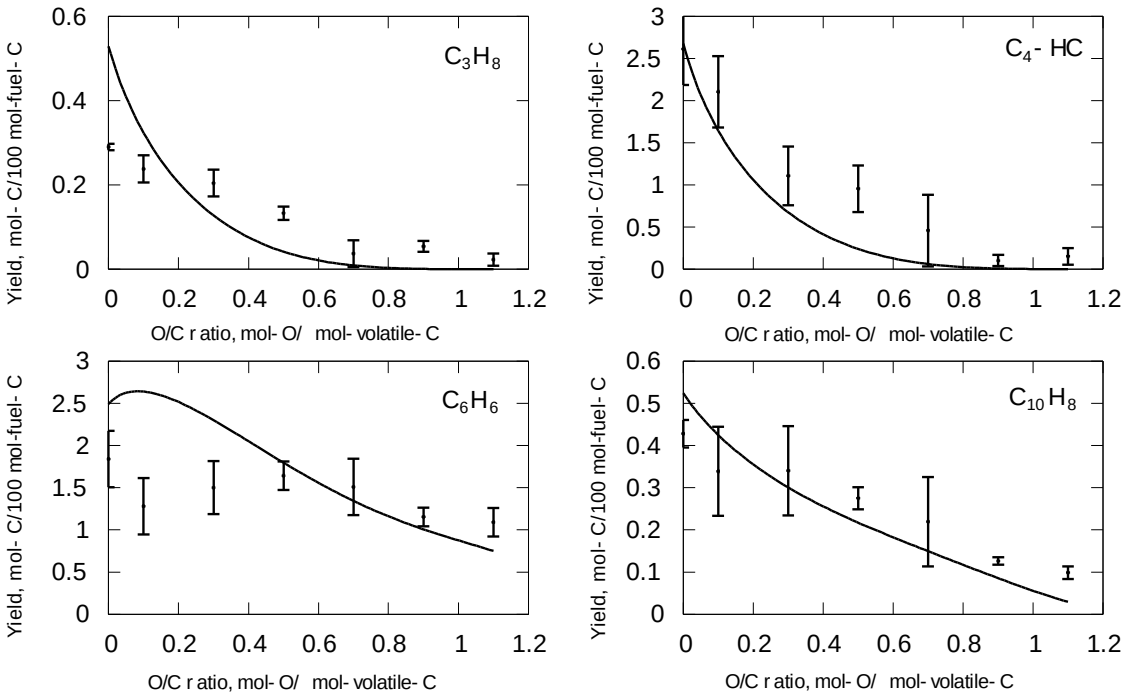

Fig. 7 Comparisons between model predictions and experimental observations under isothermal conditions (700°C) for the minor gas-phase species C_3H_8, C_4 (C_4H_{10} and C_4H_8), C_6H_6, and $C_{10}H_8$. Error bars show the standard error in the experimental measurements and solid lines show the model predictions.

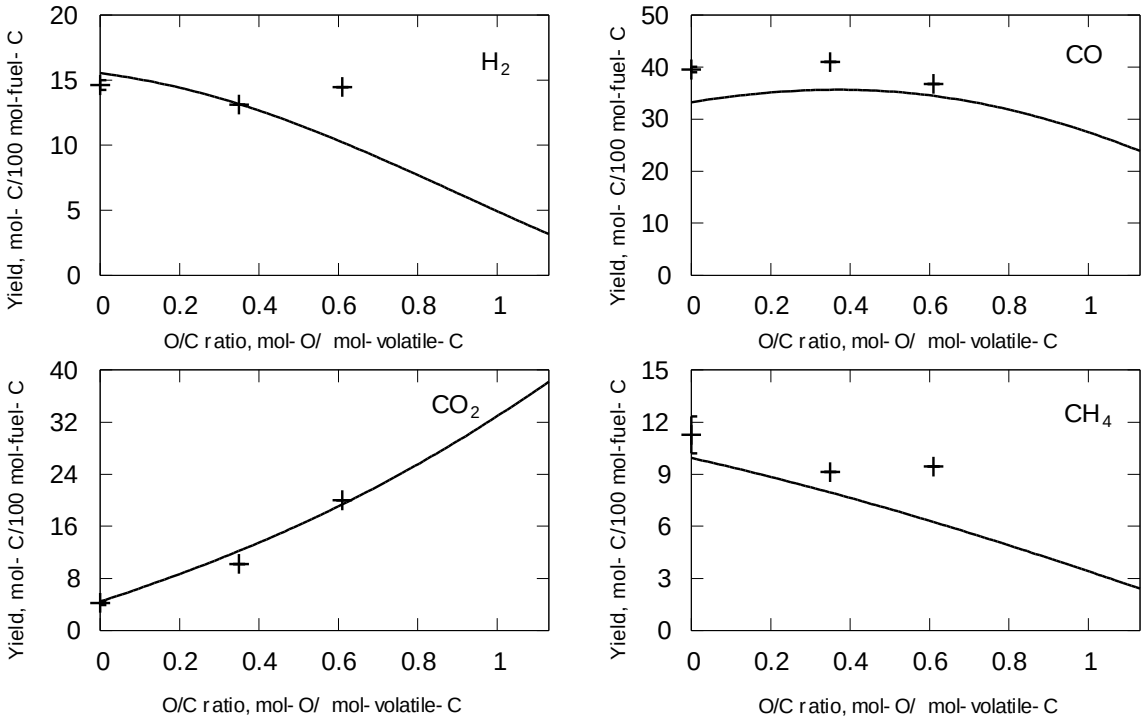

Fig. 8 Comparisons between model predictions and experimental observations under isothermal conditions (800°C) for the major gas-phase species H_2, CO, CO_2, and CH_4. Error bars show the standard error in the experimental measurements and solid lines show the model predictions.

Chapter 3

Numerical study on the steam reforming of biomass tar using a detailed chemical kinetic model

3.1. Introduction

Efficient and effective technologies are required to promote the utilisation of renewable energy from biomass resources. A report on world energy consumption predicts an increased energy demand of 56% from 2010 to 2040,[1] which impacts fossil carbon fuel prices. Concerns about energy requirements and environmental effects, such as greenhouse gas emissions as well as the consequences of climate change, motivate the search for renewable energy sources. Thermochemical conversions, such as pyrolysis and gasification, are effective in converting biomass into valuable fuels/products.[2] The thermochemical processes for biomass are diverse, yet some problems are always associated with biomass conversion. One of the major problems is unavoidable products or impurities from the gasification process, such as tars, solid particles, NH_3, H_2S, HCl, and SO_2, which affect the quality of syngas and cause problems in downstream applications.[3,4]

Tar is a major problematic by-product. It consists of stable aromatic compounds, such as polycyclic aromatic hydrocarbons. Tars are formed during biomass thermochemical conversion and condense at reduced temperatures. Although tar is only a minor component in biomass gasification, even small amounts can significantly affect downstream applications by blocking and/or fouling the process lines. Therefore, the

removal or control of tar is necessary before syngas can be used in any downstream equipment.[4–7]

There are several ways to remove tar,[8] both physically[9,10] and chemically.[11–14] Chemical methods using a catalyst have been applied for potential tar elimination, but they are expensive and require good technology to manage and regenerate the deactivated catalyst.[9,15,16] Non-catalytic partial oxidation or steam reforming is a practical and effective method for tar removal from the thermochemical conversion of biomass.[11,15] Many studies have successfully applied a partial oxidation approach to control the tar concentration.[11,13,17,18] In addition to partial oxidation, steam reforming provides additional advantages not only for tar removal, but also in terms of ensuring a hydrogen-rich content in the end product.

Non-catalytic reforming of the nascent volatiles (NV) derived from biomass fast pyrolysis is a complex process that likely consists of uncountable chemical reactions. A deeper understanding of the complex reactions in the reforming process associated with tar formation and consumption is required for better process design and optimisation.

A detailed chemical kinetic model (DCKM) consisting of thousands of elementary step-like reactions of stable species experimentally and theoretically established for volatile components derived from biomass, as well as intermediates including radical species for biomass thermochemical conversion, has been developed to understand both the conversion of feedstocks and formation of products.[6,19–22] The DCKM was developed to overcome the limitations of the lumping approach, in which species are grouped into one or more different lumps and kinetic parameters are determined by numerical fitting.[23,24] In contrast, the concentration of each individual molecule in the

gas phase can be used directly as input information for a DCKM, and the kinetic parameters of individual elementary reactions are provided based on experimental and theoretical studies. In a recent report, we used a DCKM for the partial oxidation of the NV derived from cedar sawdust fast pyrolysis. [22] However, there are no reports of using a DCKM to analyse steam reforming of the NV derived from biomass fast pyrolysis to predict the tar characteristics.

The purpose of this study was to examine the capability of using an existing DCKM [6,19,21,22] to predict the experimentally observed trends of steam reforming (SR) of the NV derived from woody biomass (cedar chips) fast pyrolysis under various reforming conditions. This is the first such attempt. The DCKM is used to describe the vapour phase reforming of the volatiles. The initial molecular compositions are required input for the DCKM computations, and were derived from analytical pyrolysis experiments.[6] Global reactions accounting for the decomposition of the experimentally undefinable portion included in the NV and soot reforming were also tested to improve the model capabilities. Finally, the model was critically evaluated by comparing the predicted and experimental results obtained using a two-stage reactor.[15]

3.2. Methodology

3.2.1 Experimental

3.2.1.1 Biomass sample

Japanese cedar wood chips with particle sizes of 1.5–2.0 mm were used. The results of proximate and ultimate analyses have been described in Table 1.[15]

3.2.1.2 Reforming of nascent volatiles by steam or air reagents

The experimental study of the partial oxidation (POx) and steam reforming (SR) of NV to examine the effect of steam and air reagents on tar destruction by Wang et al.[15] was used to critically evaluate the DCKM. It should be noted that no experiment was carried out for the POx and SR of NV. The experimental data was taken from Wang et al..[15] The experiment was designed for pyrolysis in the first reactor followed by reforming in the second reactor. Biomass (1.0 g/min) together with carrier nitrogen (1 NL/min) were continuously fed into the pyrolyser where the temperature was held at 750°C. The generated NV were immediately flowed into the reformer reactor and reacted with the reforming reagent (air/steam) at 900°C. Products were collected from the sampling ports between the pyrolysis and reformer reactors and along the flow direction inside the reformer reactor. Detailed descriptions of the experimental set-up as well as the product analysis have been reported previously [15].

3.2.1.3 Analytical pyrolysis

The molecular composition of the NV is required for the DCKM computations and was derived from analytical pyrolysis experiments with an original set-up.[6,19] These experiments were also used to monitor the secondary gas-phase cracking of the NV at different residence times. Unlike the experiments for the POx and SR of NV, these experiments were done by us and the data given here is all original. In addition, these data were used to develop a global reaction for the unidentified products to be applied along with the DCKM. The pyrolyser was designed as a U-shaped two-stage tubular reactor (UTSR) divided into two zones by quartz wool filter, one for the fast pyrolysis of cedar wood chips and the other for the cracking of the NV. Approximately 1.0 mg of cedar

sample wrapped with stainless steel (SUS) wire mesh was fixed by a magnet to the upper part of the UTSR. After heating the UTSR to the desired temperature, the sample was dropped to the bottom of the first zone. Char product remained over the quartz frit at the reactor bottom and the char yield was determined by weighing method. The NV formed by fast pyrolysis were separated from char product and immediately carried from the first zone into the second zone by carrier gas (helium and/or nitrogen). The residence time of the volatiles in the second zone was varied from 0.2 to 4.1 s by adjusting the heated volume (moving the furnace in the vertical direction) of the second reactor. The UTSR was connected to the streamline of a gas chromatograph (GC). The detailed experimental procedure and product analysis have been described elsewhere.[6]

3.2.2 Numerical simulation

3.2.2.1 Vapor phase cracking of NV in the UTSR

The vapour-phase cracking of NV derived from cedar sample fast pyrolysis in the UTSR was numerically simulated using the BATCH code in the DETCHEM program package. DETCHEM^{BATCH} was designed for computational analysis of time-dependent homogeneous reaction systems.[25] Simulations were performed under isobaric and isothermal conditions for residence times of 0 – 4.1 s. The boundary conditions required for the computations are listed in Table 2.

Table 3 shows the product yields when the sample was fast pyrolysed with the UTSR at 750°C and a vapour-phase residence time of 0.2 s. There were 52 identifiable pyrolysates from the NV quantified by three different GC instrumental configurations. The total amount of identified products including char accounted for 83 wt%. However, 17 wt% of the NV was not detected by the GC. The missing materials most likely

condensed on the inner wall of the line between the UTSR and the GC and/or were not separated chromatographically due to the high molecular mass. Notwithstanding, the C:H:O atomic ratios of the missing products at this temperature could be estimated as 4:6:1 based on the elemental balances of the feedstock and the identified NV with char.

3.2.2.2 Reforming of NV in the two-stage reactor

The partial oxidation and steam reforming of NV in the two-stage reactor were considered to occur as depicted in Fig. 1. The numerical simulations were performed using the PLUG model in the DETCHEM program package ($DETHCEM^{PLUG}$).[25] The PLUG model was designed for modelling the non-dispersive one-dimensional flow of a chemically reacting ideal gas mixture under steady-state conditions. First, numerical simulations were performed for the NV in the pyrolysis reactor at 750°C. The input information for the molecular composition of the simulation was derived from pyrolysis experiments in the UTSR. The reaction mechanism and boundary conditions (such as velocity of the feed gas at the inlet of the pyrolysis reactor and temperature along the flow direction) are listed in Table 2.

The ouput information from the pyrolysis reactor consists of more than 500 chemical species and was used as the input for the numerical simulation of the reformer reactor (second reactor). The computations were performed at a reforming temperature of 900°C for both steam and air-reforming reagents with varying steam and air ratios, separately. The air ratio (ER) is the ratio of oxygen moles supplied to the reformer to the oxygen moles required for the complete combustion of the feedstock. The steam ratio (H_2O/C) is the ratio of steam moles supplied to the reformer to the carbon moles in the feedstock. The flow rates and residence times depended on the amount of pyrolysis gas

from the first stage and the amount of reforming agent in the second stage.

3.2.2.3 Reaction mechanism

The detailed chemical kinetic model (DCKM) has been used to predict the biomass secondary gas-phase reactions; it consists of 560 species and 8170 elementary step-like reactions, and has been critically evaluated for the secondary vapour-phase reactions of cellulose,[6,19] coffee extraction residue,[21] and cedar sawdust.[22] The results have suggested that the DCKM has predictive capbility for the vapour-phase cracking of NV generated from fast pyrolysis of cellulose and coffee extraction residue, as well as predictive ability for the vapour-phase partial oxidation of NV generated from biomass (cedar) fast pyrolysis.

A global reaction was developed and used with the DCKM to account for the decomposition of the gas-chromatographically inseparable components included in the NV. A global reaction for soot reforming was also added and used along with the DCKM.

3.3. Results and Discussion

3.3.1 Global reactions for the conversion of missing components included in the NV

To understand the significance of missing products on the product distributions in the subsequent vapour-phase reactions, the pyrolysis experiment in the UTSR was numerically simulated by the DCKM using the BATCH reactor model. The amounts of major products (hydrogen, carbon monoxide, carbon dioxide, and methane) were under-predicted when compared with the UTSR experiments when the reactions of the missing products were neglected (Fig. 2). The under-predictions for those yields are likely due to the lack of information about the reactions of the missing products included in the NV.

The under-predictions of the computational yields versus the experimental ones could potentially be minimised by assuming that the missing products undergo chemical reactions converting them to under-predicted products. Hence, the reaction of the missing products (global reaction) was developed and formulated as

$$C_{36}H_{54}O_9 \rightarrow 14\ H_2 + CO + 3\ CH_4 + 4\ CO_2 + C_2H_4 + \text{soot}\ (C_{26}H_{10}) \quad (1)$$

The kinetic constants (k) of the global reaction were optimised to minimise the gaps between the predictions which corresponding to CALC1 results and experimental results. The k of the global reaction was optimised as 1.5 and 3.0 s^{-1} for temperatures of 750 (k_{G750}) and 900 °C (k_{G900}), respectively. The result for 750 °C is shown in Fig. 2.

It was assumed that the cracking of the missing product occurs first and then the reforming of the cracked products occurs. This assumption was confirmed by the fair agreement between the model predictions and previous experimental results of the partial oxidation of the NV derived from cedar sawdust fast pyrolysis.[22]

3.3.2 Product distributions inside the pyrolysis and reformer reactors from the DCKM

Fig. 3 (a) illustrates the product distributions for CALC2 and CALC5 along the axial length of the pyrolysis reactor (750 °C) and reformer reactor (900 °C) under steam reforming conditions with H_2O/C = 0.5. The figure shows the behaviour of gaseous species inside the reactor that could be profiled individually when using the DCKM with the plug flow reactor model. More than 500 species of product distributions were derived from the reformer reactor, though not shown all the profiles in Fig. 3 (a). Fig. 3 (b) presents the mass fraction profiles of major and minor species in the vapour-phase steam reforming of NV derived from cedar wood chips fast pyrolysis at 900 °C with H_2O/C =

0.5 (CALC5). According to this figure, the most abundant product species from vapour-phase steam reforming was carbon monoxide, followed by major products such as carbon dioxide, water, methane, and hydrogen. Steam was gradually consumed from the initial part of the reactor, and major changes were observed between the reactor inlet and the next 0.2 m length of the reactor.

3.3.3 Numerical simulation of NV cracking in the pyrolysis reactor

A plug-flow reactor model coupled with the DCKM along with the global reaction for the missing products was used to simulate the pyrolysis of NV derived from cedar wood chips at 750 °C. The predictions of pyrolysis gas products for CALC2, including hydrogen, carbon monoxide, methane, carbon dioxide, ethylene, ethane, and propane, compared with the experimental results from the pyrolysis reactor are depicted in Fig. 4. The predictions with the global reaction showed fairly good agreement with the experimental results, indicating that the DCKM along with the global reaction successfully reproduced the pyrolysis gas compositions of the NV in the pyrolysis reactor. The pyrolysis gas compositions were under-predicted only when the DCKM was used alone, especially for hydrogen species. This is likely because the global reaction assumed that the missing products (high molecular mass compounds) were decomposed into the major products (hydrogen, carbon monoxide, methane, carbon dioxide, and ethylene) during NV pyrolysis.

3.3.4 Critical evaluation of the DCKM for reforming NV

The numerical results of the species concentrations at the reactor outlet as a function of both the ER and H_2O/C ratios were compared with the experimental results of Wang et al.[15] Figure 5 compares the predictions (CALC3) and experimental data under partial

oxidation (air reagent) conditions at 900 °C. The DCKM predicted well the vapour-phase POx of the NV at 900 °C under varying ER. The results show the major products (hydrogen and carbon monoxide) and tar residual rate against the residence time for three air-reforming ratios (0, 0.15, and 0.3). When the ER increased, yields of hydrogen (Fig. 5 a) decreased; these predictions are well correlated with the experimental data at different ER values, and are also consistent with the previous study of gas-phase POx.[22] The decreasing trend in hydrogen yield is explained by the oxidation of hydrogen when abundant oxygen is available. In contrast, carbon monoxide (Fig. 5 b) was slightly overestimated at ER = 0.15 and 0.3. However, the behaviour of the yield of carbon monoxide agrees with the experimental results, whereas the carbon monoxide gradually decreased with increasing residence time.

The tar residual rate was defined as amount of tar in the reformed gas per amount of tar in the pyrolysis gas. In this prediction, the amount of tar in the pyrolysis gas was calculated as 1.81 wt% by numerical simulation of NV cracking in the pyrolysis reactor. The tar was calculated as the sum of the product species having a molecular size greater than that of benzene except radical species. Good agreement between predictions and experiments was generally observed for the tar residual rate under POx conditions (Fig. 5 c). The tar residual rate predictions were well predicted at all ER values. Such good agreement suggests that the DCKM can predict minor products such as aromatic hydrocarbons, which are precursors/constituents of tar, and even those products generated at very low yields from NV reforming.

The effects of steam on the reformed gases and tar residual rate at 900 °C from CALC4 are depicted in Fig. 6. The yields of hydrogen (Fig. 6 a) against residence time at three H_2O/C ratios (0, 0.5, 1.0) were under-predicted, especially for longer residence

times. Similarly, Fig. 6 b shows the carbon monoxide yields at different residence times. The trends were erroneously predicted for both hydrogen and carbon monoxide concentrations at longer residence times in steam reforming; this may be associated with a lack of certain reactions related to hydrogen and carbon monoxide formations. Nevertheless, fair agreement can be seen in Fig. 5 c for the tar residual rate under SR conditions. In addition, comparisons between Fig. 5 c and Fig. 6 c reveal that supplying air to the reformer was more effective than supplying steam for tar decomposition.

3.3.5 Critical evaluation of the DCKM with two global reactions for reforming NV

Extending the present model to account for the formation of hydrogen and carbon monoxide must be considered to improve the SR predictions of NV. Soot reforming significantly affected the predictions of hydrogen and carbon monoxide. In this experiment, soot was assumed to be converted to gaseous products under steam reforming conditions.

According to the soot composition derived from the global reaction for the missing products, the reaction of soot reforming may be formulated as follows:

$$\text{Soot } (C_{26}H_{10}) + 26\ H_2O \rightarrow 26\ CO + 31\ H_2 \qquad (2)$$

The kinetic constant (k) for the soot reforming reaction was optimised at k_{G900} = 0.25 $cm^3/mol\ s^{-1}$ by numerical fitting to reproduce the experimental results.

The numerical predictions (CALC5) obtained from a plug-flow reactor model coupled with the DCKM and two global reactions (for the missing products and soot reforming) for SR of NV at 900 °C are presented in Fig. 7. With the reforming of soot as one of the global reactions, the predictions agreed with the experimental results. The hydrogen and carbon monoxide products gradually increased for longer residence times,

similar to the experimental trends. The yields of hydrogen (Fig. 7 a) were overestimated slightly, but the trend of increasing yields with increasing residence time was well estimated. Figure 7 b indicates that the carbon monoxide yield was improved. The yield of carbon monoxide increased with increasing residence time and showed good agreement with the experimental data. Although the concentration of carbon monoxide was slightly under-predicted at H_2O/C = 0.5 and 1.0, this may be explained by the abundance of steam promoting the water-gas shift reaction, resulting in decreased carbon monoxide.

The tar residual rates at 900 °C with different H_2O/C ratios are compared with the experimental data in Fig. 7 c. The tar residual rate was well predicted, and the predicted trends captured the experimental trends at each H_2O/C ratio. No difference from Fig. 6 c was observed when the global reaction for soot reforming was added.

Overall, the model predictions showed satisfactory agreement with the experimental concentration profiles of the major species and the tar residual rate. With no adjustable parameters, the DCKM can capture the experimentally observed trends for the effects of not only POx, but also SR on the product distributions obtained during the reforming of NV from cedar wood chips.

3.4. Conclusions

A detailed chemical kinetic model (DCKM) consisting of more than 8000 elementary step-like reactions, including more than 500 chemical species, was applied to simulate the non-catalytic POx and SR of NV derived from cedar wood chips fast pyrolysis. Approximately 52 chemical species of the NV were identified experimentally and used for input data for simulations of the pyrolysis reactor. The computational output

from the pyrolysis reactor, which consisted of more than 520 species, was used as input for the simulation of the reformer reactor. The POx predictions agreed well with the experimental concentration profiles for the major products as well as the tar residual rate. The experimentally observed characteristics for the SR of the NV were well reproduced for the major products and tar residual rate by using extended global reactions including soot reforming along with the DCKM. The good agreement between the predictions and experimental observations suggests that the DCKM is a potentially useful kinetic model for understanding the complex thermochemistries of NV reforming of biomass.

References

[1] A. Pandey, T. Bhaskar, M. Stöcker, R.K. Sukumaran, Recent Advances in Thermo-Chemical Conversion of Biomass, 2015.

[2] H. Knoef, ed., Handbook Biomass Gasification.pdf, 2005.

[3] M. Verma, S. Godbout, S.K. Brar, O. Solomatnikova, S.P. Lemay, J.P. Larouche, Biofuels production from biomass by thermochemical conversion technologies, Int. J. Chem. Eng. 2012 (2012).

[4] M. Asadullah, Biomass gasification gas cleaning for downstream applications: A comparative critical review, Renew. Sustain. Energy Rev. 40 (2014) 118–132.

[5] C. Li, K. Suzuki, Tar property, analysis, reforming mechanism and model for biomass gasification—An overview, Renew. Sustain. Energy Rev. 13 (2009) 594–604.

[6] K. Norinaga, H. Yang, R. Tanaka, S. Appari, K. Iwanaga, Y. Takashima, et al., A mechanistic study on the reaction pathways leading to benzene and naphthalene in cellulose vapor phase cracking, Biomass and Bioenergy. 69 (2014) 144–154.

[7] K. Maniatis, A.A.C.M. Beenackers, Introduction: tar protocols., IEA gasification tasks, Biomass and Bioenergy. 18 (2000) 1–4.

[8] J. Han, H. Kim, The reduction and control technology of tar during biomass gasification/pyrolysis: An overview, Renew. Sustain. Energy Rev. 12 (2008) 397–416.

[9] A. Paethanom, S. Nakahara, M. Kobayashi, P. Prawisudha, K. Yoshikawa, Performance of tar removal by absorption and adsorption for biomass gasification, Fuel Process. Technol. 104 (2012) 144–154.

[10] A.V. Bridgwater, The technical and economic feasibility of biomass gasification for power generation, Fuel. 74 (1995) 631–653.

[11] S. Hosokai, K. Kishimoto, K. Norinaga, C.-Z. Li, J. Hayashi, Characteristics of Gas-Phase Partial Oxidation of Nascent Tar from the Rapid Pyrolysis of Cedar Sawdust at 700−800°C, Energy & Fuels. 24 (2010) 2900–2909.

[12] S. Schmidt, S. Giesa, A. Drochner, H. Vogel, Catalytic tar removal from bio syngas—Catalyst development and kinetic studies, Catal. Today. 175 (2011) 442–449.

[13] Y. Su, Y. Luo, Y. Chen, W. Wu, Y. Zhang, Experimental and numerical investigation of tar destruction under partial oxidation environment, Fuel Process. Technol. 92 (2011) 1513–1524.

[14] L. Ma, J.F.M. Denayer, G. V. Baron, Improving catalytic hot gas cleaning in biomass gasification by oxygen addition, in: AIChE 100 - 2008 AIChE Annu. Meet. Conf. Proc., 2008. http://www.scopus.com/inward/record.url?eid=2-s2.0-79953828165&partnerID=tZOtx3y1.

[15] Y. Wang, T. Namioka, K. Yoshikawa, Effects of the reforming reagents and fuel species on tar reforming reaction., Bioresour. Technol. 100 (2009) 6610–4.

[16] R. Trane, S. Dahl, M.S. Skjøth-Rasmussen, A.D. Jensen, Catalytic steam reforming of bio-oil, Int. J. Hydrogen Energy. 37 (2012) 6447–6472.

[17] P.A. Jenssen, E. Larsen, K.H. Jørgensen, Tar reduction by partial oxidation, in: Proceedings of the 9th European bioenergy conference (1996), pp. 1371–1375, 1996: p. 1996.

[18] J. Ahrenfeldt, H. Egsgaard, W. Stelte, T. Thomsen, U.B. Henriksen, The influence of partial oxidation mechanisms on tar destruction in TwoStage biomass gasification, Fuel. 112 (2013) 662–680.

[19] K. Norinaga, T. Shoji, S. Kudo, J. Hayashi, Detailed chemical kinetic modelling of vapour-phase cracking of multi-component molecular mixtures derived from the fast pyrolysis of cellulose, Fuel. 103 (2013) 141–150.

[20] K. Norinaga, H. Yatabe, M. Matsuoka, J. Hayashi, Application of an Existing Detailed Chemical Kinetic Model to a Practical System of Hot Coke Oven Gas Reforming by Noncatalytic Partial Oxidation, Ind. Eng. Chem. Res. 49 (2010) 10565–10571.

[21] T. Shoji, K. Norinaga, O. Masek, J. Hayashi, Numerical Simulation of Secondary Gas Phase Reactions of Coffee Grounds with a Detailed Chemical Kinetic Model, J. Japan Inst. Energy. Vol. 89 (2010) 955–961.

[22] N. Thimthong, S. Appari, R. Tanaka, K. Iwanaga, S. Kudo, J. Hayashi, et al., Kinetic modeling of non-catalytic partial oxidation of nascent volatiles derived from fast pyrolysis of woody biomass with detailed chemistry, Fuel Process. Technol. (2015).

[23] J. Corella, M.A. Caballero, M.-P. Aznar, C. Brage, Two Advanced Models for the Kinetics of the Variation of the Tar Composition in Its Catalytic Elimination in Biomass Gasification, Ind. Eng. Chem. Res. 42 (2003) 3001–3011.

[24] P. Morf, P. Hasler, T. Nussbaumer, Mechanisms and kinetics of homogeneous secondary reactions of tar from continuous pyrolysis of wood chips, Fuel. 81 (2002) 843–853.

[25] O. Deutschmann, S. Tischer, C. Correa, D. Chatterjee, S. Kleditzsch, V.M. Janardhanan, et al., DETCHEM Software package, 2.5 ed., (2014).

Table 1. Properties of cedar wood chips

	Cedar wood chips
Proximate analysis	
Vol., wt%	80.8
FC., wt%	18.9
Ash, wt%	0.3
HHV, MJ/kg	19.3
Untimate analysis	
C, wt% (d.a.f.)	49.7
H, wt% (d.a.f.)	6.6
O, wt% (d.a.f.)	43.3
Others, wt% (d.a.f.)	0.4

Table 2. Calculation conditions for numerical simulation

Experiment	Reactor model	Mechanism	Reagent	Conditions		Calcula-tion number
				Temper-ature	Linear velocity	
Thermal cracking of NV in UTSR pyrolysis during the first stage of a two-stage gasifier	BATCH	DCKM	-	750ºC	-	CALC1
Pyrolysis at 1st stage in two – stage gasifier	PLUG	DCKM Global reaction for missing products	-	750ºC	0.092 m/s	CALC2
POx in the second stage of a two-stage gasifier	PLUG	DCKM Global reaction for missing products	Air [ER ratio =0] [ER ratio = 0.15] [ER ratio = 0.3]	900ºC	 0.1650 m/s 0.2626 m/s 0.3603 m/s	CALC3
SR in the second stage of a two-stage gasifier	PLUG	DCKM Global reaction for missing products	Steam [H_2O/C ratio = 0] [H_2O/C ratio = 0.5] [H_2O/C ratio = 1.0]	900ºC	 0.1650 m/s 0.2334 m/s 0.3017 m/s	CALC4
SR in the second stage of a two-stage gasifier	PLUG	DCKM Global reaction for missing products Global reaction for soot reforming	Steam [H_2O/C ratio = 0] [H_2O/C ratio = 0.5] [H_2O/C ratio = 1.0]	900ºC	 0.1650 m/s 0.2334 m/s 0.3017 m/s	CALC5
The DCKM consists of 8170 elementary step-like reactions and 560 species						

Table 3. Nascent volatiles product distribution from cedar wood chips used in the numerical simulation of gas – phase reforming

	Mass fraction	Temperature: 750°C		
		C	H	O
Products (volatiles)				
Hydrogen	0.60	0.00	0.60	0.00
Carbon monoxide	33.00	14.15	0.00	18.85
Carbon dioxide	8.20	2.24	0.00	5.96
Water	13.90	0.00	1.56	12.34
Methane	4.00	2.99	1.01	0.00
Acetylene	0.21	0.19	0.02	0.00
Ethylene	3.40	2.91	0.49	0.00
Ethane	0.40	0.32	0.08	0.00
Propadiene	0.03	0.03	0.00	0.00
Methyl-acethylene	0.11	0.10	0.01	0.00
Propylene	0.65	0.56	0.09	0.00
Propane	0.04	0.03	0.01	0.00
Methanol	0.85	0.32	0.11	0.42
Acetaldehyde	0.80	0.44	0.07	0.29
1-Butene	0.40	0.34	0.06	0.00
n-Butane	0.04	0.03	0.01	0.00
Ethanol	0.04	0.02	0.01	0.01
2-Butyne	0.17	0.09	0.01	0.06
Cyclopropene	0.18	0.12	0.01	0.05
Furan	0.22	0.16	0.01	0.05
Acetone	0.16	0.10	0.01	0.05
2-Propanol	0.00	0.00	0.00	0.00
2-methyl-1,3-Butadiene	0.01	0.01	0.00	0.00
1,4-Pentadiene	0.10	0.08	0.01	0.00
1-Pentene	0.01	0.01	0.00	0.00
Acetic-acid	0.40	0.16	0.03	0.21
Cyclopentadiene	0.27	0.25	0.02	0.00
Methyl-furan	0.08	0.06	0.01	0.02
2,5-Dimethylfuran	0.06	0.04	0.01	0.01
Hydroxy-acetone	0.20	0.10	0.02	0.09
Benzene	0.10	0.09	0.01	0.00
Dimethyl-furan	0.01	0.00	0.00	0.00
Toluene	0.53	0.48	0.05	0.00
Fural	0.17	0.11	0.01	0.06
Ethylbenzene	0.07	0.07	0.01	0.00
Phenylacetylene	0.01	0.01	0.00	0.00
Styrene	0.17	0.15	0.01	0.00
Phenol	0.25	0.19	0.02	0.04
Benzofuran	0.11	0.09	0.01	0.01
Indene	0.14	0.13	0.01	0.00
Cresol	0.16	0.12	0.01	0.02
3-Methyl-1, 2-Benzenediol	0.09	0.06	0.01	0.02
Naphthalene	0.13	0.12	0.01	0.00

Naphthalene,1-methyl-	0.03	0.03	0.00	0.00
Naphthalene,2-methyl-	0.04	0.03	0.00	0.00
1-Butene-3-yne	0.02	0.02	0.00	0.00
1,2-Butadiene	0.01	0.00	0.00	0.00
1,3-Butadiene	0.53	0.47	0.06	0.00
1-Butyne	0.00	0.00	0.00	0.00
1-Hexen-3-yne	0.02	0.02	0.00	0.00
Cyclohexane	0.01	0.01	0.00	0.00
2,3-Butanedione	0.03	0.02	0.00	0.01
Total (volatiles)	71.13	28.07	4.46	38.60
Char [a]	12.35	10.67	0.12	0.68
Feed biomass	100	50.00	6.6	43.3
Unknown (difference)	16.52	11.26	2.02	4.02

[a] Char is substituted with nitrogen in the simulation

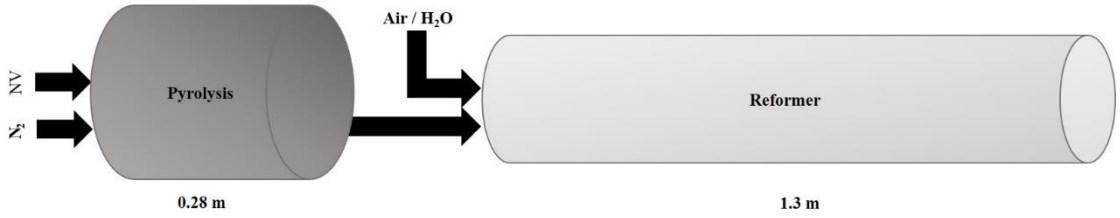

Fig. 1 Schematic representation of the two idealised plug-flow reactors for numerical simulations of pyrolysis and reforming.

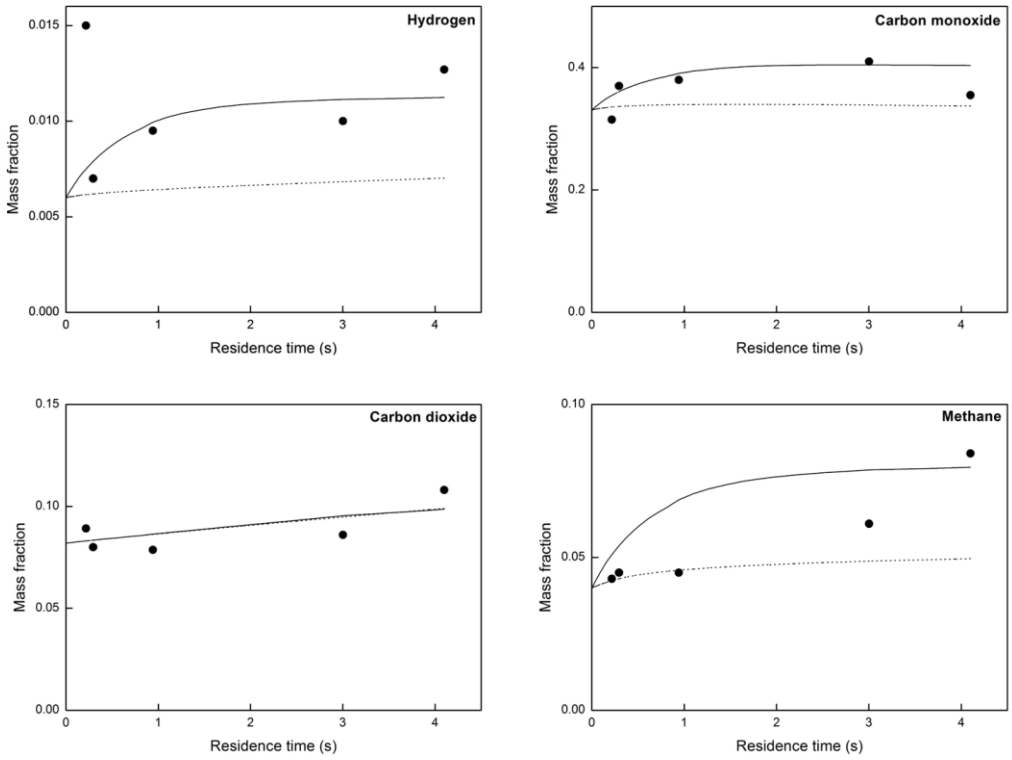

Fig. 2 Comparison between the model predictions (CALC1) for kinetic constant (*k)* = 0 and 1.5 s^{-1}, and the fast pyrolysis experiment of cedar wood chips at 750 °C for the major gas-phase species of hydrogen, carbon monoxide, carbon dioxide, and methane. The solid lines (*k* = 0) and the dashed lines (*k* = 1.5) represent the model predictions without the global reaction and those with the global reaction at 750 °C, respectively.

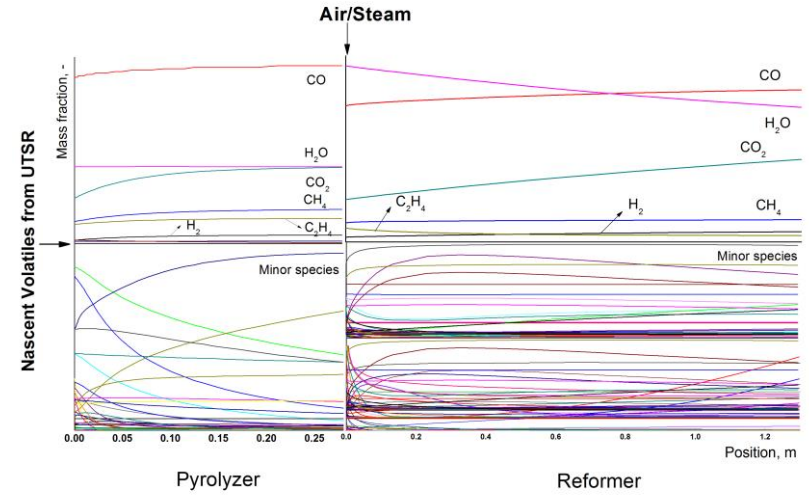

(a)

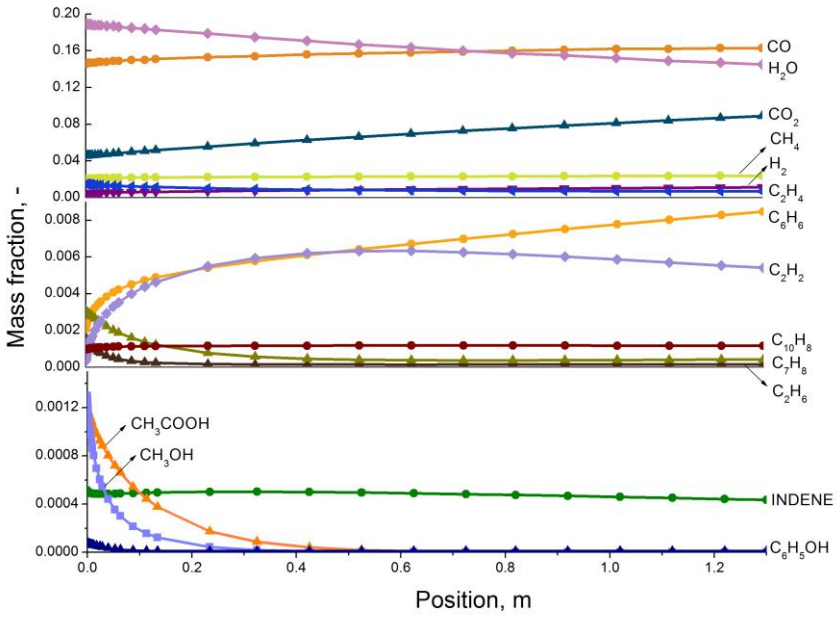

(b)

Fig. 3 (a) Distributions of species concentrations along the axial length of the plug-flow reactors for pyrolysis (length = 0.28 m) for CALC2 and reforming (length = 1.3 m) for CALC5, respectively. (b) Profiles of the mass fractions of major and minor species in the vapour-phase steam reforming of volatiles derived from cedar wood chips fast pyrolysis at 900 °C at H_2O/C = 0.5 (CALC5).

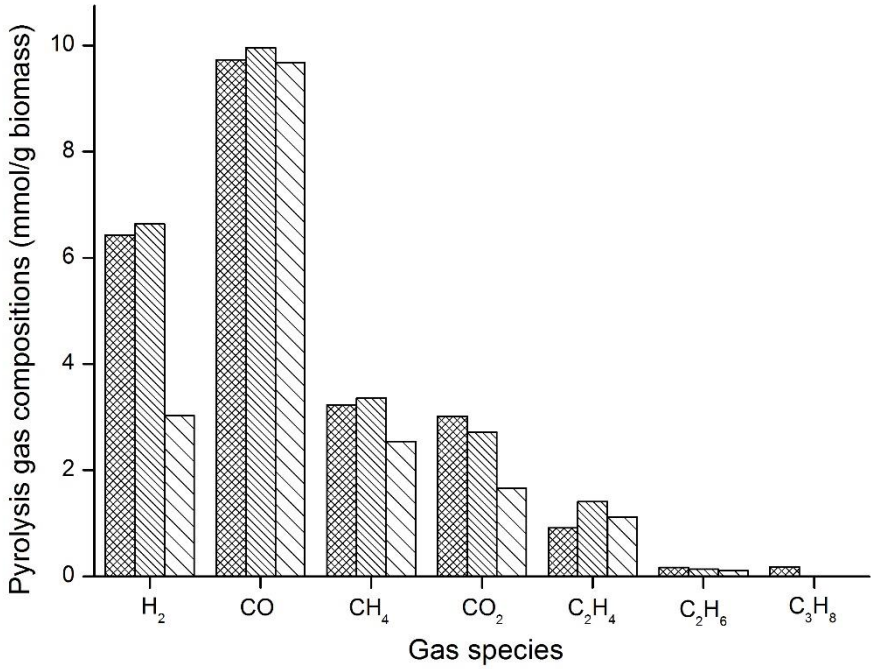

Fig. 4 Comparisons between the model predictions (CALC2) and experimental observations for the pyrolysis reactor under isothermal conditions (750 °C) for the pyrolysis gas compositions of H_2, CO, CH_4, CO_2, C_2H_4, C_2H_6, and C_3H_8. The dense bars represent the experimental measurements, and the thin-stripe and thick-stripe bars indicate the model predictions with and without the global reaction for the missing products, respectively.

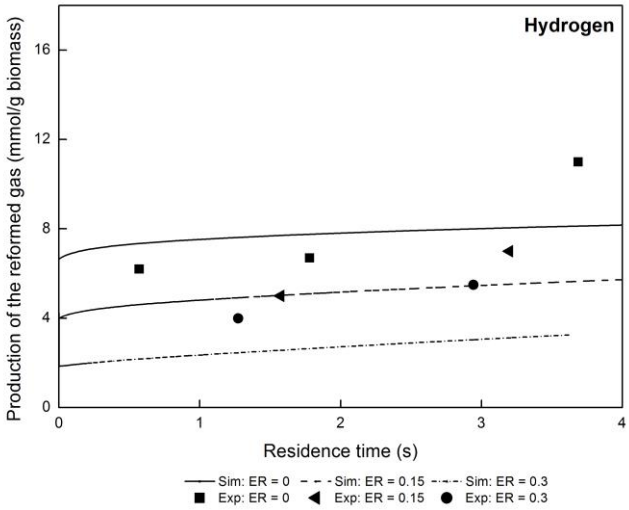

(a)

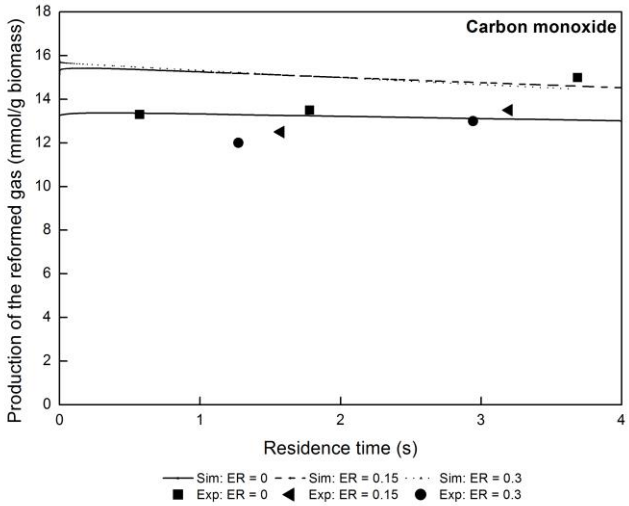

(b)

Fig. 5-1 Comparisons between the model predictions (CALC3) and experimental observations for the reformer reactor under partial oxidation (air reagent) conditions at 900 °C for the product gas species H_2 and CO, and the tar residual rate. The computations were performed using the plug-flow reactor with the DCKM and a global reaction for the missing products. The symbol and the solid line represent the experimental data and the model predictions, respectively.

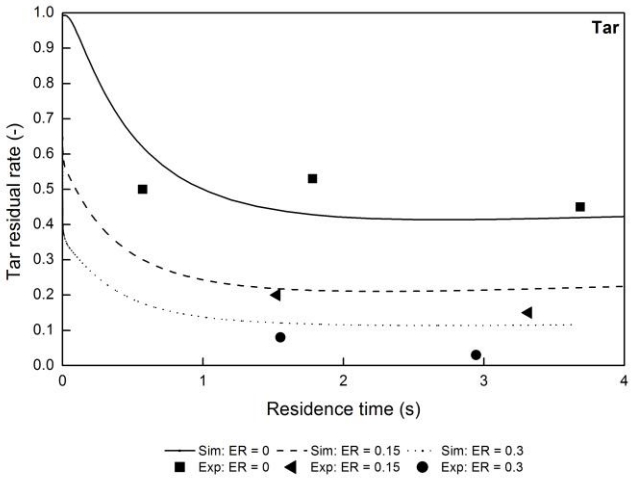

(c)

Fig. 5-2 Comparisons between the model predictions (CALC3) and experimental observations for the reformer reactor under partial oxidation (air reagent) conditions at 900 °C for the product gas species H_2 and CO, and the tar residual rate. The computations were performed using the plug-flow reactor with the DCKM and a global reaction for the missing products. The symbol and the solid line represent the experimental data and the model predictions, respectively.

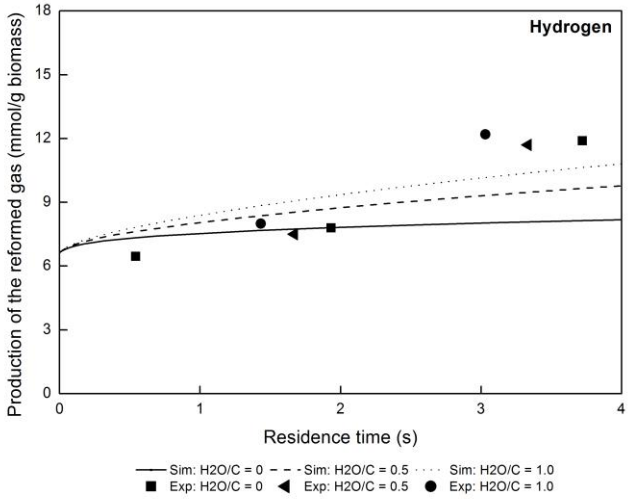

(a)

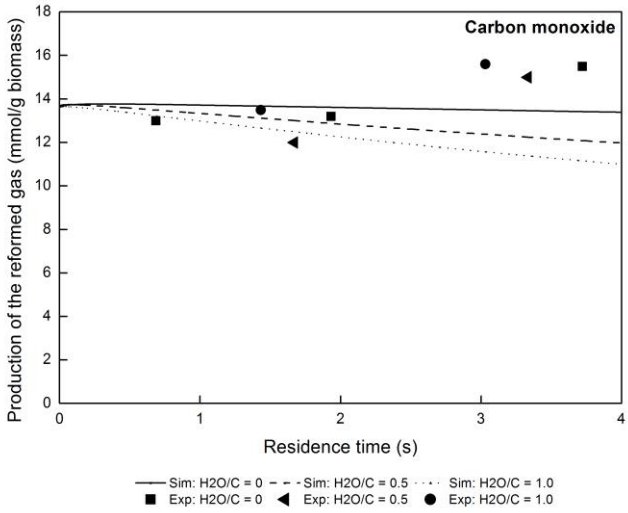

(b)

Fig. 6-1 Comparisons between the model predictions (CALC4) and experimental observations for the reformer reactor under steam reforming (steam reagent) conditions at 900 °C for the product gas species H_2 and CO, and the tar residual rate. The computations were performed using the plug-flow reactor with the DCKM and a global reaction for the missing products. The symbol and the solid line represent the experimental data and the model predictions, respectively.

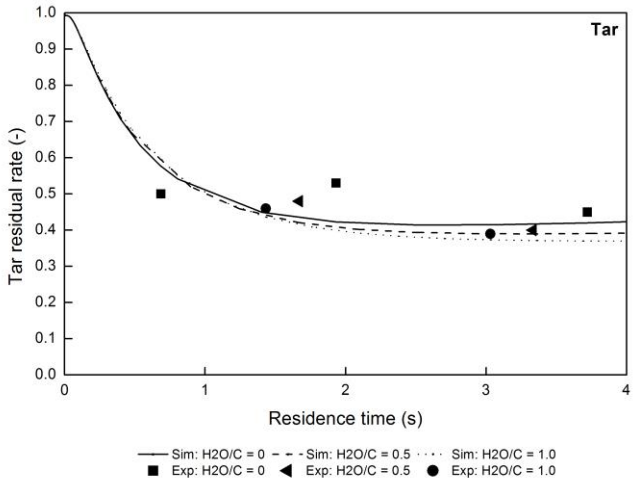

(c)

Fig. 6-2 Comparisons between the model predictions (CALC4) and experimental observations for the reformer reactor under steam reforming (steam reagent) conditions at 900 °C for the product gas species H_2 and CO, and the tar residual rate. The computations were performed using the plug-flow reactor with the DCKM and a global reaction for the missing products. The symbol and the solid line represent the experimental data and the model predictions, respectively.

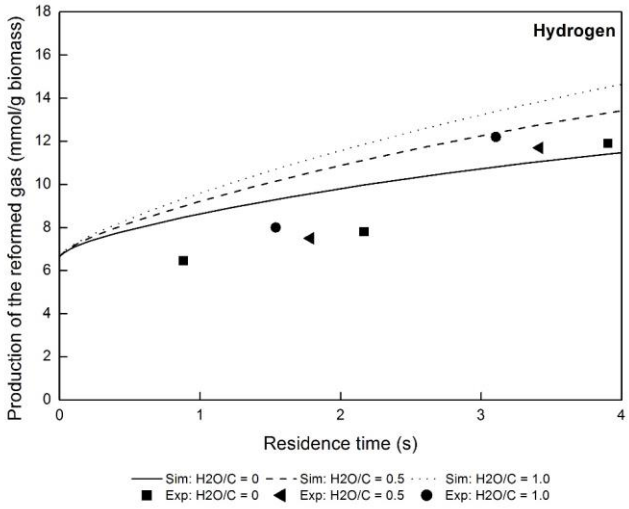

(a)

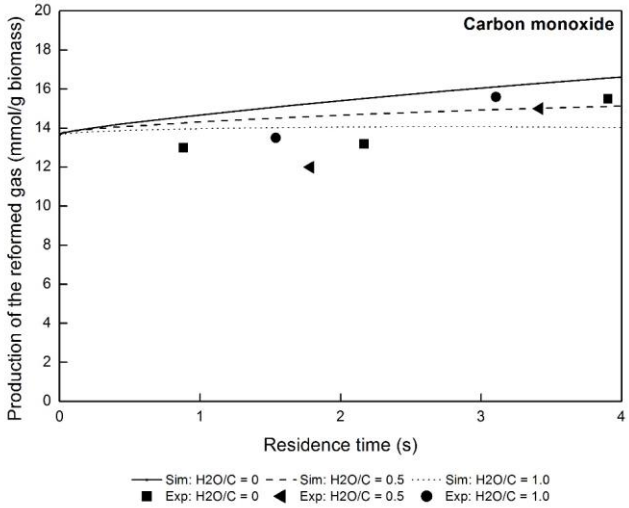

(b)

Fig. 7-1 Comparisons between the model predictions (CALC5) and experimental observations for the reformer reactor under steam reforming (steam reagent) conditions at 900 °C for the product gas species H_2 and CO, and the tar residual rate. The computations were performed using the plug-flow reactor with the DCKM and two global reactions for the missing products and soot reforming. The symbol and the solid line represent the experimental data and the model predictions, respectively.

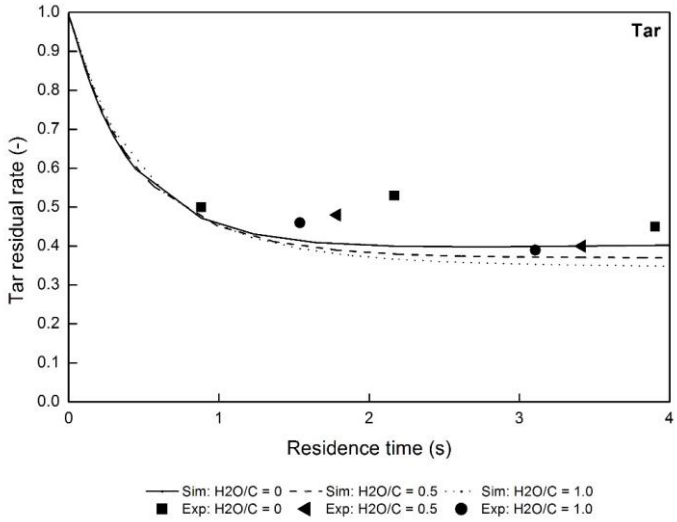

(c)

Fig. 7-2 Comparisons between the model predictions (CALC5) and experimental observations for the reformer reactor under steam reforming (steam reagent) conditions at 900 °C for the product gas species H_2 and CO, and the tar residual rate. The computations were performed using the plug-flow reactor with the DCKM and two global reactions for the missing products and soot reforming. The symbol and the solid line represent the experimental data and the model predictions, respectively.

Chapter 4

Predictive capability of an existing detailed chemical kinetic model for non-catalytic vapor-phase reforming of nascent volatiles derived from various woody biomass fast pyrolysis

4.1. Introduction

Thermochemical conversion of biomass requires technologies for tar removal which are one of the greatest technical challenges towards successful biomass utilizations. Tar is high molecular weight hydrocarbons. This tar tends to be refractory and will condense at low temperature leading to clogged or fouling in continuous operation of gasifier. Even tar generation is small but this small amount can significantly damage downstream equipment and worsen gasification efficiency. Most downstream applicatuons require tar free or at least part of tar removal before syngas can be used (engines, fuel cells, etc.) [1–4].

Volatile matter released during pyrolysis at the initial stage of gasification habitually contains non-condensable gases together with tarry components. Reforming this existing tar into dry gas is proven as effective tar controling and cost reduction technology due to no-requirement for further expensive facilities of gas treatment. Catalytic [5,6] and non-catalytic [7–9] approaches for tar reforming have been reported. Catalyst cracking is effective for tar elimination, but they are expensive and require good technology to manage/regenerate the deactivated catalyst [10–14].

Non-catalytic vapor-phase reforming such as partial oxidation (POx) aimed at a more robust and simple technique [7,8,15,16]. Several reported claimed that amount of oxygen and temperature were significantly impacts on tar concentrations [7,8]. Generally, excess air ratios between 0-0.7 and high temperature between 800 -1050°C contributed positively to tar destruction [16].

Experimental studies on the gas-phase POx characteristics of NV derived from biomass fast pyrolysis have been reported [7, 9]. However, POx process comprises of hundreds to tens of thousands of chemical reactions. To optimize, design, and understand those complex reactions require kinetic modeling. Kinetic modeling on the tar destruction have been widely studied by traditional models (lumping approach) for previous studies [17–21]. Unfortunately, the lumping approach has some limitations such as lack of predictive capability of the products in the molecular level and the rate constants are determined by numerical fitting. To date, detailed chemical kinetic model (DCKM) have been developed to overcome the limitation of lumping approach. By using DCKM, the concentration of each individual molecules in the gas phase can be directly used as input information without lumping chemical species so gas-phase products can predict in the molecular level. The DCKM had been applied to predict the kinetics of combustion [22,23], pyrolysis of hydrocarbons [24,25], vapor-phase cracking of NV generated from the fast pyrolysis of cellulose [26,27] and coffee extraction residue [28]. Narumon et al. applied DCKM which consists of >8000 elementary reaction steps and >500 chemical species to predict vapor-phase refroming both of POx and steam reforming (SR) of NV derived from cedar biomass [29,30]. Besides, there are no studies have applied the DCKM on the vapor-phase reforming of NV derived from different type of biomasses.

To extend the predictive capability of the DCKM, this study aims to examine the DCKM possibility for vapor-phase reforming of NV derived from different biomasses. There are two type of biomasses were studied namely empty fruit bunches (EFB) and bagasse (BG) which are the residual of palm and sugarcane, respectively. This is the first attempt to analyze the POx of NV derived from EFB and BG primary pyrolysis by using the DCKM. The simulation performed in batch reactor model with DCKM and global reaction for the missing products. The DCKM was critically evaluated by comparing the predictions with experimental results obtained from the secondary vapor-phase POx in two-stage reactor.

4.2. Kinetic model and numerical simulation

The DCKM to simulate the POx of NV derived from EFB and BG fast pyrolysis was based on reaction mechanisms for POx and SR of the NV derived from cedar fast pyrolysis [29,30]. The DCKM consists of 8159 elementary reaction steps and 548 chemical species from the smallest species (hydrogen radicals) to the largest molecule (coronene). Thermodynamic data for the species involved in the mechanisms as well as the rate constants were used without modification. The mechanisms used here is provided in appendix.

The simulations were performed under isobaric and isothermal conditions with BATCH code in DETCHEM program package ($DETCHEM^{BATCH}$) [31]. The initial molecular compositions of the NV from EFB and BG is one of input boundary conditions which derived from the primary pyrolysis experiment in a U-shaped two-stage tubular reactor (UTSR).

4.3. Experimental data

4.3.1 Primary pyrolysis experiment for EFB and BG

The molecular composition of the reactants are necessary as a boundary condition for calculations. In this study, the composition of primary pyrolysis products from EFB and BG were determined based on an analytical experiments with an originally designed set-up in a U-shaped two-stage tubular reactor (UTSR) [27]. A UTSR divided into two zones by a quartz wool filter (one part for the fast pyrolysis of cedar sawdust and the other for the cracking of the NV). The EFB and BG samples for the experiment provided from the Mitsui Engineering & Shipbuilding CO.,LTD. (MES). Biomass sample was dropped into the pyrolyzer which was heated at temperature 650°C. NV and char formed by pyrolysis were immediately separated, only NV were swept into the second zone. The UTSR was connected to the streamline of a gas chromatograph (GC) to indentify gas-phase products. The residence times of the volatiles in the second zone was set at 0.1 s by adjusting the volume of the second reactor. A detailed description of the experimental set-up can be found elsewhere [26,27].

4.3.2 Gas-phase POx of NV derived from EFB and BG fast pyrolysis

The experimental data of vapor-phase POx of NV derived from EFB and BG fast pyrolysis were used for critical evaluation of the DCKM. All the experimental data in this study performed by MES. The experiment is briefly introduced here.

EFB and BG were used as biomass feedstock with particle sizes ranging from 350 to 590 μm. Ultimate analysis of EFB and BG were shown in Table 1. A two-stage reactor (Fig. 1) was employed for the experiment of vapor-phase POx. The first and second stages were designed for fast pyrolysis of the biomass sample and the partial oxidation of the

NV, respectively. The sample was fed continuously with primary nitrogen into the first stage at a rate of 0.23 g/min. The temperature of the first stage was held at 650°C where biomass fuel was rapidly pyrolyzed to form char and NV products. Char product was retained on the quartz frit at the first reactor bottom, while the NV product were swept through the frit under a forced flow of secondary nitrogen into the second stage. In the second stage of the reactor, oxygen was introduced to mix with the NV at the amount of O_2/C = 1.23 and 0.08 for EFB and BG, respectively. The O_2/C ratio is defined as the ratio of the number of oxygen atoms in the supplied oxygen gas to the total number of carbon atoms in the NV. The temperature of the second stage was set at 700^{o}C for the experiment of EFB and varying temperature at 700, 800, and 900^{o}C for the experiment of BG. All the products passing through the second reactor were collected and analyzed.

4.4. Results and discussion

4.4.1. Molecular compositions of primary pyrolysis of EFB and BG

The molecular composition of the reactants are necessary as one of input for DCKM. Yield of the primary pyrolysis products of EFB and BG are listed in Table 1 at the pyrolysis temperatures 650°C and residence time 0.1 s. Overall, there are 44 pyrolysates were identified and quantified with three different GC instrumental configurations. Total mass of the products accounted for 68 and 61 wt.% for the EFB and BG, respectively. Accordingly, 32 and 39 wt.% are undetectable or are not separated chromatographically by current GC. Unidentified products were considered as missing products in this time. The missing products were likely correspond to high molecular components which condensed at the inner wall of the line between the UTSR and the GC. The C:H:O atomic ratios of missing products were estimated as 7:11:6 and 6:9:5 for EFB and BG,

respectively based on the information of elemental balance between feedstock, NV and char product (Table 1).

To account the missing products into the simulation, the global reactions were developed based on the information of elemental balance. The missing products were assumed to converte into major products (hydrogen, carbon monoxide, carbon dioxide, and methane) and formulated as;

EFB; $C_7H_{11}O_6 \rightarrow 2.5\ H_2 + 1.5\ CH_4 + 2\ CO + 2\ CO_2 + \text{Soot}\ (C_1)$. (1)

BG; $C_6H_9O_5 \rightarrow 2\ CH_4 + CO + 2\ CO_2 + \text{Soot}\ (C_1H_1)$. (2)

The kinetic constant (k) for global reactions were optimized by numerical fitting, $k_{700} = 1.0\ s^{-1}$ and $k_{700} = 0.3$, $k_{800} = 0.8$, and $k_{900} = 1.5\ s^{-1}$ for EFB and BG, respectively. For detailed of developing the global reaction was mentioned elsewhere [29].

4.4.2. Experimental results of POx of NV derived from EFB and BG

Experimentally observed results for effect of oxygen on gas-phase of NV derived from different biomasses fast pyrolysis were investigated. Fig. 2 shows yields of major products (hydrogen, carbon monoxide, carbon dioxide, and methane) as a function of residence time at temperature 700^{o}C with the $O_2/C = 1.23$ mol/mol for EFB sample. The yields of hydrogen, carbon monoxide, and carbon dioxide decrease when increasing residence times from 0-2 s. Besides, yield of carbon dioxide increase as longer residence times. Changes in the yields of major products mainly explain by the abundant oxygen that is available for oxidation reaction. Hydrogen oxidation results in decreasing hydrogen yield. The formation of steam derived from hydrogen partial oxidation enhanced methane steam reforming reaction which results in a decreasing of methane yield. The decreasing of carbon monoxide is because of carbon monoxide partial

oxidation. The increasing yield in carbon dioxide is due to carbon monoxide oxidation in addition with water gas shift reaction.

Fig. 3 shows the experimental yields of minor products (ethylene, ethane, benzene, phenol, and naphthalene) obtained from POx of EFB at temperature 700^{o}C as function of residence times. Although the POx products contain very low yields of minor products, however, these products are important for tar precursors. The yields of minor products dramatically decrease between residence time 0-0.5 s. It seemed that oxygen is effect on the decreasing of minor products due to POx process.

The POx of NV derived from BG fast pyrolysis at temperature 700, 800, and 900^{o}C with O_2/C = 0.08 mol/mol of EFB at 700^{o}C shown in Fig. 4. The effect of O_2/C on the major product yields are shown as the function of residence times. It is obvious that yields of major products increase as increasing residence times; the most abundant product is carbon monoxide, which is followed by carbon monoxide, methane, and hydrogen, respectively. In addition, changes in trends of major products increase when increasing reforming temperature from 700-900^{o}C.

4.4.3. Mole fraction profiles of major products in the vapor-phase POx

Numerically obtained profiles of mole fractions found in the vapor-phase POx of NV derived from EFB are shown in Fig.5. The DCKM along with a batch reactor model and a global reaction were used to simulate the distribution of the species concentrations as a function of residence times at temperature 700°C. Prediction results (Fig. 5) are roughly divided into two patterns; one shows increasing mole fractions as longer residence times with the most abundant product is carbon dioxide and carbon monoxide. And the other patterns show decreasing mole fractions over times such as hydrogen and

methane, followed by minor products (phenol, benzene, naphthalene). Oxygen is gradually consumed from the top of reactor. These trends are used to compare with experimental results for critical evaluation of DCKM model.

4.4.4. Critical evaluations of the DCKM

To evaluate the predictive capability of an existing DCKM, the predicted product yields by numerical simulations are compared with those experiments.

4.4.4.1. Computational POx of NV derived from EFB fast pyrolysis

The numerical results of species concentrations as a function of residence times (0-2 s) were compared with experimentally obtained results from the gas-phase POx in the two-stage reactor. Figure 6 shows comparisons for POx of the NV derived from EFB fast pyrolysis at 700^{o}C with the O_2/C = 1.23 mol/mol. When the oxygen was introduced, predicted trend of hydrogen (Fig. 6 a) decrease and the decreasing trend of hydrogen could capture the trend of the experiment. Predictions show that carbon monoxide (Fig. 6 b) decreased when increasing residence time, on the contrary, carbon dioxide (Fig. 6 c) increased as longer residence times. Decreasing trend of methane yield (Fig. 6 d) also could be observed from the simulation. These trends of major products captured the trends of experiment under varying residence times.

The comparisons made for minor products of POx for EFB are given in Fig. 7. The minor products are important due to they are typically found in the refractory post-gasification tar. DCKM could individually predict the yields of minor products namely for ethylene (Fig 7 a), ethane (Fig 7 b), benzene (Fig 7 c), phenol (Fig 7 d), and naphthalene (Fig 7 e). However, discrepancies were observed between the calculations and experiments which is somewhat under-prediction at the shorter residence times (0-

0.5 s). The under-predictions are likely explained by premixed assumption used for simulation which is different from experiment (Fig. 8). Experiments likely involve incomplete mixing between oxygen and NV before 0.5 s. Besides, numerical simulation assumed complete mixing of oxygen and NV at the top of the reforming zone (0 s).

4.4.4.2 Computational POx of the NV derived from BG fast pyrolysis

The comparisons between the model predictions and experimental results obtained in the POx of BG fast pyrolysis were discussed in this section. The computational predictions were calculated based on mass of product yield per mass of biomass feedstock. The product yields of hydrogen, carbon monoxide, carbon dioxide, and methane at different reforming temperature 700, 800, and 900^{o}C with a constant O_2/C = 0.08 mol/mol are shown in Figs. 9-11.

Fig. 9 shows comparisons of computation and experiment at reforming temperature 700^{o}C. In present of oxygen at the residence times 0-2 s, hydrogen slightly increased. Carbon monoxide and carbon dioxide also increased when increasing resident times. While methane slightly increase when increasing residence times. Yields of major products were fairly reproduced the experimentally observed trends.

Fig. 10 shows the yields of major products for the POx of BG at temperature 800^{o}C. As the results, trends of major products (hydrogen, carbon monoxide, carbon dioxide, and methane) agree well with experimental trends. Whereas yield of major products gradually increased at increasing residence times from 0-2 s. In addition, Yields of major products at reforming temperature 800^{o}C tends to higher than the yields of major products at reforming temperature 700^{o}C.

Such agreements between predictions and measurements for major product yields derived from POx of BG at reforming temperature 900^{o}C shown in Fig. 11. Excellent agreements can be seen between predictions and experiment at all residence times (0-2 s). These predicted trends of major products could reproduce the increasing trends of experiment. Generally, yields of major products at 900^{o}C are more higher than yields at lower temperature (700 and 800^{o}C).

4.4.5. Predictions of vapor-phase POx at different reforming temperature

The effect of various reforming temperatures (700, 800, and 900^{o}C) on the yields of major products at the residence time 1.0 s for POx of the NV derived from BG fast pyrolysis shown in Fig. 12. Experimental values for hydrogen, carbon monoxide, carbon dioxide, and methane yields exhibit the increasing trends when increasing reforming temperatures from 700 to 900^{o}C. These trends are well captured by numerical simulation of DCKM.

Although there are slight disagreements with some of the experimental observations, the DCKM shows capability to predict the concentration profiles of major and minor products in the vapor-phase POx of the NV derived from different biomasses. The erroneous predictions would be attribute to the way of model improvement together with more sophisticated experimental approach to approximate the composition of NV.

4.5. Conclusions

A detailed chemical kinetic model (DCKM) was applied to examine its predictive capability for non-catalytic partial oxidation (POx) of nascent volatiles (NV) derived from different biomasses fast pyrolysis. The DCKM was critically evaluated by exhaustive comparisons between the computational predictions and experimental results.

The experimental data obtained from the POx of empty fruit bunches (EFB) and bagasse (BG) in two-stage reactor. The overall predictions agree well with the experimetal trends for major and minor products. Nevertheless, some disagreement still found between predictions and experiment especially for the minor products at short residence times. However, DCKM is the one of a comprehensive kinetic modeling approach for understanding the complex thermochemistries of vapor-phase reforming at mechanistic level. More accurate predictions require further challenge tasks such as model improvement and experimental analysis.

References

[1] C. Li, K. Suzuki, Tar property, analysis, reforming mechanism and model for biomass gasification-An overview, Renew. Sustain. Energy Rev. 13 (2009) 594–604.

[2] P. McKendry, Energy production from biomass (part 3): gasification technologies, Bioresour. Technol. 83 (2002) 55–63.

[3] H. Knoef, ed., Handbook Biomass Gasification.pdf, 2005.

[4] M. Asadullah, Biomass gasification gas cleaning for downstream applications: A comparative critical review, Renew. Sustain. Energy Rev. 40 (2014) 118–132.

[5] S. Anis, Z.A. Zainal, Tar reduction in biomass producer gas via mechanical, catalytic and thermal methods: A review, Renew. Sustain. Energy Rev. 15 (2011) 2355–2377.

[6] M.P. Aznar, M.A. Caballero, J. Gil, J.A. Martín, J. Corella, Commercial steam reforming catalysts to improve biomass gasification with steam-oxygen mixtures. 2. Catalytic tar removal, Ind. Eng. Chem. Res. 37 (1998) 2668–2680. http://www.scopus.com/inward/record.url?eid=2-s2.0-0032105553&partnerID=tZOtx3y1.

[7] S. Hosokai, K. Kishimoto, K. Norinaga, C.-Z. Li, J. Hayashi, Characteristics of Gas-Phase Partial Oxidation of Nascent Tar from the Rapid Pyrolysis of Cedar Sawdust at 700−800°C, Energy & Fuels. 24 (2010) 2900–2909.

[8] Y. Su, Y. Luo, Y. Chen, W. Wu, Y. Zhang, Experimental and numerical investigation of tar destruction under partial oxidation environment, Fuel Process. Technol. 92 (2011) 1513–1524.

[9] Y. Wang, T. Namioka, K. Yoshikawa, Effects of the reforming reagents and fuel species on tar reforming reaction., Bioresour. Technol. 100 (2009) 6610–4.

[10] R. Trane, S. Dahl, M.S. Skjøth-Rasmussen, A.D. Jensen, Catalytic steam reforming of bio-oil, Int. J. Hydrogen Energy. 37 (2012) 6447–6472.

[11] S. Schmidt, S. Giesa, A. Drochner, H. Vogel, Catalytic tar removal from bio syngas—Catalyst development and kinetic studies, Catal. Today. 175 (2011) 442–449.

[12] R.N. Singh, S.P. Singh, J.B. Balwanshi, Tar removal from Producer Gas : A Review, 3 (2014) 16–22.

[13] J. HEPOLA, P. SIMELL, Sulphur poisoning of nickel-based hot gas cleaning catalysts in synthetic gasification gasII. Chemisorption of hydrogen sulphide, Appl. Catal. B Environ. 14 (1997) 305–321.

[14] K. Tomishige, T. Miyazawa, T. Kimura, K. Kunimori, N. Koizumi, M. Yamada, Resistance to sulfur poisoning of hot gas cleaning catalysts for the removal of tar from the pyrolysis of cedar wood, Appl. Catal. B Environ. 60 (2005) 299–307.

[15] P.A. Jenssen, E. Larsen, K.H. Jørgensen, Tar reduction by partial oxidation, in: Proceedings of the 9th European bioenergy conference (1996), pp. 1371–1375, 1996: p. 1996.

[16] J. Ahrenfeldt, H. Egsgaard, W. Stelte, T. Thomsen, U.B. Henriksen, The influence of partial oxidation mechanisms on tar destruction in TwoStage biomass gasification, Fuel. 112 (2013) 662–680.

[17] J. Corella, M.A. Caballero, M.-P. Aznar, C. Brage, Two Advanced Models for the Kinetics of the Variation of the Tar Composition in Its Catalytic Elimination in Biomass Gasification, Ind. Eng. Chem. Res. 42 (2003) 3001–3011.

[18] E. Ranzi, A. Cuoci, T. Faravelli, A. Frassoldati, G. Migliavacca, S. Pierucci, et al., Chemical Kinetics of Biomass Pyrolysis, Energy & Fuels. 22 (2008) 4292–4300.

[19] C. Dupont, L. Chen, J. Cances, J.-M. Commandre, A. Cuoci, S. Pierucci, et al., Biomass pyrolysis: Kinetic modelling and experimental validation under high temperature and flash heating rate conditions, J. Anal. Appl. Pyrolysis. 85 (2009) 260–267.

[20] E.-J. Shin, M.R. Nimlos, R.J. Evans, Kinetic analysis of the gas-phase pyrolysis of carbohydrates, Fuel. 80 (2001) 1697–1709.

[21] P. Morf, P. Hasler, T. Nussbaumer, Mechanisms and kinetics of homogeneous secondary reactions of tar from continuous pyrolysis of wood chips, Fuel. 81 (2002) 843–853.

[22] J.M. Simmie, Detailed chemical kinetic models for the combustion of hydrocarbon fuels, Prog. Energy Combust. Sci. 29 (2003) 599–634.

[23] J. Warnatz, U. Maas, R.W. Dibble, Combustion, 3rd ed., Springer-Verlag, Heidelberg,New York, 2000.

[24] K. Norinaga, O. Deutschmann, Detailed Kinetic Modeling of Gas-Phase Reactions in the Chemical Vapor Deposition of Carbon from Light Hydrocarbons, Ind. Eng. Chem. Res. 46 (2007) 3547–3557.

[25] M. Nowakowska, O. Herbinet, A. Dufour, P.-A. Glaude, Detailed kinetic study of anisole pyrolysis and oxidation to understand tar formation during biomass combustion and gasification, Combust. Flame. 161 (2014) 1474–1488.

[26] K. Norinaga, H. Yang, R. Tanaka, S. Appari, K. Iwanaga, Y. Takashima, et al., A mechanistic study on the reaction pathways leading to benzene and naphthalene in cellulose vapor phase cracking, Biomass and Bioenergy. 69 (2014) 144–154.

[27] K. Norinaga, T. Shoji, S. Kudo, J. Hayashi, Detailed chemical kinetic modelling of vapour-phase cracking of multi-component molecular mixtures derived from the fast pyrolysis of cellulose, Fuel. 103 (2013) 141–150.

[28] T. Shoji, K. Norinaga, O. Masek, J. Hayashi, Numerical Simulation of Secondary Gas Phase Reactions of Coffee Grounds with a Detailed Chemical Kinetic Model, J. Japan Inst. Energy. Vol. 89 (2010) 955–961.

[29] N. Thimthong, S. Appari, R. Tanaka, K. Iwanaga, S. Kudo, J. Hayashi, et al., Kinetic modeling of non-catalytic partial oxidation of nascent volatiles derived from fast pyrolysis of woody biomass with detailed chemistry, Fuel Process. Technol. (2015).

[30] N. Thimthong, S. Appari, R. Tanaka, K. Iwanaga, T. Namioka, S. Kudo, et al., Numerical study on the steam reforming of biomass tar using a detailed chemical kinetic model, J. Japan Inst. Energy. (2015) 2015.

[31] O. Deutschmann, S. Tischer, C. Correa, D. Chatterjee, S. Kleditzsch, V.M. Janardhanan, et al., DETCHEM Software package, 2.5 ed., (2014).

Table 1: Carbon, hydrogen, and oxygen balances in the primary pyrolysis of empty fruit bunches (EFB) and bagasse (BG)

Feed biomass	**Empty fruit bunches (EFB)**				**Bagasse (BG)**			
	Mass fraction	**650° C**			**Mass fraction**	**650° C**		
		C	**H**	**O**	100	**C**	**H**	**O**
	100	47.28	5.74	46.42		46.17	6.15	44.16
Products (Volatiles)								
Hydrogen	0.34	0.00	0.34	0.00	0.32	0.00	0.32	0.00
Carbon monoxide	5.40	2.32	0.00	3.09	6.71	2.88	0.00	3.83
Carbon dioxide	9.53	2.60	0.00	6.93	9.06	2.47	0.00	6.59
Water	13.77	0.00	1.54	12.23	11.96	0.00	1.34	10.62
Methane	2.00	1.50	0.50	0.00	2.01	1.50	0.50	0.00
Acetylene	0.10	0.10	0.01	0.00	0.12	0.11	0.01	0.00
Ethylene	1.47	1.26	0.21	0.00	1.65	1.41	0.24	0.00
Ethane	0.35	0.28	0.07	0.00	0.41	0.33	0.08	0.00
Propadiene	0.05	0.04	0.00	0.00	0.04	0.03	0.00	0.00
1-propyne	0.29	0.26	0.03	0.00	0.10	0.09	0.01	0.00
Propene	0.74	0.63	0.11	0.00	0.87	0.75	0.13	0.00
Propane	0.06	0.05	0.01	0.00	0.07	0.06	0.01	0.00
Methanol	1.67	0.63	0.21	0.84	1.54	0.58	0.19	0.77
Acetaldehyde	1.51	0.82	0.14	0.55	2.04	1.11	0.19	0.74
But-1-ene, But-2-ene	0.11	0.09	0.02	0.00	0.10	0.08	0.01	0.00
Iso-Butane	0.07	0.05	0.01	0.00	0.08	0.06	0.01	0.00
Ethanol	0.10	0.05	0.01	0.03	0.12	0.06	0.02	0.04
Acraldehyde	0.52	0.33	0.04	0.15	0.79	0.51	0.06	0.22
Furan	0.45	0.32	0.03	0.11	0.76	0.54	0.05	0.18
Acetone	0.40	0.25	0.04	0.11	0.65	0.41	0.07	0.18
Cyclopentadiene	0.43	0.39	0.04	0.00	0.93	0.85	0.09	0.00
1,2-Pentadiene	0.12	0.11	0.01	0.00	0.13	0.11	0.01	0.00
1,4-Pentadiene	0.67	0.59	0.08	0.00	1.02	0.90	0.12	0.00
Pentane	0.20	0.17	0.03	0.00	0.23	0.20	0.03	0.00
Acetic acid	0.80	0.32	0.05	0.43	0.85	0.34	0.06	0.45
2-Methyl-furan	0.10	0.08	0.01	0.02	0.12	0.09	0.01	0.02
But-3-en-2-one	0.00	0.00	0.00	0.00	0.00	0.00	0.00	0.00
Hydroxy acetone	0.60	0.29	0.05	0.26	1.07	0.52	0.09	0.46
Benzene	0.82	0.50	0.04	0.00	0.65	0.60	0.05	0.00
Toluene	0.18	0.16	0.02	0.00	0.21	0.20	0.02	0.00
Furan-2-carbaldehyde	0.37	0.23	0.02	0.12	0.49	0.31	0.02	0.16
Ethyl-benzene	0.00	0.00	0.00	0.00	0.00	0.00	0.00	0.00
Anthracene	0.00	0.00	0.00	0.00	0.00	0.00	0.00	0.00
Stylene	0.00	0.00	0.00	0.00	0.00	0.00	0.00	0.00
Phenol	3.67	0.40	0.03	0.09	0.34	0.26	0.02	0.06
Phenanthlene	0.00	0.00	0.00	0.00	0.00	0.00	0.00	0.00

Indene	0.00	0.00	0.00	0.00	0.00	0.00	0.00	0.00
O-cresol	0.11	0.09	0.01	0.02	0.13	0.10	0.01	0.02
M-cresol+P-cresol	0.23	0.18	0.02	0.03	0.21	0.16	0.02	0.03
Naphthalene	0.25	0.00	0.00	0.00	0.00	0.00	0.00	0.00
Methylnaphthalene	0.00	0.00	0.00	0.00	0.00	0.00	0.00	0.00
Methylnaphthalene	0.00	0.00	0.00	0.00	0.00	0.00	0.00	0.00
1-Butene-3-yne	0.06	0.05	0.00	0.00	0.05	0.05	0.00	0.00
1,3-Butadiene	0.44	0.39	0.05	0.00	0.44	0.39	0.05	0.00
1-hexene	0.00	0.00	0.00	0.00	0.00	0.00	0.00	0.00
char	24.00	17.11	0.35	6.54	14.33	10.21	0.21	3.91
Unknown (difference)	28.05	14.65	1.62	14.89	39.42	17.92	2.11	15.87
Total	100.00	47.28	5.74	46.42	100.00	46.17	6.15	44.16

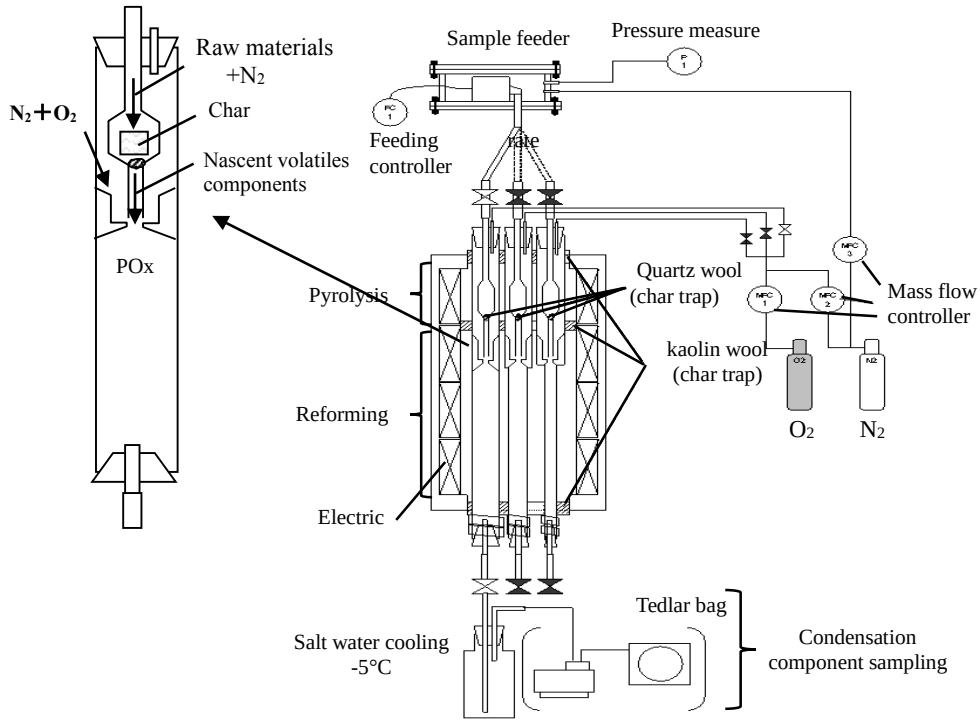

Fig. 1 A schematic representation of the experimental set-up and enlarged view of a two-stage tubular reactor consisting of two sections divided by a quartz filter. The upper one indicates fast pyrolysis of biomass particles in order to generate nascent volatiles, and the lower one indicated the in situ secondary gas-phase partial oxidation of the nascent volatiles.

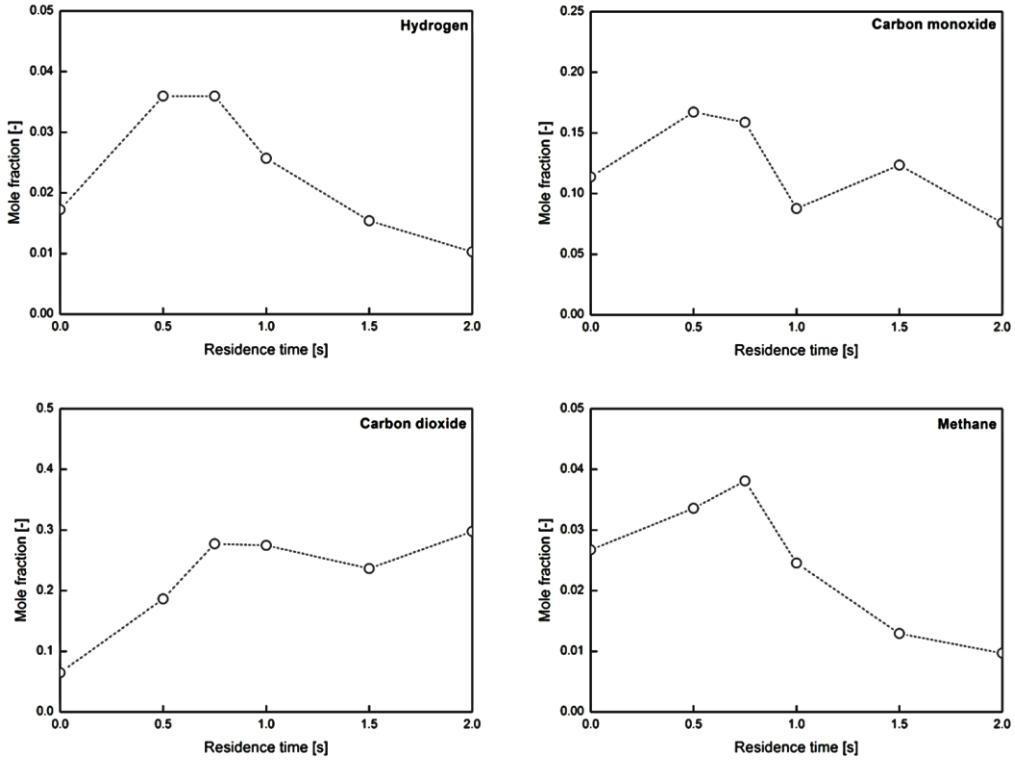

Fig. 2 Experimental results for major gases (hydrogen, carbon monoxide, carbon dioxide, and methane) found in the secondary gas-phase partial oxidation of EFB at temperature 700^{o}C and at varying residence times (0-2 s).

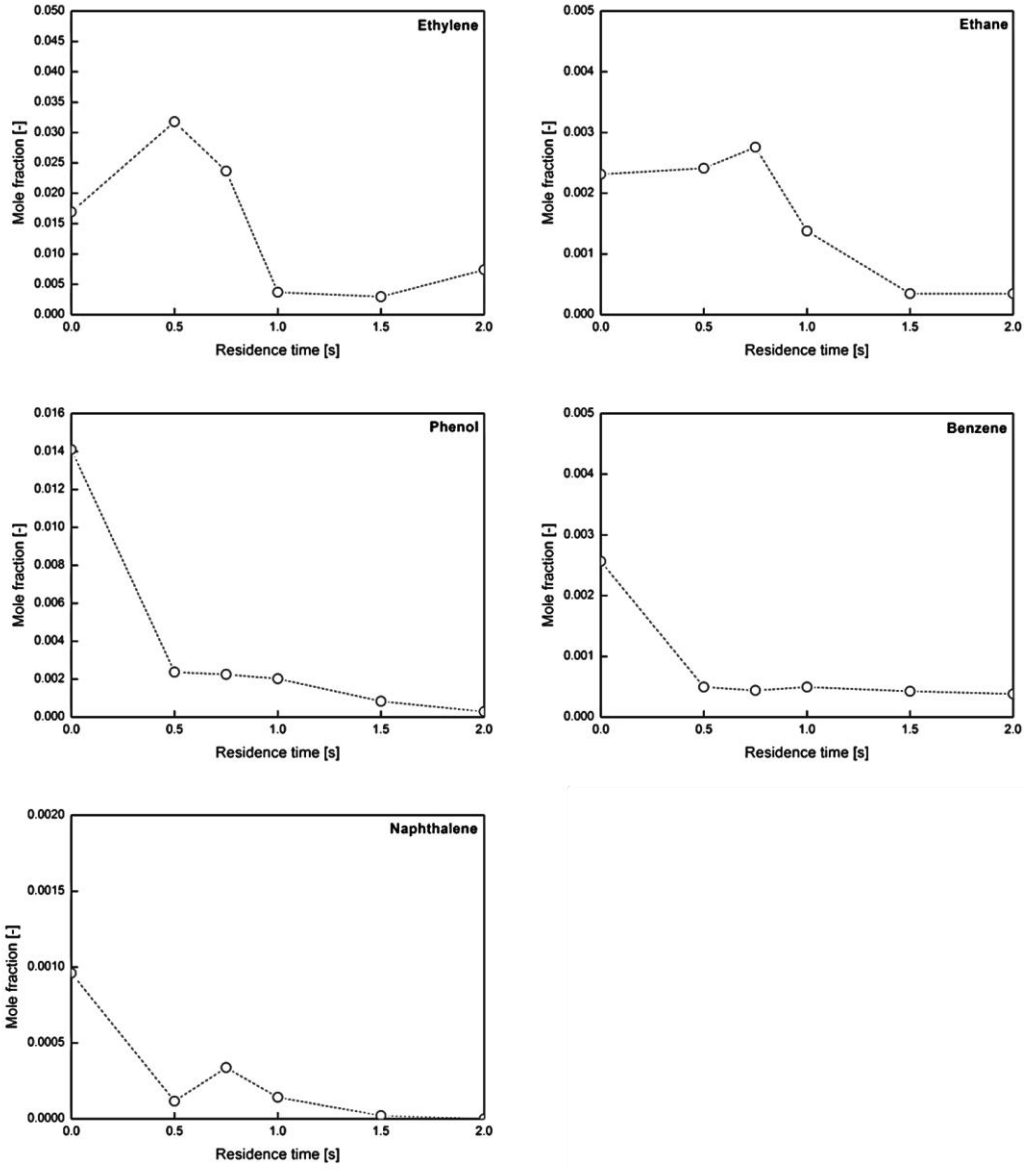

Fig. 3 Experimental results for minor gases (ethylene, ethane, phenol, benzene, and naphthalene) found in the secondary gas-phase partial oxidation of EFB at temperature 700^{o}C and at varying residence times (0-2 s).

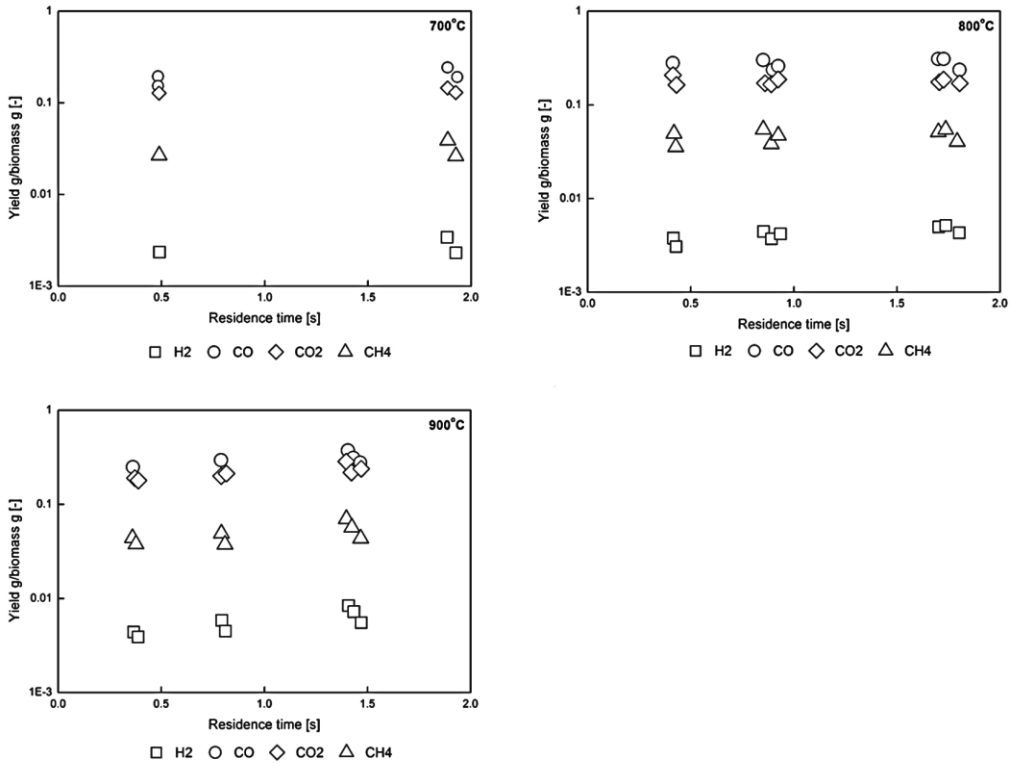

Fig. 4 Experimental results for major gases (hydrogen, carbon monoxide, carbon dioxide, and methane) found in the secondary gas-phase partial oxidation of BG at three temperatures (700, 800, and 900ºC) and at varying residence times (0-2 s).

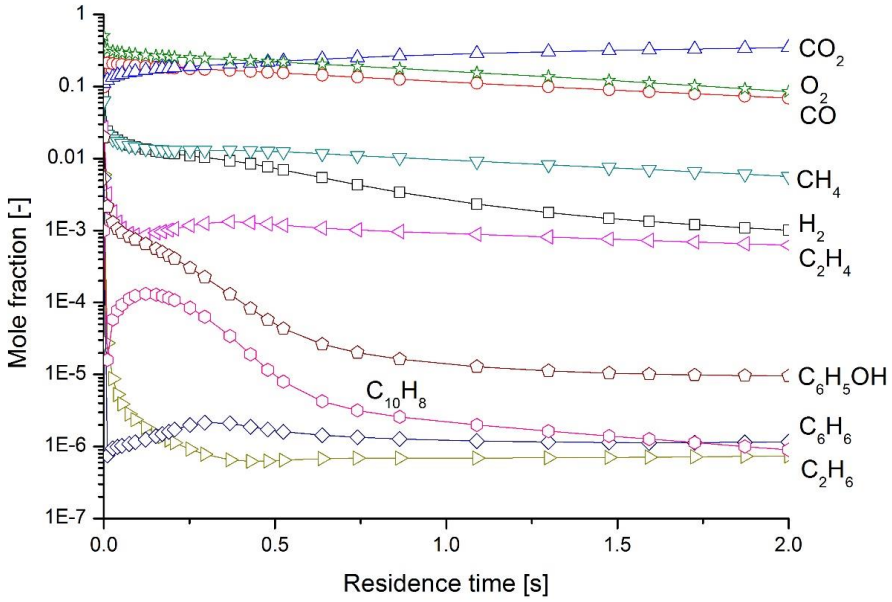

Fig. 5 Profiles of predicted mole fractions with a detailed chemical kinetic model (DCKM) of major species in the partial oxidation of nascent volatiles derived from EFB fast pyrolysis at 700^{o}C as function of residence times.

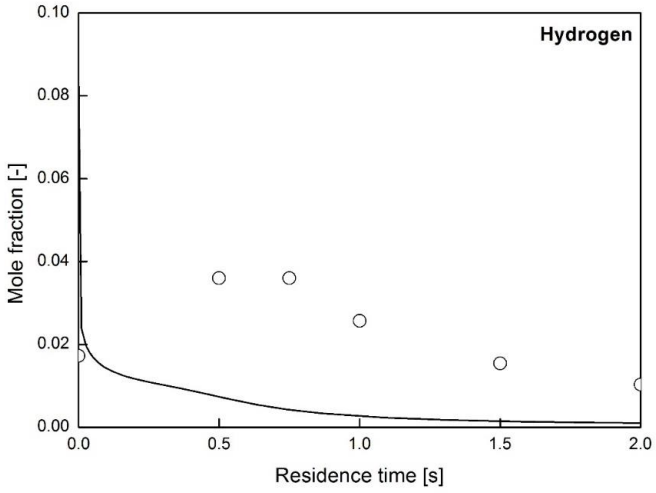

(a)

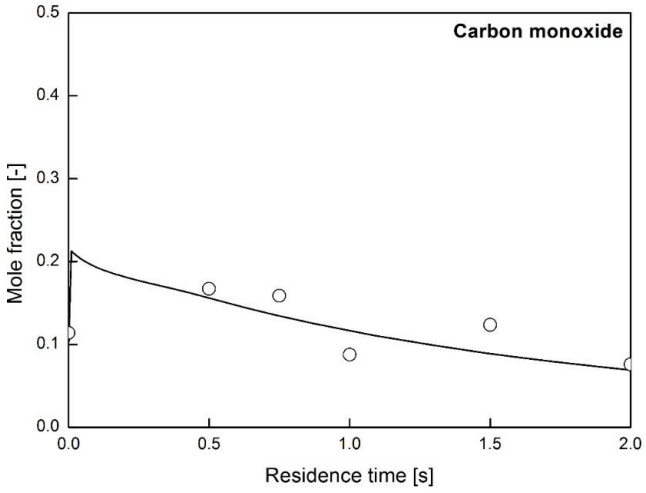

(b)

Fig. 6-1 Comparison of the computational predictions and the experimental data for major gas phase species such as hydrogen, carbon monoxide, carbon dioxide, and methane found in the vapor-phase partial oxidation of nascent volatiles derived from EFB fast pyrolysis at 700^{o}C as the function of residence times. Lines and symbols represent computational predictions and experimental data, respectively.

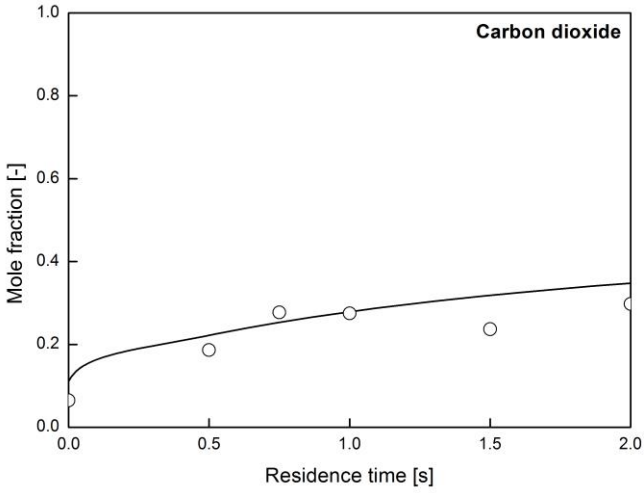

(c)

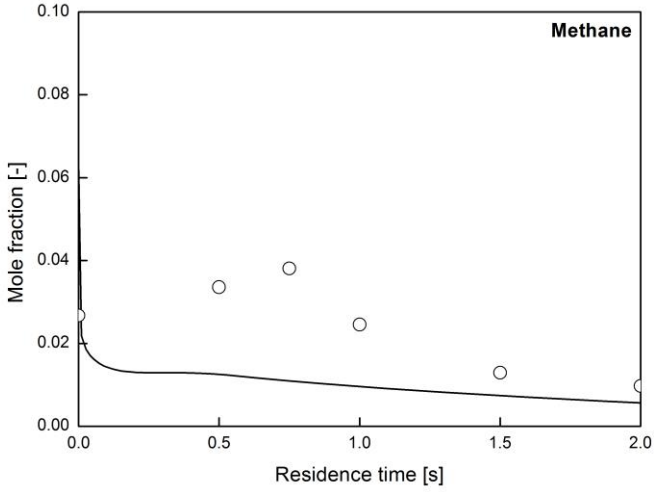

(d)

Fig. 6-2 Comparison of the computational predictions and the experimental data for major gas phase species such as hydrogen, carbon monoxide, carbon dioxide, and methane found in the vapor-phase partial oxidation of nascent volatiles derived from EFB fast pyrolysis at 700^{o}C as the function of residence times. Lines and symbols represent computational predictions and experimental data, respectively.

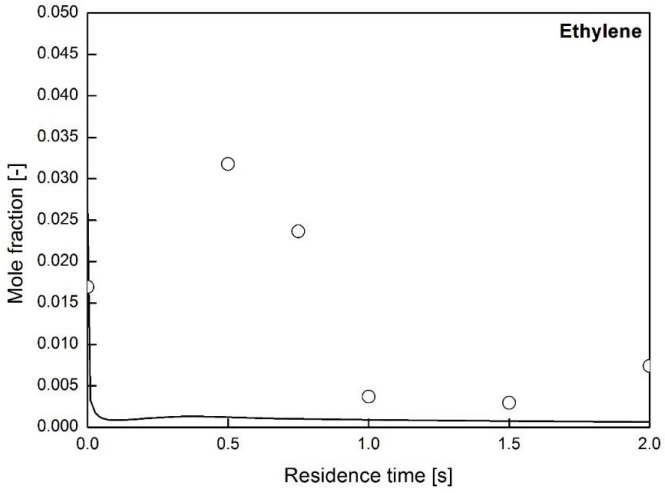

(a)

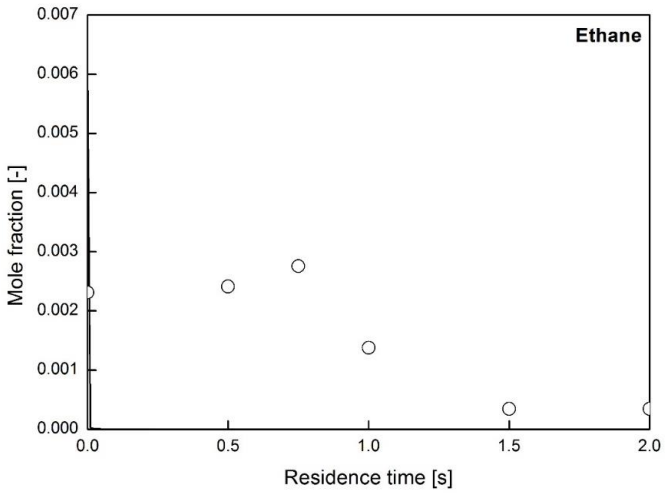

(b)

Fig. 7-1 Comparison of the computational predictions and the experimental data for minor gas phase species such as ethylene, ethane, benzene, phenol, and naphthalene found in the vapor-phase partial oxidation of nascent volatiles derived from EFB fast pyrolysis at 700^{o}C as the function of residence times. Lines and symbols represent computational predictions and experimental data, respectively.

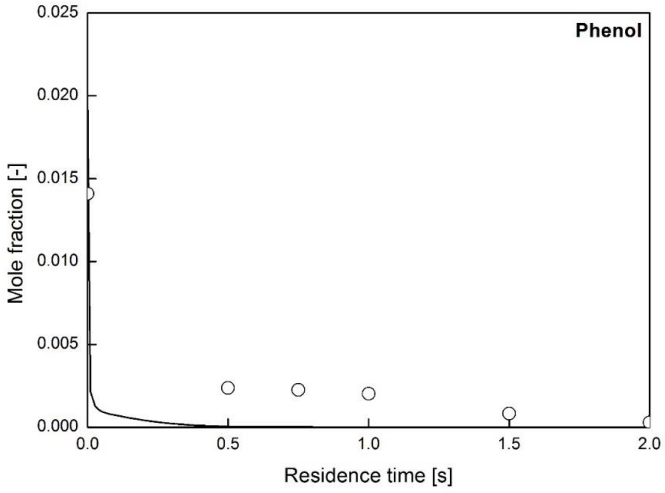

(c)

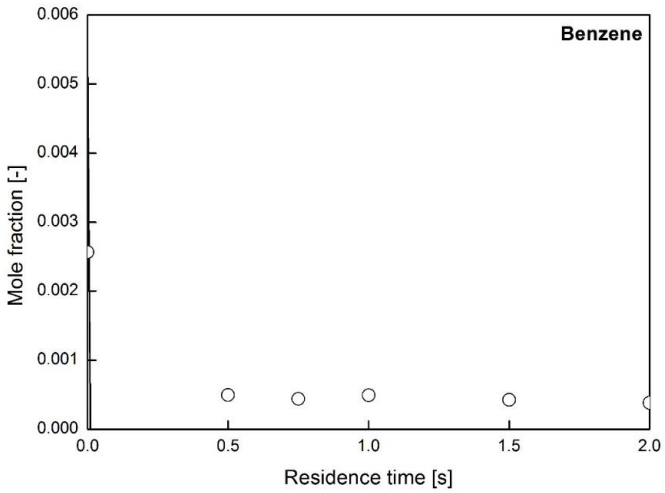

(d)

Fig. 7-2 Comparison of the computational predictions and the experimental data for minor gas phase species such as ethylene, ethane, benzene, phenol, and naphthalene found in the vapor-phase partial oxidation of nascent volatiles derived from EFB fast pyrolysis at 700^{o}C as the function of residence times. Lines and symbols represent computational predictions and experimental data, respectively

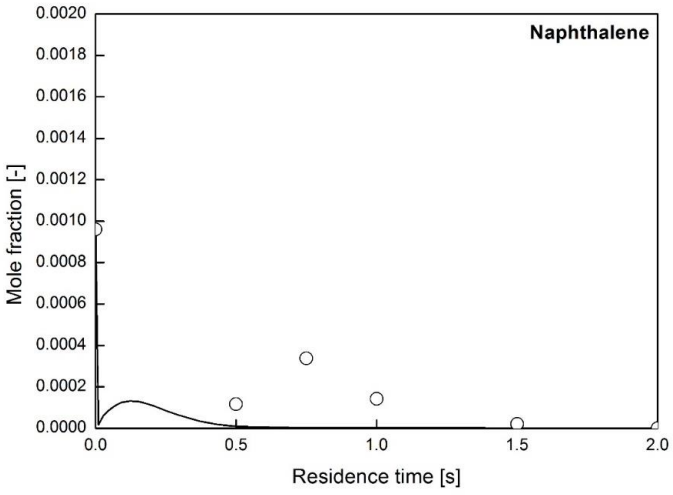

(e)

Fig. 7-3 Comparison of the computational predictions and the experimental data for minor gas phase species such as ethylene, ethane, benzene, phenol, and naphthalene found in the vapor-phase partial oxidation of nascent volatiles derived from EFB fast pyrolysis at 700^{o}C as the function of residence times. Lines and symbols represent computational predictions and experimental data, respectively.

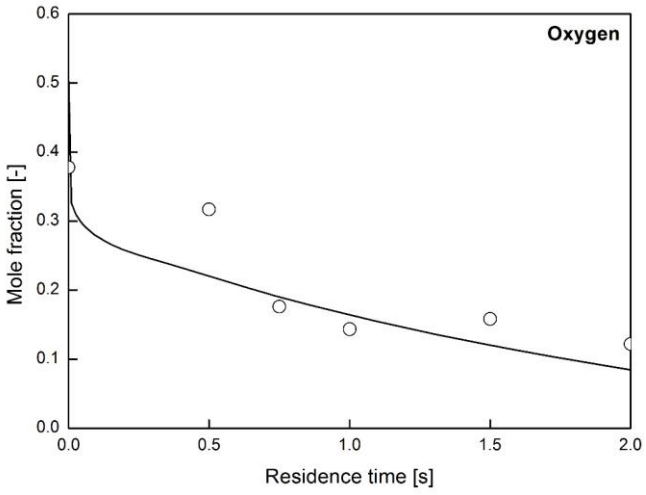

Fig. 8 Comparison of the numerical simulation and the experimental data for mole fraction of oxygen in the vapor-phase partial oxidation of nascent volatiles derived from EFB at temperature 700^{o}C as the function of residence times. Lines and symbols represent computational predictions and experimental data, respectively.

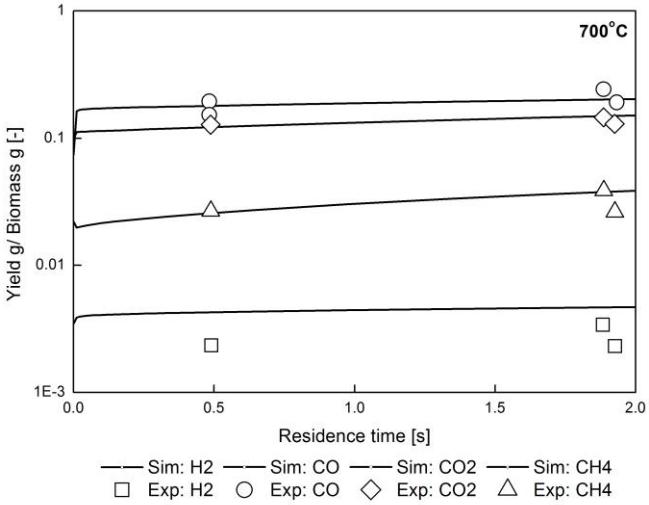

Fig. 9 Comparison of the computational predictions and the experimental data for major gas phase species such as hydrogen, carbon monoxide, carbon dioxide, and methane found in the vapor-phase partial oxidation of nascent volatiles derived from BG fast pyrolysis at temperature 700ºC as the function of residence times. Lines and symbols represent computational predictions and experimental data, respectively.

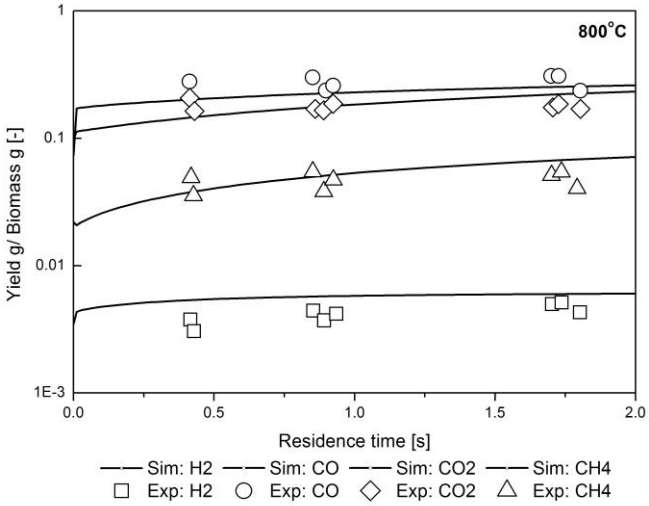

Fig. 10 Comparison of the computational predictions and the experimental data for major gas phase species such as hydrogen, carbon monoxide, carbon dioxide, and methane found in the vapor-phase partial oxidation of nascent volatiles derived from BG fast pyrolysis at temperature 800ºC as the function of residence times. Lines and symbols represent computational predictions and experimental data, respectively.

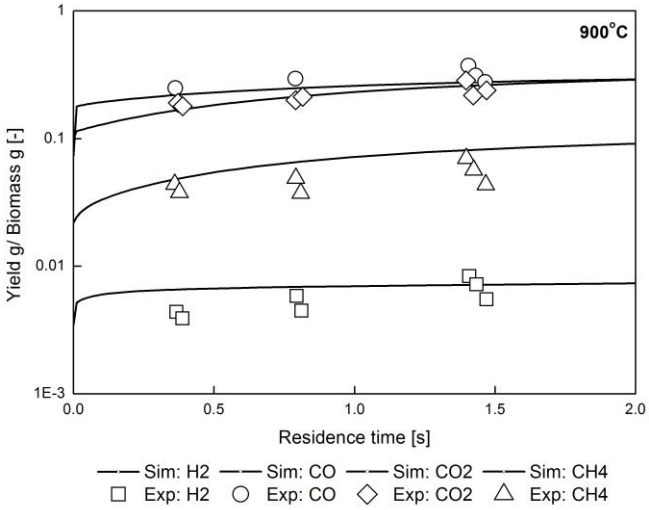

Fig. 11 Comparison of the computational predictions and the experimental data for major gas phase species such as hydrogen, carbon monoxide, carbon dioxide, and methane found in the vapor-phase partial oxidation of nascent volatiles derived from BG fast pyrolysis at temperature 900ºC as the function of residence times. Lines and symbols represent computational predictions and experimental data, respectively.

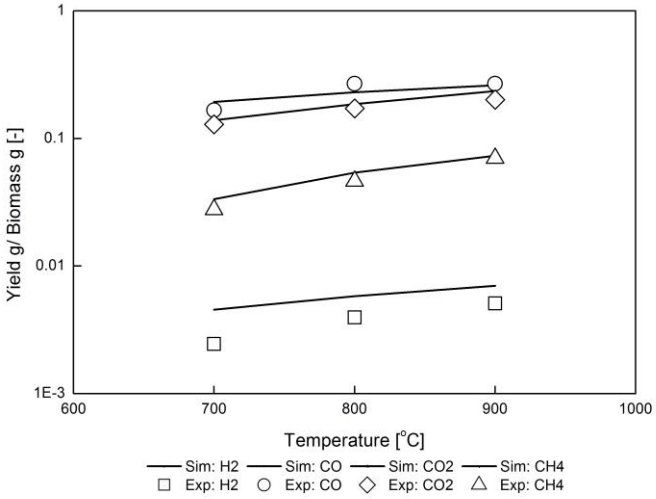

Fig. 12 Comparison of the computational predictions and the experimental data for major gas phase species such as hydrogen, carbon monoxide, carbon dioxide, and methane found in the vapor-phase partial oxidation of nascent volatiles derived from BG fast pyrolysis at the residence time 1.0 s as the function of temperature (700, 800, and 900°C). Lines and symbols represent computational predictions and experimental data, respectively.

Chapter 5

General conclusions

Thermochemical conversion of biomass such as gasification and pyrolysis are proven as an effective technology to convert organic materials into useful valuable products. Tar removal technologies are still a challenge for thermochemical conversion process. As even small amounts of tar can significantly damage downstream equipment and deteriorate gasification efficiency. Tar can be removed by process of non-catalytic vapor-phase reforming of nascent volatiles (NV) derived from biomass fast pyrolysis. To achieve a deeper understanding of the tar reforming in the vapor-phase reforming process, it is important to understand tar formation or destruction as molecular level. This work is the first attempt simulating tar reforming under non-catalytic partial oxidation and steam reforming conditions using detailed chemical kinetic model (DCKM).

The conclusion of achievements in this thesis are summarized here.

In chapter 2, the DCKM consisting of 560 species and 8170 elementary step-like reactions was used to predict gas phase behaviors and tar formations in vapor-phase partial oxidation of nascent volatiles (NV) derived from cedar sawdust fast pyrolysis at different reforming trmperature (700 and 800^{o}C) under varying O/C conditions (0~1.1). Analytical pyrolysis experiments were also conducted to approximate the molecular composition of the NV, which is required input for computations using DCKM. The NV were approximated by 52 chemical species which accounted for 77 and 89% of the sample

fed at 700 and 800°C, respectively. The missing products 23 and 11% mass fractions in NV are the products with current GC and/or could not separated chromatographically due to their high molecular mass. A global reaction for the decomposition of missing products portion of the NV accounted into the simulation with the DCKM. The DCKM was critically evaluated by comparing computational results with the obtained experimental results from partial oxidation in a two-stage reactor: the first stage was designed for fast biomass pyrolysis and the second effected the partial oxidation of the NV. The predictions reproduced the observed trends in the product yields with respect to both temperature and oxygen-to-fuel ratio, for not only the major products namely hydrogen, carbon monoxide, carbon dioxide, and methane, but also minor products such as aromatic hydrocarbons which are typically found in the refractory post-gasification tar.

Chapter 3, in addition to partial oxidation; steam reforming provides additional advantages not only for tar removal, but also in terms of ensuring a hydrogen-rich content in the end product. An existing DCKM which successfully predicted partial oxidation of NV, was firstly applied to predict the steam reforming of NV derived from cedar wood chips fast pyrolysis. The DCKM was applied to simulate the pyrolysis of nascent volatiles (NV); pyrolysis reactor at 750°C and the second effected of the NV partial oxidation and steam reforming at 900°C; reformer reactor, respectively. The computations were performed in the plug-flow reactor model for both steam and air-reforming reagents with varying steam (H_2O/C = 0, 0.5, 1.0) and air ratios (ER = 0, 0.15, 0.3), separately. The predictions could fairly reproduce the experimentally observed trends for the effects of oxygen on the yields of major products and tar residual rate, exception for the effects of steam. Additionally, global reaction of soot reforming were also tested to improve the model capabilities which the experimentally observed characteristics for the steam

reforming were well reproduced both for major products and tar residual rate. The successful predictions suggested DCKM approach is one of the potential kinetic models to understand the complex thermo-chemistries of NV reforming of biomass.

Chapter 4 is aimed to examine the capability of an existing DCKM. Partial oxidation of nascent volatiles (NV) derived from different biomasses namely empty fruit brunch (EFB) and baggage (BG) fast pyrolysis was further simulated. The compositions of the primary pyrolysis products of EFB and BG were determined based on an analytical pyrolysis experiments in a U-shaped two-stage tubular reactor (UTSR). The missing products were assumed and accounted into the simulation by developing global reactions. The computation performed at partial oxidation temperature 700^{o}C with O_2/C 1.23 mol/mol and at partial oxidation temperature 700, 800, and 900^{o}C with O_2/C 0.08 mol/mol, for EFB and BG respectively. The model was critically evaluated with experimental results in a two-stage reactor. The predictions as the function of residence times 2 s showed capability to reproduce the experimentally observed trends of EFB and BG under various reforming conditions. This emphasises that the DCKM approach is comprehensive for any type of biomassese to understand the modeling complex thermo-chemistries. In addition, more sophisticated approach to approximate the missing products for both experimentally (to identify the species) and numerically (to provide the appropriate kinetic parameters) need to be studied.

This work applied DCKM to predict the complex reactions of vapor-phase reforming of NV derived from various type of biomassese under various reforming condition. The results of this study provides comprehensive advantage in the deeper understanding for vapor-phase reforming in the molecular level. These data are useful towards successful thermochemical conversion technology for biomass utilization.

Acknowledgements

This thesis could be successfully completed with the huge supports and contributions from many people who are gratefully acknowledged here.

Firstly my sincere deepest gratitude placed for Associate Professor Koyo Norinaga, my supervisor, who gave me a chance to complete Ph.D. in Kyushu University. More than appreciation for his numerous effort to guide, encourage, and support in every part of my studies. Discussing with him often motivates and inspires me to improve my performance for growing as a research scientist. Without his intelligent guidance and enormous supporting, it would be impossible to succeed this work.

Equally important, I would like to express my cordial appreciation to Professor Jun-ichiro Hayashi, for his productive discussion, helpful suggestions, and always kindness supporting related to both of my study and daily life. His advice always brings me tremendous of knowledge which are very useful allowing me to grow up carefully as a research scientist.

In addition, my special appreciation to Professor Jun Fukai for his valuable comments and suggestion which surely improved this thesis.

My especially grateful to Assistant Professor Shinji Kudo for his kindly assist, precious guidance, patient support, and always care in both of my study and daily life.

I really praise all members in Hayashi-Norinaga laboratory who are belong to laboratory at present and who already leaved the laboratory for their kindly help and

support throughout my study. I could enjoy the daily life and get smoothly environment as always. I wish express my thanks to Mr. Ryota Tanaka, Mrs. Kyoko Hanao, and Mr. Srinivas Appari for his/her great support to make completely succeed on numerical simulation study. I also would like to thank for Yang Hua, Yang Huamei and Li Cheng Yi who always support and care me all the time.

I would like to acknowledge for Japanese Government Scholarship (MEXT) for providing financial support during my doctoral course for 3 years. I also would like to thank the Global COE Program (Novel Carbon Resource Sciences) program (GCOE), Kyushu University for giving me scholarship of oversea research internship in Institute of Energy Process Engineering and Chemical Engineering, TU Bergakademie Freiberg, Germany.

Finally but foremost, my deepest indebtedness declared to my parents, Mr. Thiam Thimthong and Mrs. Lamiat Thimthong, along with my dearest sister, Miss Sasithorn Thimthong for their selfless love, endless support, constant encouragement, and always beside me no matter how hard the situation is. This is including for all my relatives and the all my beloved people for their caring and kindness relations.

Narumon Thimthong

Journal Paper

- **Narumon Thimthong**, Srinivas Appari, Ryota Tanaka, Keita Iwanaga, Shinji Kudo, Jun-ichiro Hayashi, Tetsuya Shoji, and Koyo Norinaga. *Kinetic Modeling of Non-Catalytic Partial Oxidation of Nascent Volatiles Derived from Fast Pyrolysis of Woody Biomass with Detailed Chemistry*. Fuel Processing Technology 134 (2015) 159-167.

- **Narumon Thimthong**, Srinivas Appari, Ryota Tanaka, Keita Iwanaga, Shinji Kudo, Jun-ichiro Hayashi, and Koyo Norinaga. *Numerical study on steam reforming of biomass tar with detailed chemical kinetic model.* Journal of Japan Institute of Energy, Special issue for Asia Biomass (2015).

Conference Publication

- 01/2015 The 2nd Asian Conference on Biomass Science (ACBS2015). Auditorium, AIST Tukuba Central 1, Tsukuba, Japan (Poster presentation).
- 11/2014 The 4th ASCON-IEEChE 2014 Innovative Energy & Environmental Chemical Engineering: ISBN 978-89-5708-249-2. The Ocean Resort, Yeosu, Korea (Oral presentation).
- 09/2014 The 23rd International Symposium on Chemical Reaction Engineering (ISCRE23) and the 7th Asia-Pacific Chemical Reaction Engineering Symposium (APCRE7). Centara Grand & Bangkok Convention Centre, Bangkok, Thailand

(Poster presentation).

- 01/2014 1st Asian Conference on Biomass Science (ACBS2014). Kochi Prefectural Culture Hall, Kochi, Japan (Oral presentation).
- 12/2013 The 26th International Symposium on Chemical Engineering (ISChE 2013). BEXCO in Busan, Korea (Oral presentation).
- 11/2013 2nd Joint Conference on "Renewable Energy and Nanotechnology" (JCREN2013). Hiroshima University Faculty Club, Higashi-Hiroshima, Japan (Oral presentation).
- 10/2013 The 12th Japan-China Symposium on Coal and C1 Chemistry. Fukuoka, Japan (Poster presentation).

Award

- 01/2014 **Excellent Paper award for Oral Presentation.** The 1st Asian Conference on Biomass Science (ACBS2014).
- 09/2014 **The Best Poster Presentation Award.** The 23rd International Symposium on Chemical Reaction Engineering (ISCRE23) and the 7th Asia-Pacific Chemical Reaction Engineering Symposium (APCRE 7).

Appendix

論文提出者	Narumon Thimthong（ナルモン ティムトン）
論文題名	Detailed chemical kinetic modeling study on gas phase partial oxidation and steam reforming of species released during biomass pyrolysis （バイオマス熱分解生成物の気相部分酸化および水蒸気改質の詳細化学反応速度モデリングに関する研究）
論文調査委員	主査　九州大学　准教授　則永　行庸 副査　〃　教　授　林　潤一郎 〃　〃　〃　深井　潤

論文調査の要旨

持続可能な循環型社会形成に向けて、再生可能エネルギーの有効利用の促進が求められている。バイオマスは他の再生可能エネルギーである太陽光、風力などよりも、現状で一桁以上大きい量のエネルギーを供給している。その一方で、バイオマスは、エネルギー密度が低いため運搬コストがかさみ、集積が困難という課題がある。そこで、バイオマス発生場所近辺でのオンサイト小規模利用技術の開発が進められており、その有望な技術の一つとして、バイオマスを熱化学的に有用ガスへと転換するガス化がある。

高効率ガス化の達成には、原料バイオマスが持つ化学エネルギーの燃焼による損失をできるだけ抑え、より低温でガス化することが要求される。そこでは、多環芳香属化合物を主成分とする、凝縮性の混合物であるタールが不可避的に生成、残留する。タールはガス化炉下流での配管閉塞やスス生成を招くため、これを非凝縮性成分へと転換する改質操作が必要である。酸素、水蒸気を酸化剤とする気相改質によるタール分解は、堅牢かつ簡便な技術であるが、改質炉の設計や運転条件の最適化によって、必要最小限の酸化剤導入量を決定し、限界までの高効率化を目指す場合、バイオマスガス化で生成するタール含有ガスの気相改質を網羅的かつ詳細に記述できる反応速度モデルの構築が必要である。

そこで本研究では、バイオマス熱分解生成物の気相における部分酸化特性や水蒸気改質特性の予測を、素反応から構成される詳細化学反応速度モデルを用いた反応シミュレーションにより実現するための解析技術を開発している。本研究において得られた知見は以下のように纏められる。

（１）熱分解部と改質部で構成される二段反応器における木質バイオマス（スギ）急速熱分解生成物の気相部分酸化反応実験を対象に、詳細化学反応速度モデルを用いた反応シミュレーションを実施している。境界条件として必要となる急速熱分解生成物の分子組成を、熱分解／ガスクロマトグラフィー（GC）実験の結果に基づいて、50以上の化学種で表現する手法を確立している。GCで

検知できない重質成分については、その化学式を元素収支から求め、化学量論を満たす分解反応を仮定し、その反応速度を経験的に与えている。急速熱分解生成物に含まれる化学種および化学種間の反応を網羅する約8,000の反応から成る速度モデルを構築し、水素、一酸化炭素、二酸化炭素、メタンなどの主要成分ばかりでなく、タール前駆体となる単環芳香族類やナフタレンなどの微量成分の収率予測にも成功している。

（２）二段反応器におけるスギチップ熱分解生成物の気相水蒸気改質実験を対象に、本研究で確立した反応予測手法の、異なる改質反応系における適用性を検討している。反応シミュレーションにより、水蒸気分圧が、水素、一酸化酸素などの主要生成物の収率に及ぼす影響ばかりでなく、微量副生成物であるタールの転換特性に及ぼす影響の再現に成功している。加えて、改質反応中に生成するスス状物質のガス化反応を表現する総括反応モデルを提案し、その追加による再現精度の向上に成功している。

（３）二段反応器におけるバガス（サトウキビ搾りかす）と空果房（パーム油残渣）の

熱分解生成物の気相部分酸化実験を対象に、本研究で確立した反応予測手法の異なるバイオマス原料種に対する適用性を検討している。速度モデル中の素反応速度パラメーターを一切調整することなく、境界条件（温度、酸素量、熱分解生成物組成）を変更するだけで、実験結果の再現に成功し、本モデリング手法の汎用性を示している。

以上要するに、本論文は、熱分解／GC実験によるバイオマス熱分解生成物の分子組成決定法を提案し、熱分解生成物中に含まれる化合物及び化合物間の反応を網羅する詳細化学反応速度モデルを構築し、これに基づく反応シミュレーションによって異なるバイオマス気相改質反応系で得られた複数の実測結果の再現に成功したものであり、本論文で得られた新知見は、バイオマス熱化学転換技術開発に有用で、炭素資源利用に関する化学反応工学へ寄与する。よって、本論文は博士（工学）の学位論文に値するものと認める。

最終試験の結果の要旨

本論文に関して調査委員から、（１）シミュレーションにおけるタールの定義、（２）初期熱分解生成物の定義、（３）本モデリング手法の課題、などについて質問があったが、いずれも著者から的確な回答がなされている。また、公聴会においては、多数の出席があり活発な質問があったが、いずれも著者の説明によって質問者の理解が得られている。

以上の結果より、著者は最終試験に合格したものと認める。

Reaction mechanism and input files

DETCHEM^{BATCH} and DETCHEM^{PLUG} require following input files; reaction mechanism, thermodynamic data, transport data, and species list. Those files used in this study are provided as supplementary data in an article which has been already published in Journal of Fuel Processing Technology.

Detailed information of all data are given as follows:

Narumon et al. **Kinetic modeling of non-catalytic partial oxidation of nascent volatiles derived from fast pyrolysis of woody biomass with detailed chemistry.** Fuel Processing Technology 134 (2015) 159-167)

http://www.sciencedirect.com/science/article/pii/S0378382015000442#MMCvFirst